

POLITECNICO DI TORINO

Corso di Laurea Magistrale

in Ingegneria Meccanica

Tesi di Laurea Magistrale

**Dynamic Indentation Testing:
theory and practice**



Relatore:

Prof. Gianfranco Genta

Candidato:

Kelvyn Andres Sanchez Rojas

Anno Accademico 2020/2021



ACKNOWLEDGEMENT

Este trabajo de grado es la conclusión de un largo camino de estudio que inicio en mi país Venezuela y que después de tanto tiempo culmina en lo que se volvió mi nuevo hogar, Torino. Por todo lo vivido, por todas las experiencias y por las que faltan por vivir agradezco en primer lugar a Dios que muchas veces me ha demostrado cuan presente ha estado en mi vida.

Quiero agradecer a mis padres por todo el apoyo que me han brindado, porque su labor de padres ha sido un ejemplo que recordaré por siempre. Si no fuera por ellos, no seria la persona que soy ahora y tantas de las metas que he alcanzado no las habría ni siquiera pensado; es gracias a ustedes, Andres y Yarida que pude empezar mi camino lejos del nido.

No pienso olvidar a mis hermanos, que en la distancia siempre me apoyaron, que si tal ves nuestra relación no se basa en muchas palabras y demostrar lo que sentimos, nunca me olvido de como Emily y Juan lloraron cuando partí de Venezuela a mi nueva vida. Ustedes también fueron parte de mi motivación para seguir adelante y ser ejemplo vivo de que con perseverancia se puede.

Finalmente, quiero dar mi agradecimiento a ti, Karolay. Tu eres la razón por la cual mi vida esta completa, y agradezco infinitamente a Dios por habernos puesto en el camino del otro, porque tu me mostraste el significado del verdadero amor; ese que te hace pensar en estar juntos en las buenas y las malas, en imaginar una vida de viejitos, y cuan mas grandes se vuelven los logros cuando estas con la persona que amas.

A ti Karolay, que sin ti esta meta no se habría logrado, que me has acompañado desde el inicio en la nueva vida que empecé en Italia, quien me ha dado la mas grande de las felicidades nuestra hija Kylie. Te agradezco inmensamente por todo el amor que me das, y no me resta mas que decirte TE AMO.





ABSTRACT

The methods dedicated to the characterization of the mechanical properties of the material are vast and specific pointed to the kind of property to estimate. Among the techniques available, we can find the indentation approach; object of study in this work addressed to analyze dynamic methodologies with focus on Continuous Stiffness Measurement (CSM) or Sinus mode which is an interest procedure with the capacity of evaluate at first mechanical properties such as hardness and Young's modulus at micro and nano scale range. This work begins with studying the background behind the methodology and its connection with the ISO Standard 14577 (Instrumented Indentation Test) with particular attention to the several variables involved and the factors that affect the measurements.

All of this applied to specific applications of interest in the industries like thin film coating, heat treated materials (specific case of weld parts) and determination of properties of viscoelastic materials. In conjunction with an analysis of manufacturers' choices in the production of test equipment specifically for CSM test with the scope of supporting the potential of the method of becoming a standard procedure that can be available in the diverse normative organizations (ISO, ASTM, UNI, ...).

Keywords: Indentation, CSM, thin film, viscoelastic.





TABLE OF CONTENTS

ACKNOWLEDGEMENT	1
ABSTRACT	3
Table of Contents.....	5
LIST OF FIGURES	8
LIST OF TABLES.....	13
INTRODUCTION	15
THEORETICAL FRAMEWORK.....	20
Martens Hardness	20
Instrumented Indentation Test: Single Loading/Unloading Indentation Cycle.....	23
Power law equation – Unloading Phase	27
Contact Stiffness (S).....	28
Berkovich Indenter – Area function (A).....	31
Contact Depth (h_c) – Sinking in and Piling up considerations	32
Factors Affecting IIT Test Data.....	34
Thermal Drift.....	34
Initial Penetration Depth.....	35
Instrument Compliance (C_f)	36
Indenter Geometry.....	38
Tip Rounding.....	39
Indentation Size Effect (ISE).....	41
Pile up and Sinking in.....	43



Continuous Measurement of Stiffness (CSM).....	45
Simple Harmonic Oscillator – Indenter free hanging.....	47
Simple Harmonic Oscillator – Modelling of indenter contact	49
Indenter Contact – Pure elastic-plastic materials	51
Indenter Contact – Dissipative materials.....	52
Vibration Response of CSM System – Insights in excitement frequency selection	53
Indentation Test Machine – Scheme for Continuous Stiffness Measurement.....	55
Force Source Input Signal and Sensors	56
Computer – Phase Lock Amplifier [PLA] (Lock in Amplifier).....	58
Factors Affecting CSM Test.....	58
Instrument Compliance.....	58
Plasticity Effect – Bulk Materials.....	61
Indentation strain rate and Material Sensitivity.....	63
METHOD APPLICATIONS.....	64
Surface Mechanical Properties – Heat Treated Materials	65
Welding: CSM Hardness profile characterization.....	69
Thin Film Characterization.....	70
Film thickness known.....	71
Unknow film thickness	76
Material Characterization for Battery Cell Manufacturing	77
Viscoelastic Material – Glass Transition Temperature	79



CONCLUSIONS	82
BIBLIOGRAPHY	84
APPENDIX	90
Berkovich indenter	90
Instrument Compliance – ISO 14577-2.....	90
Fused Silica – No presence of ISE	91
Fundamental models for a viscoelastic mechanical system	92
Work of Indentation.....	92
Lock-in Amplifier Working Principle – PLA time constant effect	94



LIST OF FIGURES

Figure 1: Principle of Brinell Test (ISO Standard, 2014).....	16
Figure 2: Indenter geometry for Vickers (a) and Knoop (b) (ISO Standard, 2018)	17
Figure 3: Hardness Numbers for Non-austenitic Steels* based on data ASTM 370	17
Figure 4: Imaging creation of the print in a Brinell Test (Germak)	18
Figure 5: Schematic representation of the test procedure ISO 14577 (ISO Standard, 2016)	20
Figure 6: Deformation in the indentation loading unloading cycle (Sakai, 1993)	21
Figure 7: Load vs indenter displacement for a fully elastic contact (left) and for a plastic contact on an electropolished single crystal of tungsten (Oliver & Pharr, 1992).....	24
Figure 8: Indenter displacement (Michel Yetna, Idriss, Olivier, & Didier, 2016)	24
Figure 9: Schematic representation of load versus indenter displacement data for an indentation experiment (Oliver & Pharr, 1992).....	25
Figure 10: Force reaction (F_s) when load is applied during the indentation.....	26
Figure 11: Schematic representation of a section through an indentation (Oliver & Pharr, 2004).....	26
Figure 12: Power law equation for the unloading phase in the indentation cycle (Oliver & Pharr, 2004)	27
Figure 13: Conventional load-displacement curve resulting from indentation of a polymer (Fischer-Cripps, 2002).....	31
Figure 14: Contact depth and projected area $A_p(h_c)$ (ASMEC GmbH, s.d.)	32
Figure 15: Relation between ϵ and m (Pharr & Bolshakov, 2002)	33
Figure 16: Decision tree to assist in estimating thermal drift using a constant force hold period (ISO Standard, 2016).....	34



Figure 17: Example of indentation curve obtain after thermal drift consideration (Maculotti, et al., 2019)	35
Figure 18: Schematic of the effect of initial penetration depth on load-depth data for a depth-sensing indentation test. Depth readings must be corrected for h_i (Fischer-Cripps, 2002).....	36
Figure 19: Schematic deflection of the test machine by effect of the load application during an indentation test (Fischer-Cripps, 2002).....	36
Figure 20: Schematic of dh/dP vs h_p^{-1} (for Berkovich indenter)	38
Figure 21: Area correction function for a typical Berkovich indenter (Fischer-Cripps, 2002).....	38
Figure 22: Cross-section of a conical impression and representation of the impression profile after the withdrawal of the indenter and the elastic recovery at the bottom of the indenter represented by the dotted line (Chicot, et al., 2015).....	39
Figure 23: Evaluation of the size of the tip defect for the a) Berkovich, b) Vickers, c) Knoop and d) Spherical indenters by mean of emission field SEM analysis at different magnifications (Chicot, et al., 2013)	40
Figure 24: Cross-section of a conical impression and representation of the tip defect through the truncated length at the indenter tip (Chicot, et al., 2015).....	40
Figure 25: Contact stiffness as a function of the inverse of the square root of the contact area for a Vickers indenter (Chicot, et al., 2013)	41
Figure 26: Hardness vs indentation depth with particular attention to ISE [experimental data by (Chicot, et al., 2013)]	42
Figure 27: Measured hardness of a super-hard nano-composite nc-TiN/a-BN film ($5 \mu\text{m}$ thick) on a steel substrate. Three regimes, initial rise, plateau and fall-off can be identified (Fischer-Cripps, 2006).....	42
Figure 28: Schematic illustrations of (a) pile-up and (b) sink-in around a sharp indenter (Giannakopoulos & Suresh, 1999)	44



Figure 29: Schematic of the load-time variation during a CSM (Sudharshan Phani, Oliver, & Pharr, 2020)	46
Figure 30: Schematic of Nano Indenter indentation head (Agilent Technologies, 2013) (left) and representation of dynamic mechanical model when free indenter (right)	47
Figure 31: Illustration of solution of the simple harmonic oscillator model	47
Figure 32: Measured compliance and best fit for the Agilent G200 Nano. (Hay, Agee, & Hebert, 2010).....	48
Figure 33: Harmonic Oscillator model including contact interaction (Hay, Agee, & Hebert, 2010).....	49
Figure 34: Dynamic model contact for bulk materials (Agilent Technologies, 2013)...	51
Figure 35: CSM or Sinus mode during hold at constant force (Nohava, Dynamic mechanical analysis by nanoindentation).....	52
Figure 36: Damping factor for Anton Paar Bench (Politecnico di Torino) and Agilent Machine G200.	54
Figure 37: Suggested range of input frequency CSM test applied to test bench of Politecnico di Torino	55
Figure 38: Original schematic arrangement of a CSM test rig (United States of America Brevetto n. 4,848,141, 1989)	56
Figure 39: Force-time algorithms used for CSM and ISO 14577 tests (Hay, Agee, & Hebert, 2010).....	57
Figure 40: Model description for instrument compliance.	59
Figure 41: No apparent effect of frame stiffness on modulus (Agilent Technologies, 2013)	60
Figure 42: Variation due to sample tray position (Agilent Technologies, 2013)	60
Figure 43: Effect of frame stiffness of modulus (Agilent Technologies, 2013).....	60



Figure 44: Phase angle-displacement variation, during a constant strain rate CSM test for fused silica (Sudharshan Phani, Oliver, & Pharr, 2020).....	61
Figure 45: Experimental observation of cyclic plastic yield. (Merle, Higgings, & Pharr, 2019).....	62
Figure 46: Comparison of hardness—displacement profiles for (a) Ni SX and (b) Cr SX for tests with and without CSM. (Leitner, Maier-Kiener, & Kiener, 2017).....	63
Figure 47: Load—displacement curves of LC (multiple unloading IIT) and CSM measurements on Ni SX and Cr (Leitner, Maier-Kiener, & Kiener, 2017)	64
Figure 48: Comparison with Low strain-rate CSM experiments (Leitner, Maier-Kiener, & Kiener, 2017).....	64
Figure 49: Elastic modulus, and hardness as a function of contact depth for a magnetic rigid disk with a multilayered structure (Xiaodong & Bharat, 2002).....	66
Figure 50: Contact stiffness, elastic modulus, and hardness as a function of contact depth for hard FCA a-C/Si (Bharat Bhushan, 2002)	68
Figure 51: Geometrically necessary dislocations created by a rigid conical indentation (Nix and Gao (Nix & Gao, 1998)).....	68
Figure 52: Depth dependence of hardness plotted according to Nix-Gao model (Nix & Gao, 1998)	69
Figure 53: Discretization of welding area (Sedmak & Nohava)	69
Figure 54: Cross-section of the heat affected zone and the corresponding hardness profile at fixed indentation depth (Sedmak & Nohava)	70
Figure 55: Hardness vs impression diagonal on substrates with and without a film (Jonsson & Hogmark, 1984).....	71
Figure 56: Load-supporting areas A_f and A_s of the film and the substrate respectively (Jonsson & Hogmark, 1984).....	72



Figure 57: SEM cross section view of the coated system under investigation after fracture, showing the DLC, CrC and CNiPCr layers, as well as the NiP substrate (Puchi-Cabrera, Staia, & Lost, 2015).....	73
Figure 58: Change in the experimental values of the composite hardness as a function of penetration depth 2024-T6 aluminum alloy coated (Puchi-Cabrera, Staia, & Lost, 2015)	74
Figure 59: Change in the volume fraction of each coating contributing to the composite hard- ness, according to the JH model, as a function of penetration depth (Puchi-Cabrera, Staia, & Lost, 2015).....	74
Figure 60: Schematic representation of S variation for the coated system (hard film on soft substrate). (Tricoteasux, et al., 2010)	77
Figure 61: Lithium-ion battery structure showing approximate thickness of the components (Nohava, Characterization of electrodes in lithium-ion batteries by nanoindentation)	78
Figure 62: Distribution of hardness and elastic modulus on Li-ion cathode coating (area 300 x 300 μm).....	78
Figure 63: volution of elastic modulus of LiFePO ₄ coating after aging measured by nanoindentation (Demirocak & Bhushan, 2015).....	79
Figure 64: Storage modulus versus temperature for PDMS thin film. (Noble, 2018) ...	80
Figure 65: Loss modulus versus temperature for PDMS thin film (Noble, 2018)	80
Figure 66: Tangent delta versus temperature for PDMS thin film. The upper graph shows a zoomed view of the data around the Tg temperature (Noble, 2018)	81



LIST OF TABLES

Table 1: Hardness testing scales defined by ISO 14577-1 (ISO Standard, 2016).....	18
Table 2: Hardness Moh Scale (Emco-Test Prüfmaschinen GmbH, s.d.)	18
Table 3: Martens Hardness equations.....	21
Table 4: Martens hardness in terms of slope	22
Table 5: Sneddon's Model vs Oliver and Pharr's Model	23
Table 6: IIT hardness and parameters.....	26
Table 7: Sneddon model values of m previous the IIT theory	28
Table 8: Parameters characterizing unloading curves with Berkovich indenter (Oliver & Pharr, 1992)	28
Table 9: Contact Stiffness expression based on Sneddon model	29
Table 10: Correcting factor (β) in the evaluation of punch geometry in the contact stiffness.....	30
Table 11: General expression A_p	31
Table 12: Contact depth and sinking in depth expressions.	32
Table 13: Contact depth considering pile-up effect.....	33
Table 14: Instrument compliance	37
Table 15: ISO 14557-2 Assumptions compliance determination methods (ISO Standard, 2016).....	37
Table 16: Indentation response of material based on yield stress and mean pressure contact (Fischer-Cripps, 2002).....	43
Table 17: Type of deformation in terms of the ratio E/Y	44
Table 18: Close look into ITT hardness and elastic modulus.....	46



Table 19: Dynamic response simple harmonic oscillator.....	48
Table 20: Equivalent spring in terms of elements in harmonic oscillator model of contact stiffness.....	49
Table 21: Equivalent dashpot coefficient in terms of elements in harmonic oscillator model of contact stiffness.....	50
Table 22: Stiffness (S) and Damping coefficient of contact	50
Table 23: Storage and Loss Modulus – Dissipative energy materials (Agilent Technologies, 2013)	52
Table 24: Free hanging oscillation constant for Anton Paar Bench (Politecnico di Torino) and Agilent Machine G200.....	53
Table 25: Damping coefficient simple harmonic model	54
Table 26: Excitation force in terms of DC and AC signal (Sudharshan Phani, Oliver, & Pharr, 2020)	56
Table 27: Plasticity error estimation (Sudharshan Phani, Oliver, & Pharr, 2020)	62
Table 28: Nix and Gao Model for ISE evaluation.....	67
Table 29: Jonsson and Hogmark Model for thin film model	72
Table 30: Remarks on Volume fraction and Composite hardness	73
Table 31: Puchi-Cabrera modified Jonsson and Hogmark model for multilayered films (Puchi-Cabrera, Staia, & Lost, 2015)	75



INTRODUCTION

Determining the mechanical properties is part of the characterization of materials and one of the alternatives to evaluate the performance of fabrication processes or products. Consequently, the mechanisms applied to estimate characteristics such as hardness, elastic modulus, fatigue behavior; need to be carried out with ease and precision. When the nature of the feature of interest is connected to the surface of the object, one of the several methods to evaluate the mechanical behavior is the indentation technique; a method that consists essentially of putting in contact two materials, one whose mechanical properties are unknown with other whose characteristic are already estimated (Fischer-Cripps, 2002). In general, the scope of indentation is to determine the hardness, defined at first by Moh as the capacity of a material to leave a permanent scratch in another one (Fischer-Cripps, 2002) and nowadays this concept is understood and implemented as the resistance to localized deformation of materials.

During the measurement of hardness through indentation process, different factors are considered, these ones can be generally divided into 3 categories: geometrical parameters (because of the relevance of indenter geometry), load cycle and sources of error. In addition, depending on the technique applied, other variables may be contemplated with the aim of just not estimate hardness but other mechanical characteristic with the same data, for example, a common feature evaluated together with hardness in an indentation test is the tensile strength described as the maximum stress before the rupture of the material (Instron Company, s.d.), an usual case of a multi-scope indentation trial is when the technique is performed in metallic materials where the standard ASTM A370 defines direct correlations between hardness and strength (ASTM Standard, 2020). However, the normative previously mentioned is one of those specific cases when more than one property can be estimated, in general, the determination of multiple mechanical properties is limited by the nature of material itself, in major part of the occasions due to several factors such as anisotropy and inhomogeneity of the sample which is the reason why we can find different variants of a technique because depending on the method used to deform the material, the set of properties that can be estimated changes and conducting furtherly to the existence of a classification of indentation techniques.



Among those procedures there is one that can be pondered as a classic indentation method, we find the Brinell Test (ASTM Standard, 2020), a standard characterized by the use a tungsten carbide ball as an instrument to apply the load on the sample (see Figure 1); the aim of the test is create a print in the specimen under specific conditions: a well-defined geometry of the indent and load cycle because once indentation is performed a measurement with optical devices is fulfilled to define geometric parameters of the print in order to estimate the hardness of the component, a hardness connected to the parameters of the trial giving as result the presence in the reports of Brinell hardness values together with the diameter of the ball and peak load. Other variants of indentation tests (Vickers, Rockwell, Knoop, etc.) are applied due to the limitations of Brinell Test to estimate larger values of hardness (refer to Figure 3); or just simply to increase the velocity to perform the trial. Even though, all these types of indentation have as a common denominator the afterwards measurement through optical equipment of the print, and what it makes differ among each other is the shape of the indenter (see Figure 2).

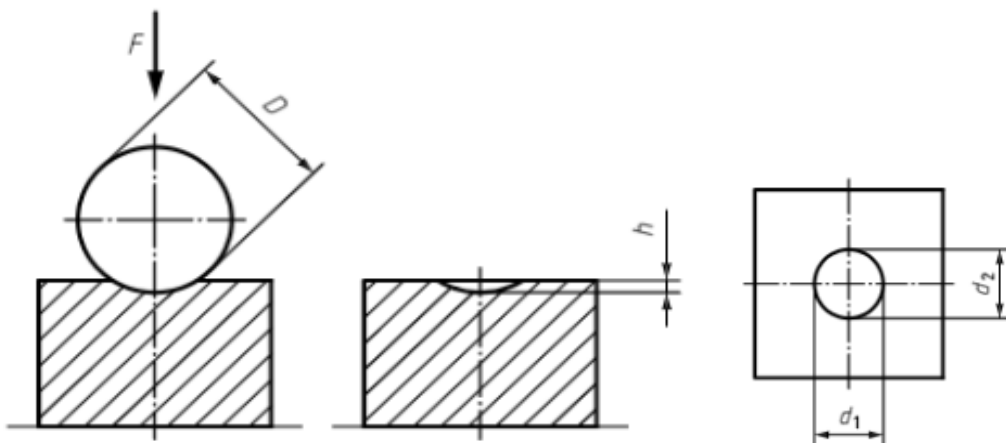


Figure 1: Principle of Brinell Test (ISO Standard, 2014)

Considering these traditional indentation tests which involve optical imaging of the indent, a fact that clearly imposes a lower limit on the length scale of the indentation (Bharat Bhushan, 2002). Because of the multiple variables present in the imaging of the print such as the position of the shadow on the boundary of the indent depending on the profile of the section of the edge of the imprint due to phenomena like sinking and pile-up later explained in more detail; and the opening angle of the lighting and observation cones, called numerical aperture (NA), a variable not fully defined in the standards (Germak) (refer to Figure 4).

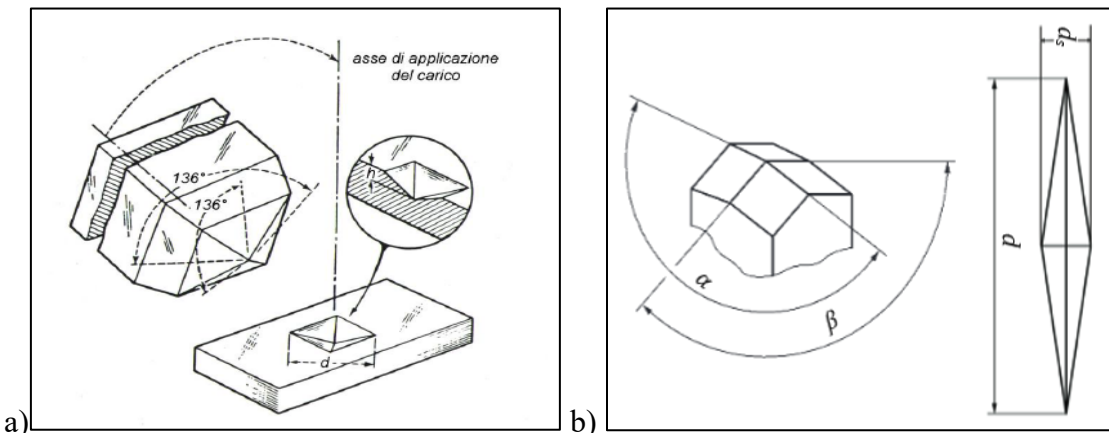


Figure 2: Indenter geometry for Vickers (a) and Knoop (b) (ISO Standard, 2018)

Hardness Range in Scale Vickers Equivalent *

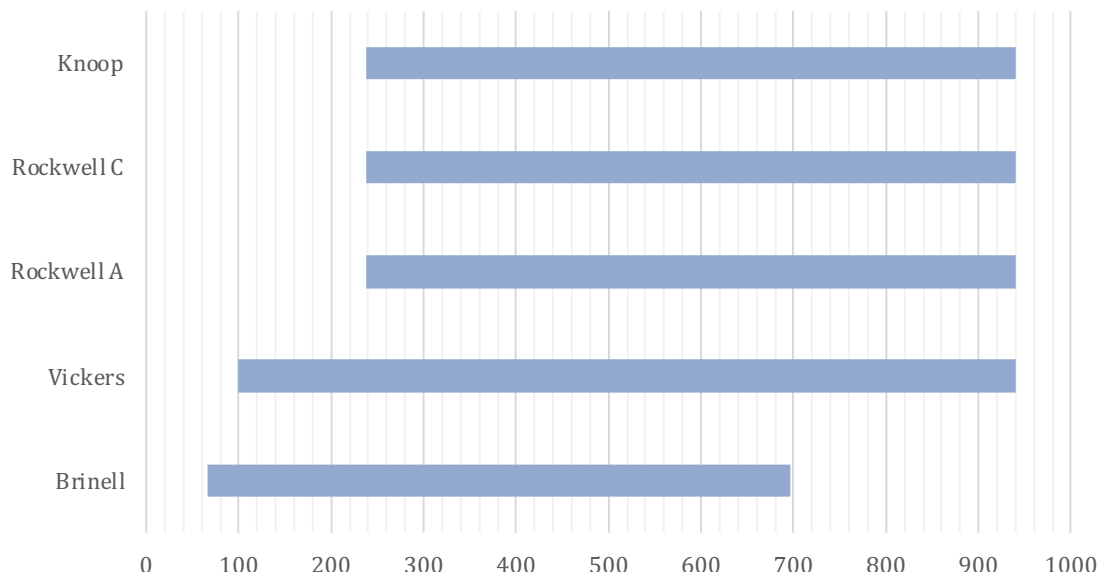


Figure 3: Hardness Numbers for Non-austenitic Steels* based on data ASTM 370

As a result of the limitation of optical measurement, another type of measurement is implemented when the nature of the desired material properties is at nanoscale length (consider values as described in ISO 14577-1 (ISO Standard, 2016), see Table 1) or optical devices are not available. In this case, the procedure to apply is a Dynamic Indentation Test, an approach of this nature is the Instrumented Indentation Test (Oliver & Pharr, 2004) adopted and used in the characterization of mechanical behavior of materials at small scales; where mechanical properties can be determined directly from load vs displacement data obtained during indentation routine without the need to image the hardness impression.



Table 1: Hardness testing scales defined by ISO 14577-1 (ISO Standard, 2016)

	Load range (N)	Penetration range (μm)
Macroscale	$2 < L < 30,000$	Not specified
Microscale	$L < 2$	$h > 0.2$
Nanoscale	Not specified	$h < 0.2$

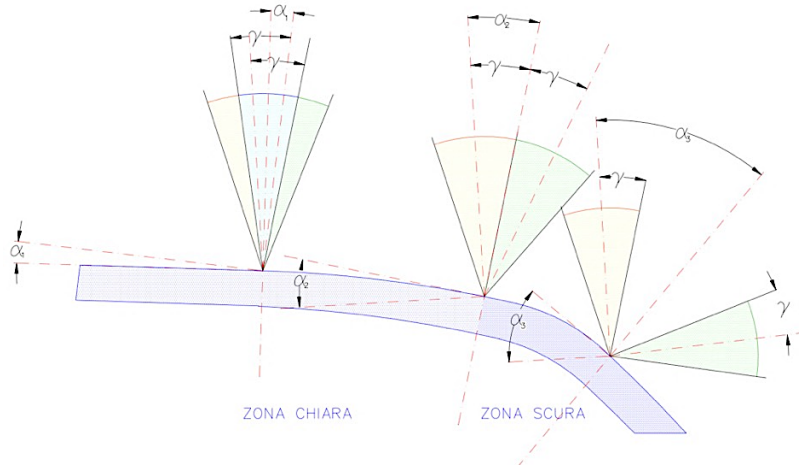


Figure 4: Imaging creation of the print in a Brinell Test (Germak)

The Instrumented Indentation Test (IIT) meant a completely different methodology in comparison with the classic methods (Brinell, Vickers, Knoop or Rockwell test); even more singular if we consider that at first the hardness of materials were evaluated with the Moh Scale (see Table 2), a ten-point scratch hardness scale in which each material can be scratched using the next harder material (Emco-Test Prüfmaschinen GmbH, s.d.), a qualitative scheme.

Table 2: Hardness Moh Scale (Emco-Test Prüfmaschinen GmbH, s.d.)

Mohs hardness	Type of mineral	Vickers hardness (HV)
1	Talcum	2HV
2	Gypsum	35HV
3	Calcite	100HV
4	Fluorspar	200HV
5	Apatite	540HV
6	Orthoclase	800HV
7	Quartz	1.100HV
8	Topaz	1.400HV
9	Corundum	2.000HV
10	Diamond	10.000HV



Hence, not relying in optical techniques represented a step forward to more accurate estimation, but just possible by the evolution of technology which allowed the improvement of equipment dedicated to the measurement of load and displacement in terms of precision and sensitivity (consider the last term as the quotient of the change in an indication of a measuring system and the corresponding change in a value of a quantity being measured (JCGM - BIPM, s.d.)).

However, this development was one of the multiple footsteps in the nanoindentation techniques, while IIT was progressing other approaches like the Work-of-Indentation and the Continuous Stiffness Measurement (CSM) also known as Sinus Mode Indentation were growing in parallel, always with the scope of defining a method to get more accurate results. Emphasizing how the methodologies are different among each other due to the different considerations applied, in one case it is used an approach of dissipation energy capacity (Work-of-Indentation) and the other one based on assumptions regarding the experimental process together with dynamic models (CSM). Although, the objective of listing variants of a specific test is to show how flexible the indentation technique is, and its capabilities as a non-destructive test.

For this reason, the objective of the author is reviewing dynamic indentation techniques, its application as a non-destructive method and discussing the effectiveness and limitation of dynamic indentation with particular attention to real cases present in manufacturing contexts. For this purpose, a set of activities were defined, the first describing analytical method for single loading-unloading indentation (Instrumented Indentation) as the base model for determining hardness and elastic modulus. The second activity is the description of Work-of-Indentation method and results, an approach that could be comprehended as a complement theory of IIT, following with CSM, an entirely well-defined method with different results in terms of properties estimated during and after the test. Consequently, it was performed a comparison among Work-of-Indentation technique, Sinus mode and single loading-unloading indentation with focus on the performance of these in testing properties of real parts.



THEORETICAL FRAMEWORK

The load-displacement sensing indentation techniques offer significant results at micro and nano scale length in the determination of mechanical properties, continuously measured during the entire indentation test, and frequently primally dependent of the penetration depth (in general measure from the tip of the punch). When we speak about the nanoindentation, it is crucial to keep in mind one of its first application.

Martens Hardness

In 1898, the person to whom this scale of measure for hardness owns its name, Martens A., developed a machine capable of measure force and displacement during an indentation test (Martens, 1898). Nowadays, the Martens hardness (HM) is a term currently implemented in the ISO Standards 14577 that is characterized by 3 aspects: hardness is interpreted as pressure by unit area, it depends primary on indentation depth (h); finally, this one considers the plastic and elastic response.

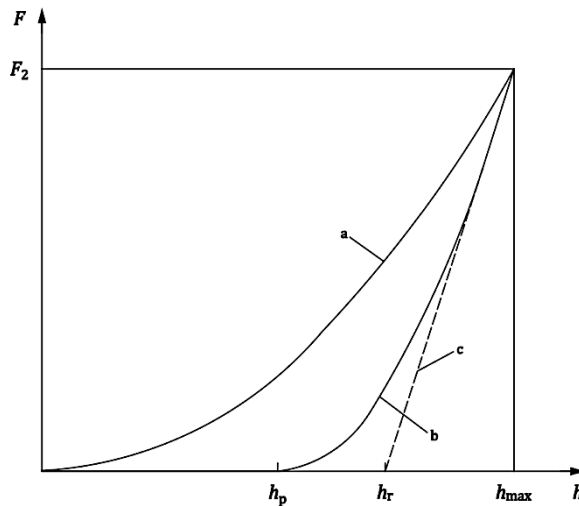


Figure 5: Schematic representation of the test procedure ISO 14577 (ISO Standard, 2016)

Regarding the last point, it is mentioned that Martens hardness involves plastic and elastic behavior because of how the author defines the equation to evaluate his scale (see Table 3); and a series of factors considered during the test, as described in ISO 14577, based on the loading-unloading path curve (see Figure 5) and the surface area of the indent definition $A_s(h)$. According to the model, in relation to the surface area, this one is not directly measured but estimated by a mathematical expression unique for the indenter



shape type and function of indentation depth considering an ideal shape of the punch; a decision motivated by the limitation of the equipment available at that time to determine the exact geometry of the indenters, that allowed to facilitate the estimation of the variable surface area but creating at the same time a limit in the scale length of the measure, as it is mentioned in the normative, in order to use model of ideal indenter is necessary to consider $h > 6\mu\text{m}$, i.e., microscale range because going to a smaller scale with this model is not possible due to the error/noise in the measure by the tip rounder factor (variable of influence explained in more detail in the next topics) as a consequence of the impossibility of produce a punch exactly as the one described in the mathematical model.

Table 3: Martens Hardness equations

Martens Hardness	Area Function	
	Vickers Indenter	Berkovich Indenter
$HM = \frac{P}{A_s(h)}$	$A_s(h) = \frac{4 \sin \alpha}{\cos^2 \alpha} h^2$	$A_s(h) = \frac{3\sqrt{3} \tan \alpha}{\cos \alpha} h^2$
α: cone semi angle in a Vickers or Berkovich indenter.		

However, the relevance of the Martens hardness is determined by 2 factors; the first one, about how the model considers the nature of the deformation in a loading-unloading indentation cycle for the material, it was assumed what later was known as an ideally plastic deformation, an aspect that other authors after Martens realized is crucial in the evaluation of the resistance of material because it determines the kind of model or implication necessary to keep in mind when we evaluate the mechanical properties of the sample. In fact, the necessity to include this phenomenon in the evaluation of hardness conducted to the characterization of deformation into ideally plastic, elastic/plastic and ideally elastic (see Figure 6)

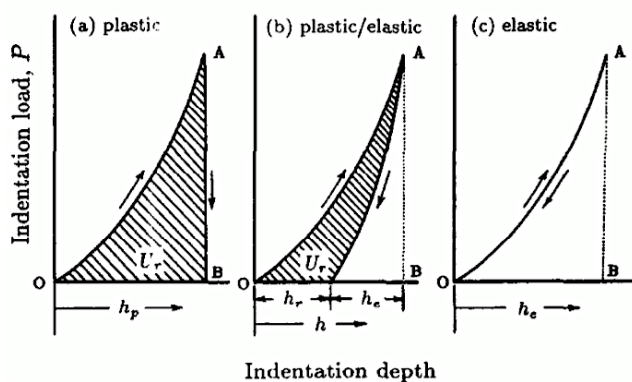


Figure 6: Deformation in the indentation loading unloading cycle (Sakai, 1993)



The second aspect of importance in the Martens model comes from the analysis in more detail of the surface area parameter. If we look the formulation of the area function, this one is primarily dependent of the indentation depth (h) because cone semi-angle (α) is constant, which means Martens hardness is measured continuously during the test resulting in an approach capable of give information layer after layer of material during a loading-unloading indentation cycle.

Considering the last point, it is necessary to mention that once the Martens hardness is estimated, it is important to proceed with the analysis of the value determined because it is important to clarify that Martens value applied for homogenous material which means if there is a significant change in the properties of the sample throughout the layers of the surface, the value obtained is unreliable. For the aim of the evaluation of material homogeneity and reliability of hardness value calculated with the equation on Table 3; it is implemented what is describe as Martens hardness from slope during loading (HM_s), which is based on a breakdown of the load-unload curves with particular emphasis in the range of 50% and 90% of peak load, summarize in the next:

Table 4: Martens hardness in terms of slope

Martens hardness - slope
$HM_s = \frac{1}{m_s^2 [A_s(h)/h^2]}$
Linear correlation h vs $F^{1/2}$
$h = m_s \sqrt{P}$

When the difference between HM and HM_s is relevant, then the values obtained are not in compliance with the model, specifically about the linear correlation for the loading portion of the curve present in Table 4 that is valid if $HM(h) = \text{const}$. However, it is good to mention that this linear correlation was evaluated by others years after, and one of those author to propose an alternative was Sneddon in his studies of elastic deformation of materials during contact of these; his result conducted to power law relationship between indentation depth and load (Harding & Sneddon, 1945) (Sneddon, 1965) which was highly accepted due to the fact is a more general approach for fitting the load – displacement data registered in the indentation test.



Although, Sneddon model represented an improvement in the nanoindentation field, this one has the same issue as Martens scheme. Both approaches refer to ideally cases of study, ideally elastic (Sneddon) and ideally plastic (Martens) deformation (see Figure 6), certainly these 2 events are feasible examples of deformation behavior of materials in real life but not necessarily the only conditions that could happen. It is due to this limitation where the instrumented indentation test comes into action.

Instrumented Indentation Test: Single Loading/Unloading Indentation Cycle

The starting point in the innovation of the Oliver and Pharr proposal born from the factors considered in the power law equation (Sneddon's Model) at that time used to describe the load-displacement curve during the loading phase in an indentation test as it is shown in Table 5 .

Table 5: Sneddon's Model vs Oliver and Pharr's Model

Sneddon's Model	Oliver and Pharr's Model
$P = \alpha h^m$	$P = \alpha(h - h_f)^m$
P: indenter load	
h: elastic displacement of indenter	
hf: final depth of the residual hardness impression	
α and m are constants determined by the least squares fitting procedure	

Both models are similar in the type of fitting function to describe the data acquired during the continuous measurement of load and displacement. In fact, Oliver and Pharr method is based on the Sneddon equation model (Harding & Sneddon, 1945) (Sneddon, 1965); the difference between the procedures is that Oliver and Pharr considered the most common case, elastic/plastic deformation, where the plastic behavior of the material is seen when the load is enough to create a non-reversible print in the sample during the indentation process at the same time an elastic recovery is observed during the test when the indenter is relief from the sample. To explore this, Oliver and Pharr analyze the unloading path in the indentation cycle instead of loading phase as shown in previous studies (Sneddon and Martens).

The reason behind of contemplating the plastic and elastic properties comes from the analysis of indentation performed in different materials, it was observed that in general after a plastic deformation the load and unload curve are not coincident, an example of this, it is the specific case of the electropolished single crystal of tungsten, in



two exact conditions. The first one, the sample is indented at low-rate increase of load with a peak of 0.5 mN, here it is noticed the unloading curve is practically the same as in the loading phase; a behavior expected because of the test conditions, the deformation suffered by the sample is entirely elastic. The second condition, the peak load is increased evidencing a jump in the displacement corresponding to the onset of plasticity and a permanent hardness impression is formed (see Figure 7).

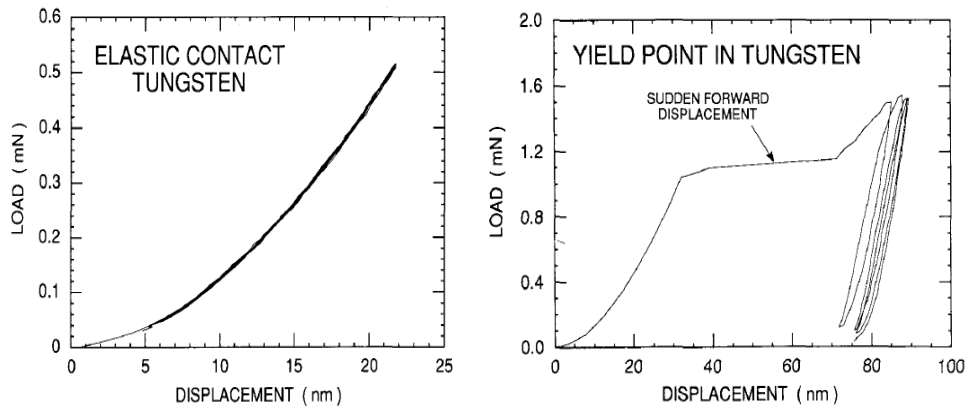


Figure 7: Load vs indenter displacement for a fully elastic contact (left) and for a plastic contact on an electropolished single crystal of tungsten (Oliver & Pharr, 1992)

The sudden forward displacement during the loading phase is a special behavior inherent to the electropolished single crystal of tungsten. In general, the curves obtained at the end of an indentation test are like Figure 8 and these can discriminate plastic and elastic energy during deformation as Oliver and Pharr implemented in their theory for instrumented indentation test.

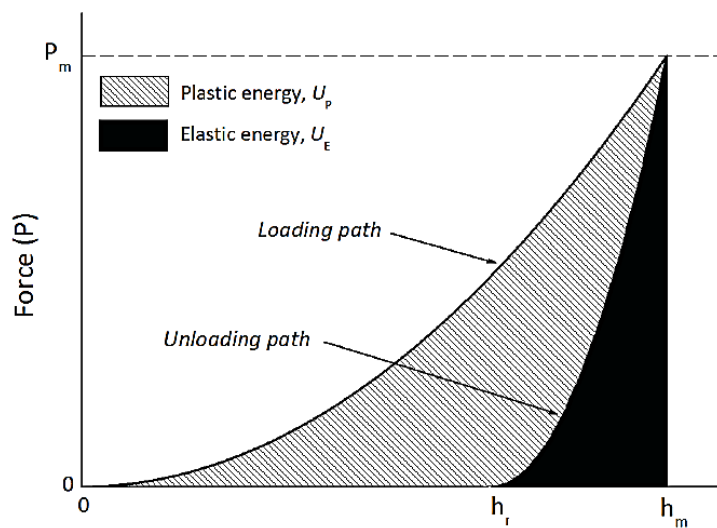
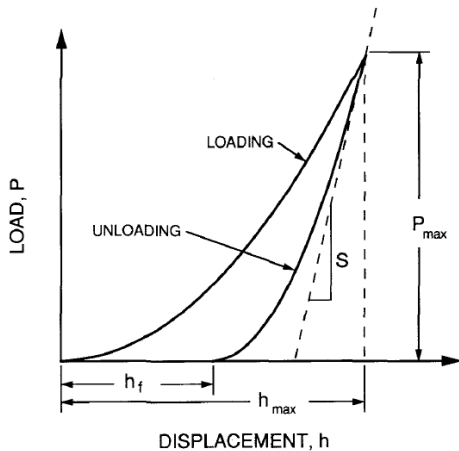


Figure 8: Indenter displacement (Michel Yetna, Idriss, Olivier, & Didier, 2016)



To consider the plastic behavior in the Sneddon's formulation to evaluate hardness after a plastic deformation, a change in the power law equation needed to be done. The result was an expression not fully dependent of the absolute displacement h , a different variable entered in the analysis, the final depth of the residual hardness impression was defined (see Figure 9) and the study is performed using a relative quantity $(h - h_f)$, due to the partially recovery to the initial state of the deformed sample because of the elastic forces.



The quantities shown are

P_{\max} : the peak indentation load; h_{\max} : the indenter displacement at peak load; h_f : the final depth of the contact impression after unloading and S : initial unloading stiffness

Figure 9: Schematic representation of load versus indenter displacement data for an indentation experiment (Oliver & Pharr, 1992).

Now, the problem is to establish the impact of using the unloading load and displacement data to determine hardness, where Oliver and Pharr used a different definition compared to the given by Martens (see Table 6) instead of the surface area, what they proposed is to use the projected area (A_p) in this way the description of hardness became the one defined by Meyer. The major difference between both definitions resides on what Sakai (Sakai, 1999) explained as the compensation of the horizontal component of the indentation load due to the axial symmetry of the indenter used when the surface area is the one to refer when calculating hardness (see Figure 10). The reference to Meyer hardness implied to do a full analysis of the resistance to penetration of the material connected to variables like plastic flow stress (yield stress), Young's modulus, ultimate strength... Although, with the objective of using the projected area to define hardness, it was needed to perform a further description in more detail of a cross section during an indentation test and consequently other variables were identified during three specific conditions, initial surface non deformed, the surface profile under load and the surface profile after the load removal (see Figure 11)

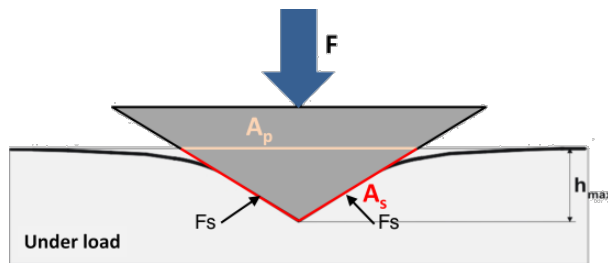


Figure 10: Force reaction (F_s) when load is applied during the indentation.

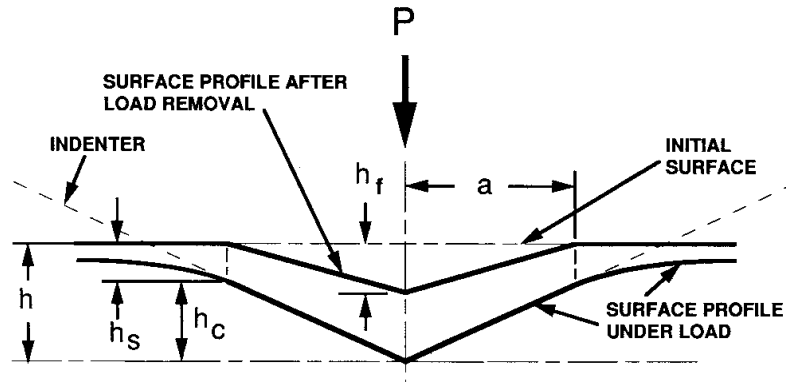


Figure 11: Schematic representation of a section through an indentation (Oliver & Pharr, 2004)

Now, once these specific moments during the trial are identified from the data, other considerations get into action too, and these have to do with the surface area. Oliver and Pharr established that the indenter surface does not touch entirely the sample, a portion of the component is deformed due to issues like sinking in and piling up. Therefore, to respect Meyer definition of hardness (mean pressure under area) for the IIT test is used what is known as contact depth (h_c), a parameter that allows to determine the indenter surface (evaluated as a projected area A_p) in real contact with the sample when a force is applied.

Table 6: IIT hardness and parameters.

IIT Hardness	Contact Area
$H_{IIT} = \frac{P_{max}}{A_p}$	$A_p = F(h_c)$

Therefore, Oliver and Pharr method add in the scene a set of new parameters to consider, but how these ones are determined is part of the approach itself. Some of them are directly measured during the test, as for example h_f , still there are others where it is necessary to establish models or equations to deal with.



Power law equation – Unloading Phase

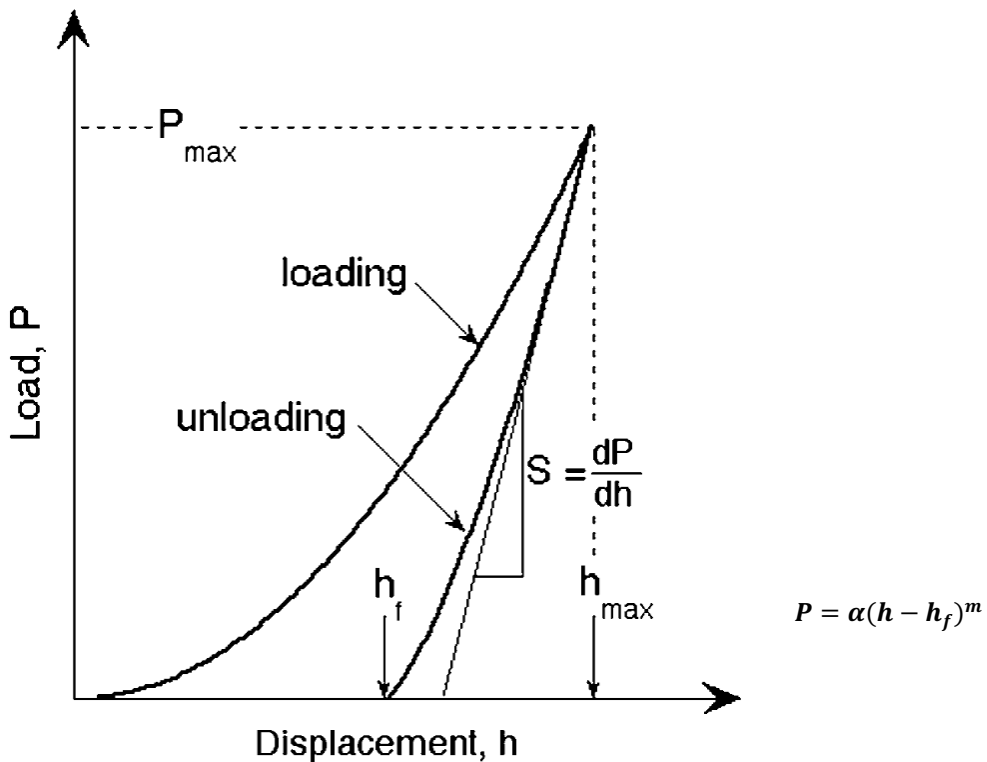


Figure 12: Power law equation for the unloading phase in the indentation cycle (Oliver & Pharr, 2004)

As per Sneddon model, the IIT method approximate the load – displacement data into a power law equation, dependent of some parameters obtained from the data. However, in relation to α and m , these are determined by a least squared procedure applied to the data which represent a further step in the technique because from Sneddon model, these variables were constants connected to the indenter geometry as a prove of these, we find in the literature tables describing for each punch (see Table 7).

Although further research showed that certainly there is a dependency of the indenter geometry, the material sample contributes too to the values of the power law equation. As a matter of fact, Oliver and Pharr in their publications gave evidence of this (see Table 8) showing that in general there is a variation of the power law exponent, approximately in a range between 1.2 and 1.6, proving that the assumptions previously done in the models to describe the indentation cycle load – displacement data were not accurate.

Table 7: Sneddon model values of m previous the IIT theory

Indenter Geometry	m
Flat cylinders	1
Cones	2
Spheres (small displacements)	1.5
Paraboloids of revolution	1.5

Table 8: Parameters characterizing unloading curves with Berkovich indenter (Oliver & Pharr, 1992)

Material	α (mN/nm ^m)	m	Correlation coefficient R
Aluminum	0.265	1.38	0.999938
Soda-lime glass	0.0279	1.37	0.999997
Sapphire	0.0435	1.47	0.999998
Fused silica	0.05	1.25	0.999997
Tungsten	0.141	1.51	0.999986
Silica	0.0215	1.43	0.99985

Once, we have available all parameters of the power law equation for the unloading curve, the next move is to start with getting other info from the curves (see Figure 12), in this case the first value of interest is the elastic unloading stiffness also known as contact stiffness (S).

Contact Stiffness (S)

It is one of the important quantities that must be measured from the data obtained during the indentation cycle, known as unloading stiffness also called contact stiffness, defined as the slope of the upper portion of the uploading curve during the initial stage of unloading (Oliver & Pharr, 2004). From the previous definition, then S could be represented as the derivate of load (P) and displacement (h), where again Sneddon provided an expression to evaluate this quantity (see Table 9) considering at the same time the deformation itself of the indenter using the approach of Stillwell and Tabor concerning the Young modulus (E) (Stillwell & Tabor, 1961).



Table 9: Contact Stiffness expression based on Sneddon model

Flat cylindrical punch - Sneddon	First S expression	Stillwell and Tabor consideration
$P = \frac{4\mu a}{1-v} h$	$S = \frac{dP}{dh} = \frac{2}{\sqrt{\pi}} \sqrt{A_p} \frac{E}{(1-v^2)}$	$\frac{1}{E_r} = \frac{(1-v^2)}{E} + \frac{(1-v_i^2)}{E_i}$
S for Flat cylindrical indenter		
$S = \frac{dP}{dh} = \frac{2}{\sqrt{\pi}} \sqrt{A_p} E_r$		

Where (a) is the radius of a cylinder used to define the projected area (A_p) as πa^2 , μ is the shear modulus and v is Poisson's ratio (always keeping present that $E=2\mu(1+v)$). In addition, it was stated other variables like Reduced Young modulus (E_r) to add in the expression the contribution of the indenter into the total deformation measured, but just in case of finite elastic constants (refer to the subindex "i" in the expressions).

In the same order of ideas, other expressions of S were identified depending on the geometry of the indenter. Although, it was later proved that with the purpose of evaluating S in the upper portion of the unloading curve, the flat cylindrical indenter expression was still accurate, as it was demonstrated by Oliver and Pharr (Oliver & Pharr, 1992) where they analyzed an general cylindrical indenter geometry and verified the same expressions of Table 9. Then, with the aim of evaluating other cases, it was checked that other authors went into more detail in the study of geometry that cannot be described as bodies of revolution like Berkovich and Vickers indenters after the work of Sneddon; in this case by (King, 1987), who developed an expression where results showed that the stiffness is almost independent of the geometry chosen for the indenter (see Table 10), these outcomes are consequence of the observation of the correcting factor (β) applied to the Sneddon equation to introduce the effect of geometry of the indenter in the determination of the contact stiffness.



Table 10: Correcting factor (β) in the evaluation of punch geometry in the contact stiffness

Contact Stiffness	β (in terms of cross section of the indenter)
$S = \frac{dP}{dh} = \beta \frac{2}{\sqrt{\pi}} \sqrt{A_p} E_r$	Circle section, $\beta=1.000$
	Square section, $\beta=1.034$
	Triangle section, $\beta=1.012$

At this point, it seems that estimate the contact stiffness could be feasible in a deterministic approach. However, this is far away of the objective because the huge problem of equations presented in Table 9 and Table 10 E_r due to the fact in a major part of the cases, it is unknown the Young modulus (E) of the material to test. Therefore, the Sneddon equations are more practical to estimate E_r when the projected area (A_p) and the contact stiffness (S) are available. Still, both quantities are sources of errors since the area is calculated using a mathematical model that need to be corrected (primarily due to the impossibility to produce an indenter exactly as the ideal one) which at the same time depends on unloading stiffness by the contact depth (h_c) explained in the dedicated section of this text.

Then we have the S value, that with the purpose of determining this, we can be tented to use derivate the power law equation described above. But, it is important to mention that the least square method used to get the relation $P-h$ guarantees the approximation of the data and not the accuracy of the derivative (due to non-linearity in the data fitted) giving as result the necessity of evaluating this parameter in other ways; at first with a graph method and then with evolution of the methods through numerical approaches which use the data itself to estimate the derivative as analyzed by (Maculotti, et al., 2019) where it was proposed alternatives to evaluate the contact stiffness in the nano-range during an instrumented indentation test.

As last point to treat in this section, it is good to mention how the contact stiffness is a parameter that can identified the presence of creep during the indentation cycle. This observation born from the analysis of load-unloading curves in indentation test in polymeric sample where the creep condition is way larger than, i.e., metallic components, resulting in a negative slope in the unloading curve having as a result the invalidity of the



models until now described, pointing how critical is to reduce the creep behavior during the indentation test (considerations of how the creep can be reduced during ITT are later explained).

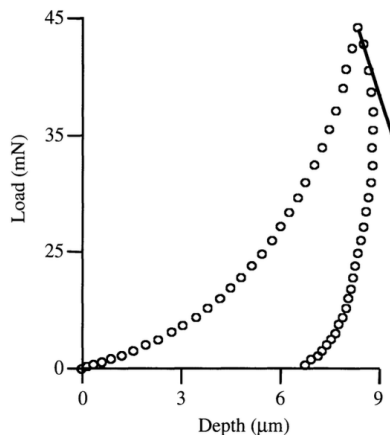


Figure 13: Conventional load-displacement curve resulting from indentation of a polymer (Fischer-Cripps, 2002)

Berkovitch Indenter – Area function (A)

In the scenario of using IIT to evaluate mechanical properties of the materials, one of the most common indenters used is the Berkovitch indenter, especially when the measurement needs to be carried out in the nanoscale range. A full description of the Berkovitch indenter is available in the appendix of this text.

The critical aspect of Berkovitch indenter is how this affects the general mathematical expression for A (Oliver & Pharr, 2004) (see Table 11). Although, due to the complexity of the equation in major part of the cases it is used the first term and utterly to consider other effects that conduct to a variation from the ideal indenter area, assumptions on the contact depth estimation.

Table 11: General expression A_p

$$\begin{aligned} A &= \sum_{n=0}^8 C_n (h_c)^{2-n} \\ &= C_0 h^2 + C_1 h + C_2 h^{1/2} + C_3 h^{1/4} + \dots + C_8 h^{1/128} \end{aligned}$$

Where $C_0 h^2$ represents the ideal indenter, the other members of the expression are the non-ideality in the punch due to several factors (manufacturing process, pile-up and sinking in effects, ...). For Berkovitch indenter, $C_0=24.56$ when $A=A_c$



Contact Depth (h_c) – Sinking in and Piling up considerations

It is the distance from the tip of the indenter that identified the portion of the indenter in real contact with the sample. The characterization of this parameter born from the need to uncoupling phenomenon like pile-up and sinking, graphically the contact area is positioned as shown in Figure 14.

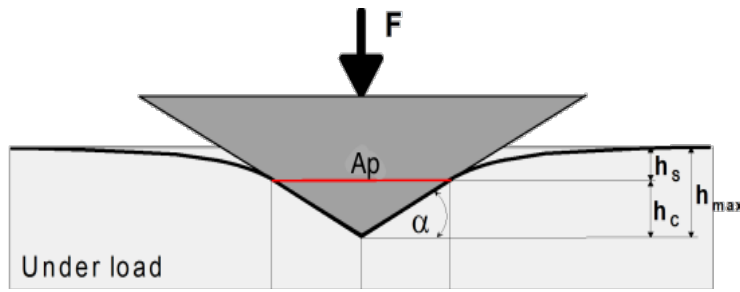


Figure 14: Contact depth and projected area $A_p(h_c)$ (ASMEC GmbH, s.d.)

From the figure about, we can observe a relation among h_c , h_s (sinking in depth) and maximum depth (h_{max}). It is at this point where the contact depth becomes a source of error in the estimation of hardness, because of how h_s is determined, a factor that is function of the contact stiffness (S) as described in the next.

Table 12: Contact depth and sinking in depth expressions.

$h_c = h_{max} - h_s$	$h_s = \epsilon \frac{P_{max}}{S}$
-----------------------	------------------------------------

In the equations above, the parameter ϵ is a constant that considers the punch geometry in the approximation of the sinking in depth. It is the Sneddon method that allows the determining of this constant, graphically represented in Figure 15 as function of the power law exponent. Notice the range of variation of ϵ within the application of Oliver and Pharr model that describes the unloading curve, even thought to not add further numerical error in the model, it is chosen to use $\epsilon=0.75$.

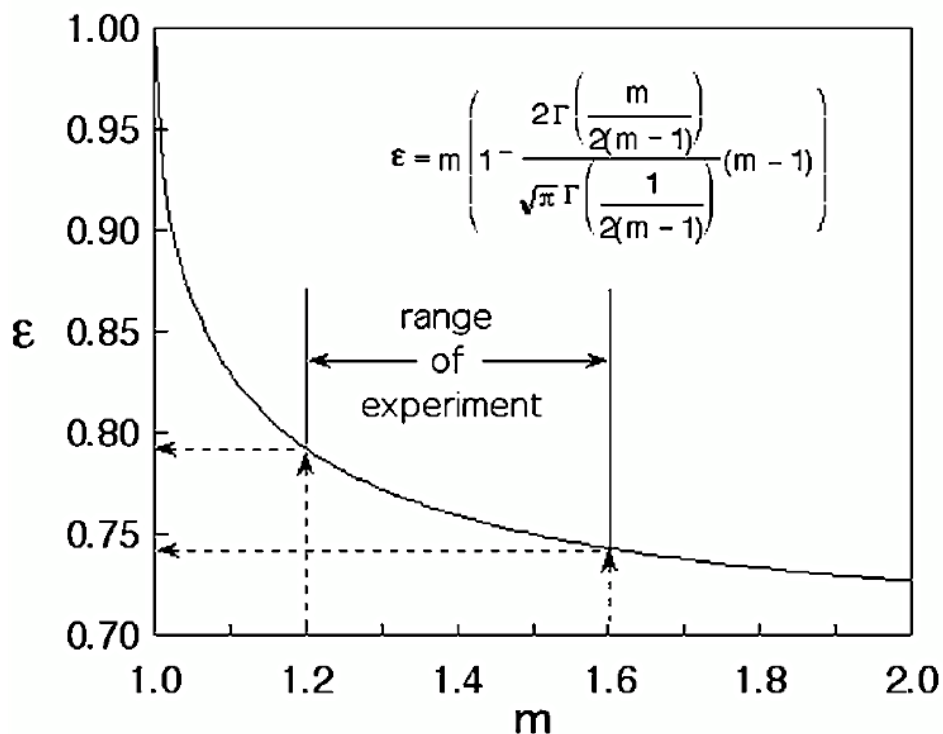


Figure 15: Relation between ϵ and m (Pharr & Bolshakov, 2002)

Still, it is important to make notice that these equations consider negligible the pile-up, due to the complexity to involve this phenomenon not feasible to quantify from a geometrical point of view; in this way this description of the contact depth introduced a constraint on the type of deformation where to guarantee the non-presence of pile-up. With the aim of considering pile-up, a different approach needs to be carried out in the contact depth estimation; the one to implement is the present in Table 13; a proposal done by (Loubet, Bauer, Tonck, Bec, & Gauthier-Manuel, 1993) and complement with a further range of application given by (Yenat, Chicot, Ndjaka, Lesage, & Decoopman, 2015)

Table 13: Contact depth considering pile-up effect.

$$h_c = 1.2 \left(h_{max} - \frac{P_{max}}{S} \right); \quad \frac{h_f}{h_{max}} > 0.83$$

As defined by (Yenat, Chicot, Ndjaka, Lesage, & Decoopman, 2015), “For materials for which this ratio is higher than 0.83 piling-up prevails while it is sinking-in when it is lower than 0.83. When the ratio equals 0.83, the two modes of deformation should coexist since the calculations made using either correction of Oliver and Pharr or Loubet et al. give the same results.”



Factors Affecting IIT Test Data

Several factors can affect the measurement during an instrumented indentation test, the most crucial errors are related to the offset in the measure, specially, at nanoscale scale length. These sources of error, in general, are connected to environmental factors, precision of the instrument, indenter shape and material properties. Consider the sensitivity of the dynamic indentation methods to these fonts of uncertainty is crucial to obtain real approximations of the mechanical behavior of the samples.

Thermal Drift

This is the first factor involved connected to the temperature. The effects of this for a nanoindentation are basically two; slow deformation under constant load, or creep (Kutz, 2006), and the expansion or contraction of the equipment which conduct to apparent displacement of the indenter.

However, depending on how relevant the thermal drift is, there are different decisions to make with the scope of evaluating properly the effect of temperature. These are linked to conditions whether the elastic limit is exceeded or the presence of vibrations during the test (see Figure 16). In practice, the hold period is applied in the unloading phase in case the creep (recovery) is less probably to occur. Meanwhile, in the opposite when creep is relevant the hold period is advised to be applied at maximum load (Fischer-Cripps, 2002).

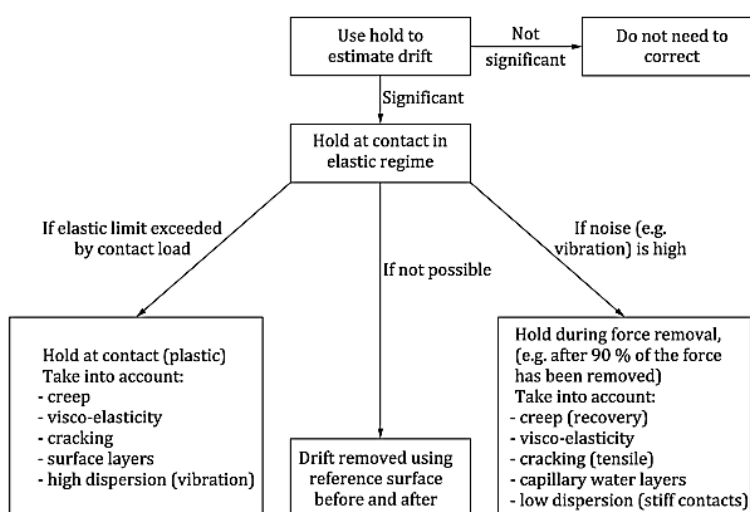
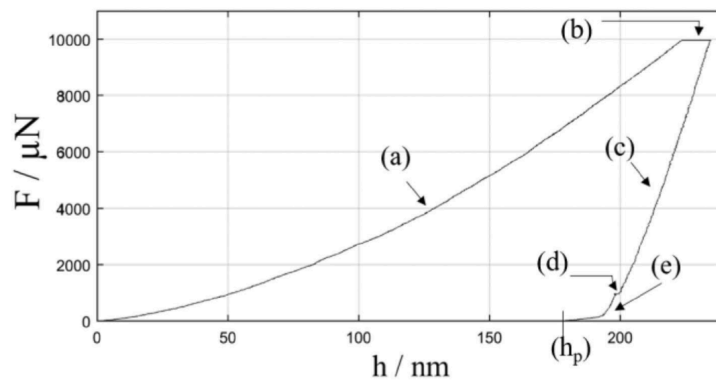


Figure 16: Decision tree to assist in estimating thermal drift using a constant force hold period (ISO Standard, 2016)



The scheme above in real test conditions gives as result what Maculotti obtained in his research in the nano-range of the contact stiffness which is summarized into the load-displacement data present in Figure 17 where there specific point/zones of interest that expressed what the decision tree implied: (a) loading curve, (b) holding at maximum load necessary for creep compensation, (c) unloading curve, (d) non-standard holding at 10% of maximum load to compensate for thermal drift (expansion/contraction of the equipment), (e) final unloading and the residual indentation h_f/h_p .



*Figure 17: Example of indentation curve obtain after thermal drift consideration
(Maculotti, et al., 2019)*

Initial Penetration Depth

Other factor of correction during the post-processing of the data after the indentation is the Initial Penetration Depth, ideally, the penetration depth is measured from the level of the specimen free surface. But, in practice it happens the opposite, the instrument needs to get in contact with the sample to generate a datum where the subsequence measurements are based. This generates an error in the values of depths which is necessary to correct.

Error correction involves specifying what values are necessary to exclude in the initial phase of the test, initial contact depth is usually made to be as small as possible and is often set using the smallest obtainable force of the instrument (Fischer-Cripps, 2002). Graphically, the correction implies to add a quantity h_i to all the measurements of displacement (see Figure 12).

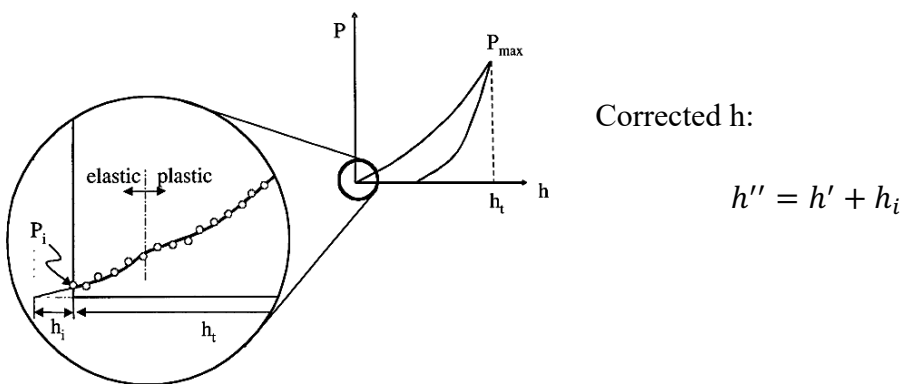


Figure 18: Schematic of the effect of initial penetration depth on load-depth data for a depth-sensing indentation test. Depth readings must be corrected for h_i (Fischer-Cripps, 2002).

Instrument Compliance (C_f)

An interest factor that in some cases can compensate the initial penetration depth is the deflection of the instrument (see Figure 19), commonly known as the instrument compliance. This is an intrinsic parameter impossible to avoid, that is measurable in terms of the stiffness which does not only depend on the instrument; there is an effect of the sample in the degree of deflection suffered by the instrument. Due to the nature of the deformation of the test rig, this issue is not constant over the range in an indentation process, it has been identified a correlation between the load applied into the sample and the deflection; this relationship involves valuing the rigidity of the bench + sample and a correction of the depth measured.

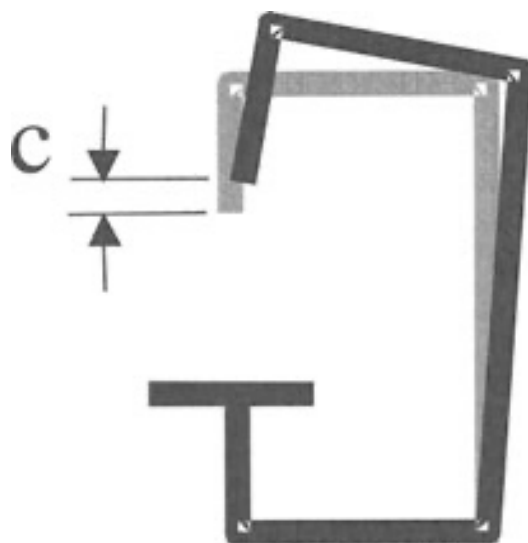


Figure 19: Schematic deflection of the test machine by effect of the load application during an indentation test (Fischer-Cripps, 2002)



About the first item, the rigidity, it is important to mention it is an estimation possible to do with the data obtain during the trial. Even though, it is advised to complement the analysis of this characteristic verifying the calibration of the test rig using a reference material. Then, depending on the case (what input parameters we have available) different methods can be used all of them part from the equations in Table 14 where it is described a total compliance at maximum force during the load removal (C) resulting from a linear combination of the reciprocal slope of the unloading curve ($1/S$) and the instrument compliance (C_f). The assumption done in this expression is that C_f is independent of the material properties of the sample tested.

Table 14: Instrument compliance

$$C = \frac{dh}{dP} = \frac{1}{S} + C_f \quad S = \frac{dP}{dh} = \frac{2}{\sqrt{\pi}} \sqrt{A_p E_r}$$

Applied to Berkovich indenter, in terms of the projected area

$$C = \sqrt{\frac{\pi}{24.56}} \left(\frac{1}{2E_r} \right) \frac{1}{h_p} + C_f$$

The procedure to determine the compliance can be summarized into the methods described in the ISO 14557-2, where the assumption presented is that Young's modulus and Poisson's ratio are independent of the indentation depth, considering this and the data in Table 14; the normative identified five scenarios where the most common one in real test conditions is related to method 2 (refer to the appendix section: instrument compliance), area function and reduced elastic modulus are unknown (see Table 15), using this approach we plot the curve C vs $(1/h_p)$ (Berkovich indenter) where the values of total compliance are estimated from test data in the unloading phase (see Figure 20).

Table 15: ISO 14557-2 Assumptions compliance determination methods (ISO Standard, 2016)

Method	$E_r = \text{const}$	$C_f = \text{const}$	Parameter input
1	yes	yes	$A_p(h_c)$
2	yes	yes	None
3	yes	no	$A_p(h_c), E_r$
4	yes	no	E_{r1}, E_{r2}
5	yes	no	$E_{r1}, E_{r2}, \text{elastic deformation}$

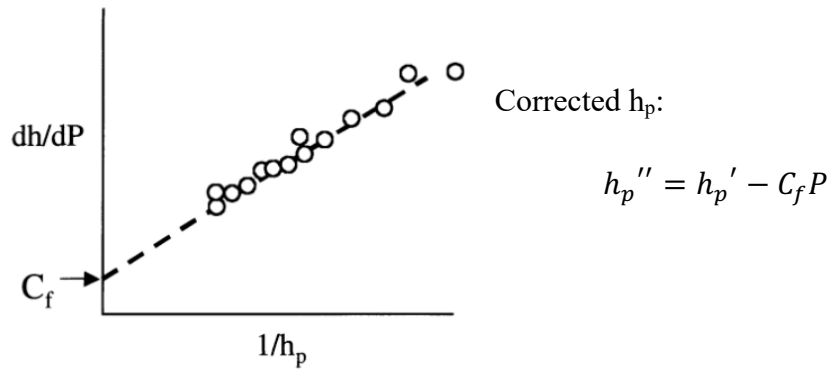


Figure 20: Schematic of dh/dP vs h_p^{-1} (for Berkovitch indenter)

Indenter Geometry

In addition to the previous factors, the next one continues with the introduction of non-ideality in the model of dynamic indentation, this element is the **Indenter Geometry**. The reason behind the influence of the geometry of the punch has to do with the fact the area during the trial is estimate from the measurement of depth. Thus, the print area is not obtained during the test, it is an indirect result connected to a correlation define by the mathematical model. In general, it is given a curved which links the real area (A), the ideal area (A_i) and the penetration depth (see Figure 21); the root cause of the asymptotic behavior at small length comes from the limitation of manufacturing processes to obtain an indenter exactly as the ideal one having consequently at small h_p the area ratio is significantly high i.e., the order of 10:1.

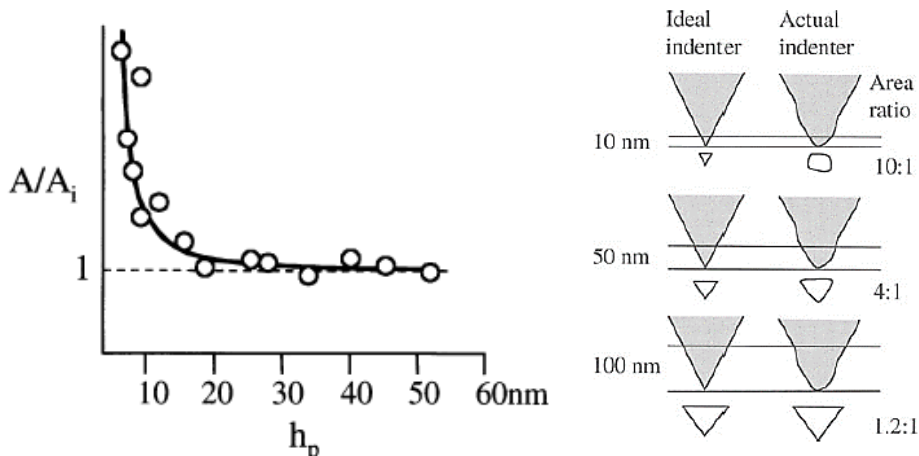


Figure 21: Area correction function for a typical Berkovitch indenter (Fischer-Cripps, 2002)



Tip Rounding

The impossibility to create an indenter geometrically exact as per mathematical model as discussed in the indentation geometry factor, furtherly conducts to the presence of other issue regarding the contact area between the indenter and the sample. In general, during the deformation, the cavity of the print under load is not fully in contact with the punch, even though this one deforms during the indentation cycle which allows the production of a hollow just about the indenter rounded tip characterized by the parameter h_b (see Figure 22) according to the work done by Chicot (Chicot, et al., 2015).

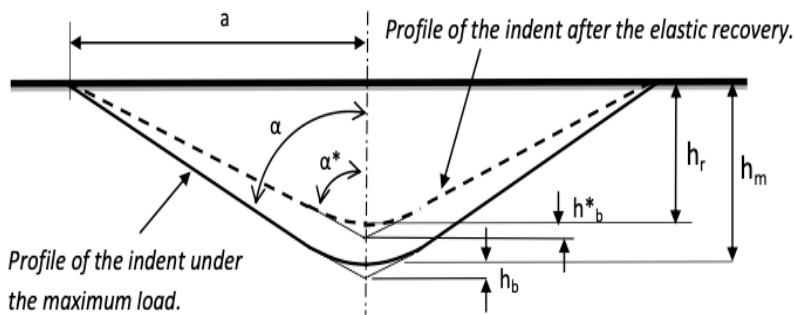


Figure 22: Cross-section of a conical impression and representation of the impression profile after the withdrawal of the indenter and the elastic recovery at the bottom of the indenter represented by the dotted line (Chicot, et al., 2015)

There is not any mathematical model that can quantify the value of h_b , especially because of the aging (usury) suffered by the indenter in its life service. Therefore, the strategy adopted in relation this factor has to do with when this needs to be considered and how we can measure it; in this way the results pointed to a definition of a criteria where the tip rounding effect is necessary to be considered when the minimum indentation depth h is on nanoscale range (refer to Table 1), in other words when $h > 0.2\mu\text{m}$, h_b can be neglected.

Instead, when the indentation test includes the analysis of indentation depth at nanoscale level, the most common approach (not related to a numerical convergence of area function as describe in ISO 14577-2) is to complement the indentation techniques with microscope ones where we find the Scanning Electronic Microscope (SEM), an example of the use of this equipment in indentation was performed by Chicot (Chicot, et al., 2013) where it was studied the effect of the tip defect at the same time making



emphasis in how the dimension h_b can be significant large in comparison with minimum indentation depth when the indenter has had some hours in service. The results for tip defect are shown in Figure 23.

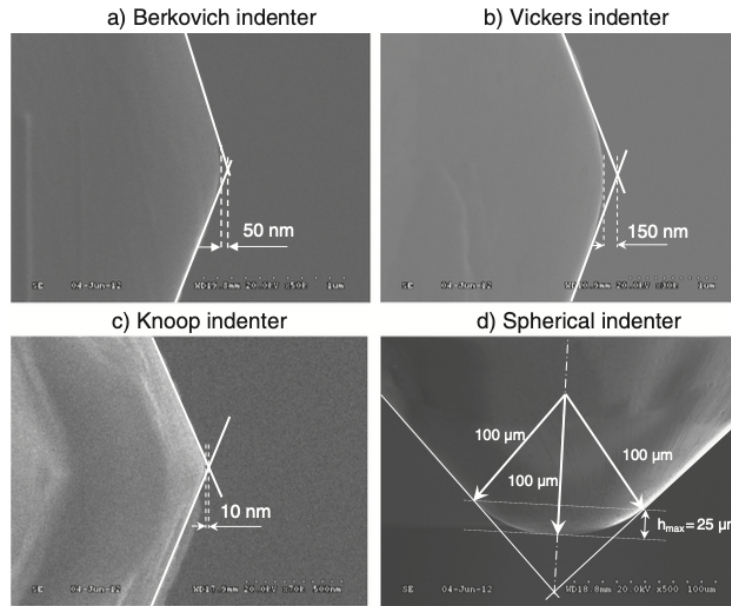


Figure 23: Evaluation of the size of the tip defect for the a) Berkovich, b) Vickers, c) Knoop and d) Spherical indenters by mean of emission field SEM analysis at different magnifications (Chicot, et al., 2013)

In the same order of ideas, the next step after determining tip rounding defect is how to include this factor into the model, for this purpose it is used the truncated cone model (see Figure 24) to describe the cavity of the print under load, this is a methodology applied in diverse studies (Tan, 2006), (Malzbender, De With, & Den Toonder, 2000), (Chicot, et al., 2015)) where a volume is added into the equation resulting in an expression of $A \sim (h+h_b)$, at this point the length h_b takes the definition of the truncated indenter tip.

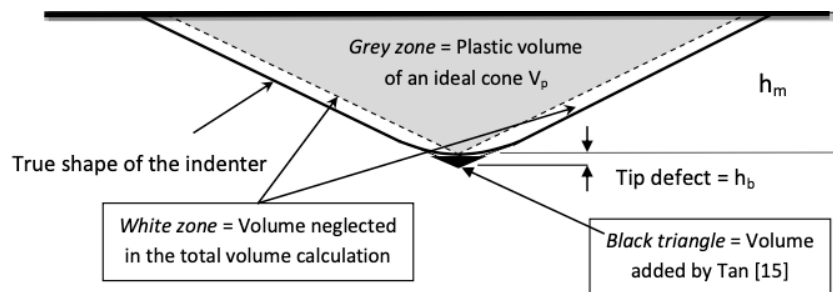


Figure 24: Cross-section of a conical impression and representation of the tip defect through the truncated length at the indenter tip (Chicot, et al., 2015)



Hence, the truncated cone model has given interesting results in the determination of the instrument compliance, where the assumption of linearity (see Table 14) at nanoscale level was having troubles, making it not valid if the tip defect is not taken account. As it was observed in the studied done by (Chicot, et al., 2013) (see Figure 25)

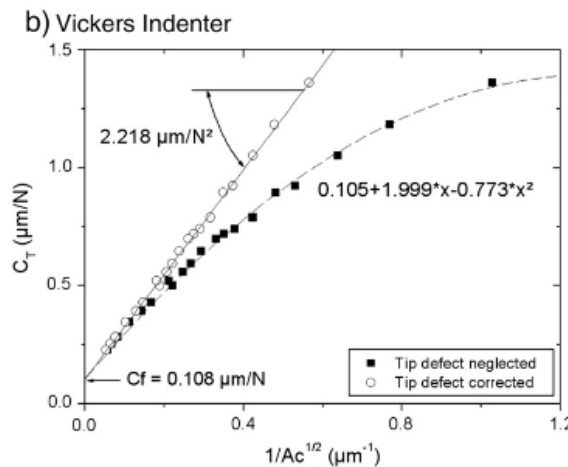
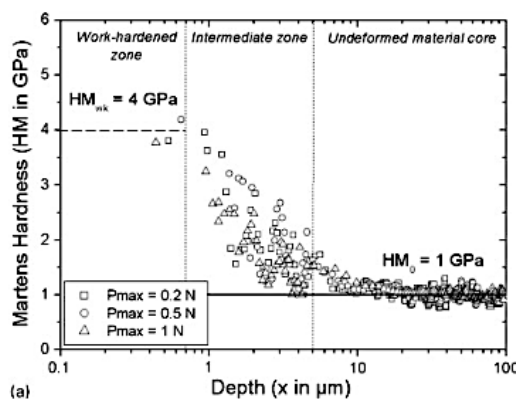


Figure 25: Contact stiffness as a function of the inverse of the square root of the contact area for a Vickers indenter (Chicot, et al., 2013)

Indentation Size Effect (ISE)

Another important variable to consider is **Indentation Size Effect (ISE)** which can be translated into the impact of indenter displacement (deep scale) has under the hardness and elastic module measurement because even when the material could be an isotropic one, the properties of the surface and core can differ between each other due to several cause, among them: presence of very thin oxide films of substantially different mechanical properties than the bulk material, or the presence of residual stresses and strain-hardening arising from the specimen preparation and polishing procedure (Fischer-Cripps, 2002).



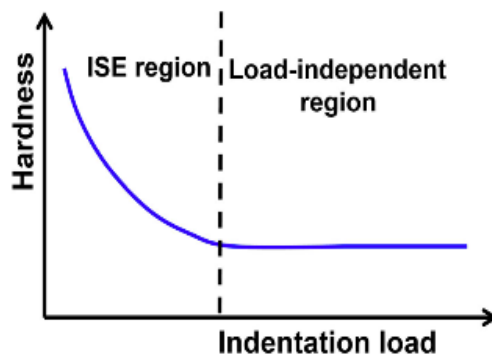


Figure 26: Hardness vs indentation depth with particular attention to ISE [experimental data by (Chicot, et al., 2013)]

The ISE can be identified graphically by plotting H vs h with the scope of identifying diverse zones of interest: work-hardened zone, intermediate zone, and undeformed material core (Chicot, et al., 2013). Each region is characterized by the way the outer layer and the core interact between each other, and the indentation response of the material (see Figure 26) where it is possible to afterward describe 2 macro-regions; one where the ISE effect is relevant, and the other which is independent of the load.

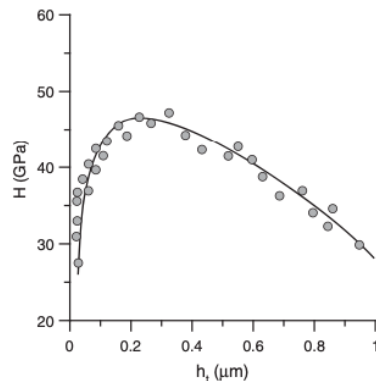


Figure 27: Measured hardness of a super-hard nano-composite nc-TiN/a-BN film (5 μm thick) on a steel substrate. Three regimes, initial rise, plateau and fall-off can be identified (Fischer-Cripps, 2006)

Although, it is important to refer always to the general behavior appreciated in Figure 26 (right). Because when indentations are performed and then plotted H vs h , it is possible to encounter correlation as described by Fischer (Fischer-Cripps, 2006) where there is an initial rise in the hardness at low penetration depths (see Figure 27) which is not consequence of the indentation size effect, instead the correct interpretation is correlated to indentation material response because at low scale (in particular in the nano range) the capability of an indentation cycle to generate a plastic deformation in the



material is highly influence by the tip round effect. Therefore, whether the indenter is sharp enough or not, it is the crucial factor, meaning that blunt indenters are highly probably sources of elastic deformation due to the fact the mean contact pressure (p_m) or hardness value (when a plastic deformation is done) based on Martens or Meyer definition does not overcome the minimum value needed to create a plastic deformation in the material according to Fischer (Fischer-Cripps, 2002) and summarized in Table 16.

Table 16: Indentation response of material based on yield stress and mean pressure contact (Fischer-Cripps, 2002)

$p_m < 1.1Y$	Full elastic response, no permanent or residual impression left in the test specimen after removal of load.
$1.1 < p_m < CY$	Plastic deformation exists beneath the surface but is constrained by the surrounding elastic material, where C is a constant, whose value depends on the material and the indenter geometry.
$P_m = CY$	Plastic region extends to the surface of the specimen and continues to grow such that the indentation contact area increases at a rate that gives little or no increase in the mean contact pressure for further increases in indenter load.

As final remark on this topic, it is important to mention the ISE factor is an aspect to keep under observation when it is necessary to characterize a material, becoming crucial to learn how to recognize it and where is not present (see appendix: Fused Silica-ISE as a material which does not describe this phenomenon). Still, even if it looks like an issue when determining the mechanical properties of a sample; this behavior opened the possibility of further studies in thin films coating where precisely the interaction between the core (substrate) and the film assume a form like the indentation size effect observed in macro homogeneous components, conducting to one of the applications of instrumented indentation techniques; characterization of multilayer component material.

Pile up and Sinking in

During the treatment of the contact depth and area function, the effect of piling-up and sinking-in was considered, but not formally explained in terms of which properties of the material influence the presence of this effect and why these are source of error (overestimation or sub-estimation) of the surface contact between the indenter and the



material. From previous studies it has been observed a certain proportionality between piling-up and sinking-in with the ratio E/Y, where E stands for Young modulus and Y for yield stress.

Table 17: Type of deformation in terms of the ratio E/Y

$\sigma = E\epsilon$	$\epsilon \leq Y/E$ Elastic deformation
$\sigma = K\epsilon^n$	$\epsilon \geq Y/E$ Elastoplastic deformation

In general, it has been identified that for materials with large value of E/Y the piling up is more likely to occur. In the opposite direction, it is noticed that sinking-in is the most predominant effect. However, this is not the only discriminant in the evaluation of these effects, in the analysis need to be studied too the strain hardening exponent (n); where in presence of materials with $n > 0$, the possibility of a predominant sinking-in effect is highly suitable.

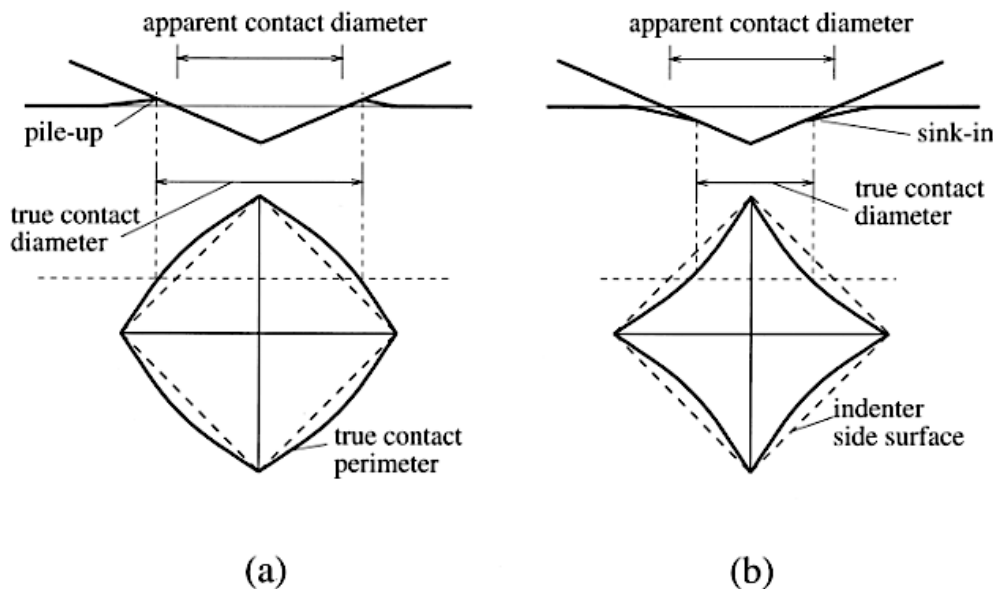


Figure 28: Schematic illustrations of (a) pile-up and (b) sink-in around a sharp indenter (Giannakopoulos & Suresh, 1999)

Although, the determination of E/Y and n, nowadays, is not enough to evaluate the presence of piling-up and sinking-in which has conducted to the application of other techniques like the energetic approach (Work of Indentation – see appendix) and finite element methods (FEM). Where the most used criteria, the energetic one has derived the expressions discussed in the contact depth theory.



CONTINUOUS MEASUREMENT OF STIFFNESS (CSM)

Load – displacement sensing techniques has become a suitable alternative to characterize mechanical properties of materials, for this reason the need to implement strategies that allow to overcome the limitations of these in the analysis for a wide range of materials and the precision of the measurements obtained. In relation to the limitations, we have verified how instrumented indentation technique as Oliver and Pharr described (Oliver & Pharr, On the generality of the relationship among contact stiffness, contact area, and elastic modulus during indentation, 1992) is restricted to non-viscoelastic materials which nowadays they represent an important slice in the material industry with particular interest in their capacity to absorb vibrations and/or impact; but due to the particular nature of their mechanical properties (difficult to describe in terms of easy equations/relationships because of the non-linearity of the model to define them), it is needed to apply empirical methods and simplification to get a better understanding of this singular materials.

In the same other of ideas, precision and resolution in the data driven from the test need in a major part of the case, be continuous over a range, and IIT for sure it was a great and it is still a method applicable in these days. However, in the indentation area, approaches that allow to get a continuous characterization of the sample over the indentation depth length are more and more wanted, especially in thin films application where in an indentation cycle is suitable to pass from film to substrate (bulk material) with not clear knowledge of at what indentation depth occurred. Therefore, how it can be measure continuously with depth all the properties previously discussed, at the same time we increase the possibilities of materials to study, e.g., viscoelastic materials. For this scope, we can find the Continuous Stiffness Measurement developed by Oliver and Pethica (United States of America Brevetto n. 4,848,141, 1989) which consist in the application of an AC oscillatory force (at known frequency) during the contact of two bodies (indenter and sample) and measuring the subsequent oscillatory displacement (see Figure 29).

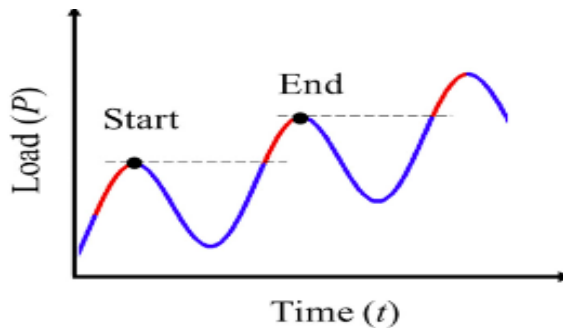


Figure 29: Schematic of the load-time variation during a CSM (Sudharshan Phani, Oliver, & Pharr, 2020)

The represented force-time curve is zoomed with the purpose of making evidence of the oscillation in the load applied into the sample. The introduction of this AC signal in the load DC driven one has the purpose to generate and output signal (indentation depth function, h) with the AC component capable to be analyzed with the objective to extract contact stiffness behavior throughout the parameter h ; it is possible to come with the doubt of why the contact stiffness is the variable of interest to characterize the material with the increasing of the depth, to answer this, a close look into the model equation for hardness and elastic modulus is necessary which is summarize into Table 18 showing how important is the correct estimation of contact stiffness.

Table 18: Close look into ITT hardness and elastic modulus

IIT Hardness	IIT Elastic modulus
$H_{IIT} = \frac{P_{max}}{A_c}$	$S = \frac{2}{\sqrt{\pi}} \sqrt{A_p E_r}$
$A_c = F(h_c)$ $h_c = h_{max} - \epsilon \frac{P_{max}}{S}$	$\frac{1}{E_r} = \frac{(1 - \nu^2)}{E} + \frac{(1 - \nu_i^2)}{E_i}$

In accordance with what is describe above, the capability of the CSM method (to be demonstrated in the next parts about the method) could be resumed in

- Continuous measurement of mechanical properties function indentation depth (depth profile properties).
- Measurement in viscoelastic materials, storage, and loss modulus of polymers as function of the frequency.
- Enhancement in situ surface detection



Simple Harmonic Oscillator – Indenter free hanging

The first step into the understanding of the continuous stiffness measurement method parts from the model used to represent the contact of indenter and sample, for a better comprehension done in two macro steps: the study of a free hanging displacement of the indenter and then a modelling of the contact interaction/ response when the punch get contact with the material. About the free indenter movement, the model has been studied as a simple-harmonic oscillator (see Figure 30)

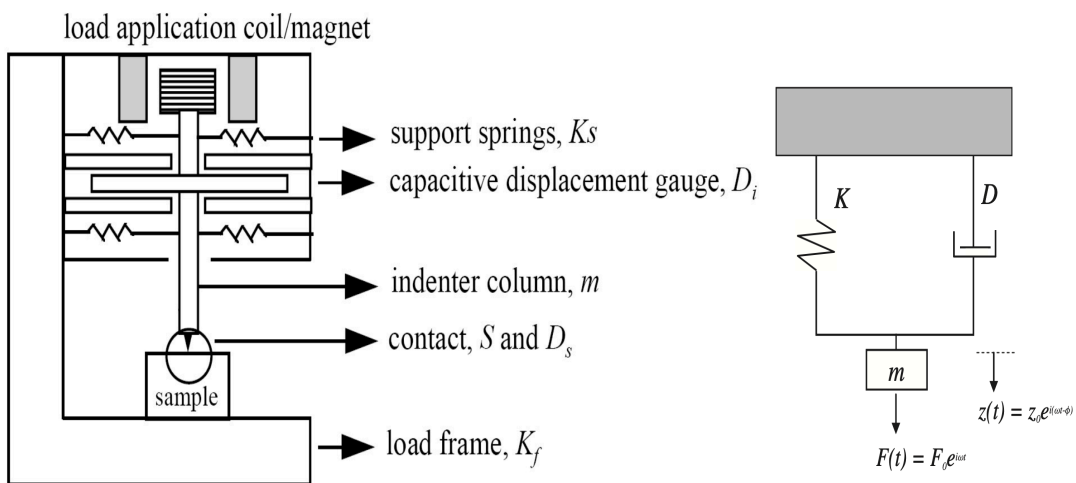


Figure 30: Schematic of Nano Indenter indentation head (Agilent Technologies, 2013) (left) and representation of dynamic mechanical model when free indenter (right)

Applying the simple-harmonic oscillator simplification, the mass (indenter) which is under the effect of the excitement force $F(t)$; it is expected to have a response similar in form to the one exhibit by the oscillating force with the same frequency, but lag in a phase angle, ϕ . The solution for the simple harmonic oscillator problem is describe graphically in Figure 31.

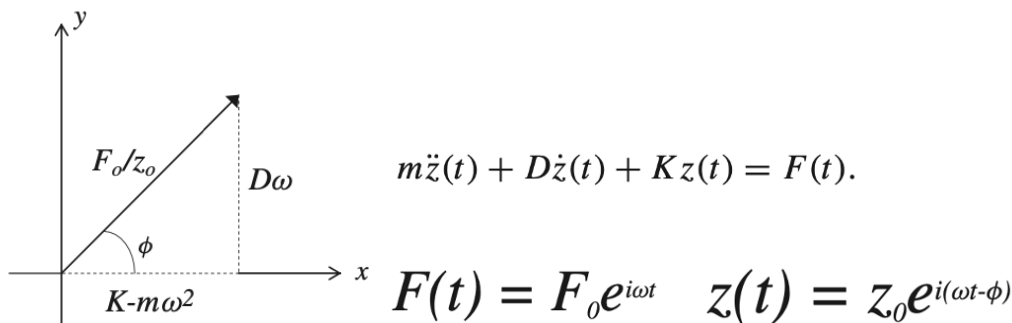


Figure 31: Illustration of solution of the simple harmonic oscillator model



In a deterministic point of view, the representation of the info in the figure above can be reduce to:

Table 19: Dynamic response simple harmonic oscillator

Ratio Z_0/ F_0	Phase angle (ϕ)
$\frac{Z_0}{F_0} = \frac{1}{\sqrt{(K - m\omega^2)^2 + (D\omega)^2}}$	$\tan \phi = \frac{D\omega}{(K - m\omega^2)}$

According to the equations above, it is possible to determine stiffness (K), mass (m) and damping coefficient when the ratio Z_0/ F_0 (some author defined it as dynamic compliance, e.g., J. Hay (Hay, Agee, & Hebert, 2010)) and the frequency ω are known. So, applying this model to the specific case of the free hanging oscillation of the indenter means to characterize the test rig in terms of the support spring stiffness ($K=K_s$), damping coefficient of the displacement gauge ($D=D_i$) and the mass of the indenter (m).

To do such analysis of the properties of the machine test, the most common approach consists in acting a frequency sweep over a wide range using a frequency-specific amplifier (for example, a lock-in amplifier) to measure the AC force and the displacement response at the same frequency with the scope of determining F_0 , Z_0 and phase shift (ϕ) by plotting Z_0/F_0 vs ω to next derive a best fit function based on equations in Table 19. This procedure is a standard process in the calibration of the test rig prior the real testing of the sample of interest, manufacturers of indentation machines in general include this calibration routine into the software of their product and the resulting plot is like the one in Figure 32.

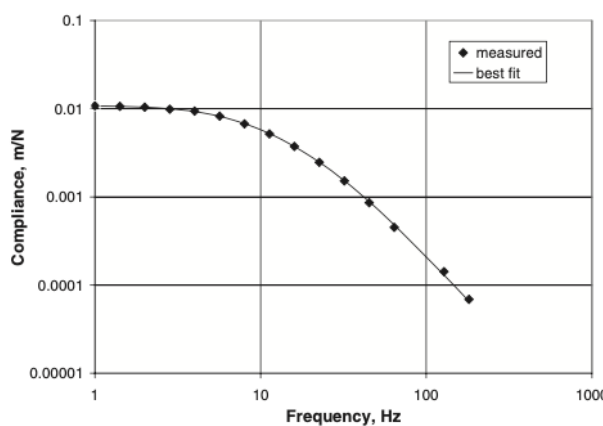


Figure 32: Measured compliance and best fit for the Agilent G200 Nano. (Hay, Agee, & Hebert, 2010)



Simple Harmonic Oscillator – Modelling of indenter contact

Once it is done the calibration of machine test parameters in relation to the variable involve in the simple harmonic oscillator apply to the free displacement of the indenter. We can proceed with modelling of the interaction with the material to test by using Voigt model (Sidney R. & Estelle, 2013) (other approaches available in the appendix); to study this phenomenon, it is identified the new variable to get in interaction with the ones already studied, at this point the schematic representation used becomes as follow.

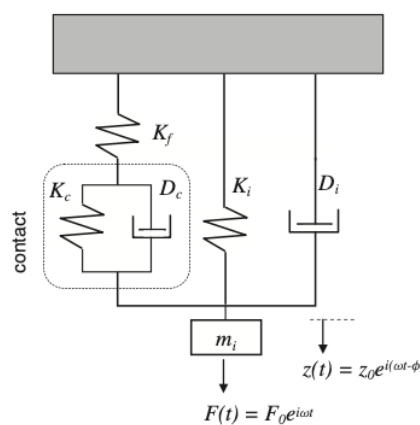


Figure 33: Harmonic Oscillator model including contact interaction (Hay, Agee, & Hebert, 2010)

The scheme presented in Figure 33 is similar to the one in Figure 30, where it was added a series of components to describe the contact interaction between the indenter and the sample, for a generic material. However, in order to model this new configuration is necessary to apply some reductions considering the relative position of the components among each other, starting from the spring elements.

Table 20: Equivalent spring in terms of elements in harmonic oscillator model of contact stiffness.

$K_e = \left[\frac{1}{K_f} + \frac{1}{K_c} \right]^{-1} + K_i$	<p>K_c: equivalent stiffness (K_e=K on Figure 30)</p> <p>K_f: Elastic stiffness of the frame (refer to Instrument compliance C_f)</p> <p>K_c: Stiffness contact (refer to parameter S in indentation theory)</p> <p>K_i: Elastic stiffness of the support</p>
---	---



Table 21: Equivalent dashpot coefficient in terms of elements in harmonic oscillator model of contact stiffness.

$D_e = D_i + D_c$	<p>D_e: equivalent damping coefficient ($D_e=D$ on Figure 30)</p> <p>D_i: Damping coefficient of the test rig (associate to capacitive displacement gauge)</p> <p>D_c: Damping coefficient of the sample</p>
-------------------	--

Regarding the mass term, when the indenter gets into contact with the material sample, the effective mass is not significantly affected (Hay, Agee, & Hebert, 2010) resulting in $m=m_i$. Consequently, we need to define the response in function of these parameters, including the fact that the variables added in the model related to the contact behavior are unknown in a major part of the cases. Thus, the objective of this approach is determining the equivalent stiffness and damping constant with the aim of utterly estimate mechanical properties of the material tested. An analysis, that starts with the premise of knowledge of the instrument compliance in accordance with the procedures established by the manufacturer to quantify it (this estimation of K_f usually is done through a procedure defined into ISO 14577-2, a summary of one of the methods describe in the standard is available in the appendix under Instrument Compliance).

Hence, the formulation that allows to determine the variables D and K is the next represented, in addition to it, a particular case of this solutions is when K_f tends to be infinity (Rigid Frame) of course an impossible real situation. Although, it is a good assumption when we are small contacts or very compliant materials (Hay, Agee, & Hebert, 2010).

Table 22: Stiffness (S) and Damping coefficient of contact

$K_c = S = \frac{K_f(K - K_i)}{K_f - (K - K_i)}$	<p>When $K_f \gg K_e$</p> <p>$K_c = S = K - K_i$</p>
--	--

Now, it has been defined the equations that describe the motion system, it is good to introduce the base guidelines in the measurement of signals. Normally, a simple harmonic oscillator or any system with a nature of the same type in the laboratory is



studied in terms of response in the frequency domain, for that reason it is common to applied sweep on the frequency (ω) and investigate the output $Z_{(t)}$ over a range.

Although, with a CSM, it is often the case where the excitation frequency is fixed and the components present in the oscillator change during the test, because of the contact variables (S and D_c) changes. For the contact stiffness from the IIT theory, it is known that is function of the contact depth (h_c).

Indenter Contact – Pure elastic-plastic materials

An important insight during the study of test data after CSM test concerns to identification of the kind of material that it is been tested. The model described parts from a generalization of the material and the indenter/sample interaction, but when going deeper in the model, it is possible to identify to different groups of material during a dynamic indentation test, bulk materials (pure elastic-plastic materials) and those one with dissipative properties (viscoelastic materials). When the case is the testing of bulk materials, the model can be simplified as next

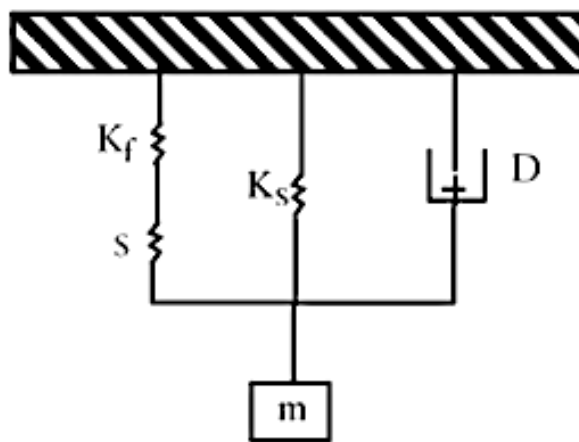


Figure 34: Dynamic model contact for bulk materials (Agilent Technologies, 2013)

It can be observed that the damping element in the contact interaction model is not present since bulk materials do not exhibit dissipative properties with deformation (even the damping itself of the machine does not contribute significantly to the phase angle due to the setup in general used where $K_e \cdot m \omega^2 \gg D_e \omega$). Still, during the continuous indentation test is possible to find an apparent dissipation of the energy because of plasticity effect later in the text studied in more detail.



Indenter Contact – Dissipative materials

In the previous section, it was mentioned how bulk materials applications simplified the model of the simple oscillator. When the materials that is being tested shows a shift in the signal of displacement (phase angle) means that the energy applied to deform the sample is going through a process of energy dissipation (introduced in the simple oscillator model as D_c) due to dislocations mechanisms during the test, mechanism that are analyzed from a macro point of view by the storage and loss modulus.

Table 23: Storage and Loss Modulus – Dissipative energy materials (Agilent Technologies, 2013)

Storage Modulus E'	Loss Modulus E''
$E' = \frac{\sqrt{\pi}S}{2\sqrt{A}}$	$E'' = \frac{\sqrt{\pi}D_e\omega}{2\sqrt{A}}$
Ratio storage modulus	
$\tan \phi = \frac{E''}{E'} = \frac{D_c\omega}{S}$	

These properties can be used for example to understand the behavior of polymeric materials by analyzing the indentation test during the hold phase of the CSM test (see Figure 35), a deeper insight of the result of this kind of study will be later explained in this work.

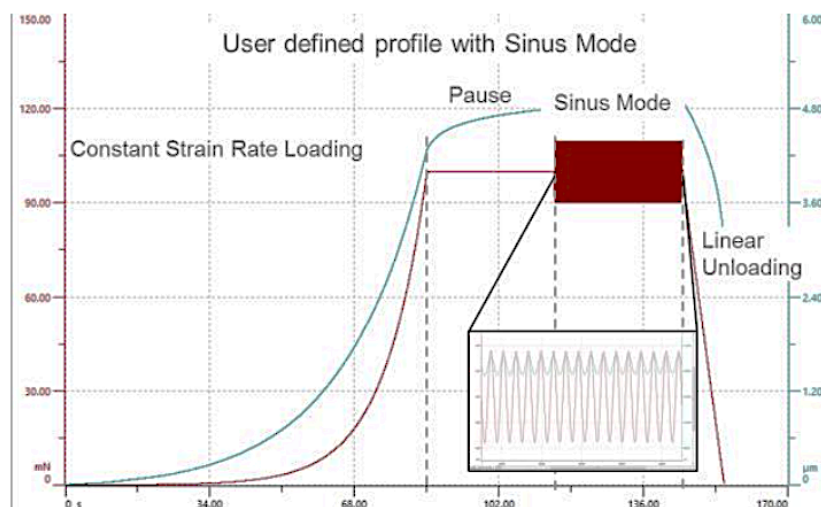


Figure 35: CSM or Sinus mode during hold at constant force (Nohava, Dynamic mechanical analysis by nanoindentation)



Vibration Response of CSM System – Insights in excitement frequency selection

It has been anticipated that the properties inherent to the contact indenter/sample description are indentation depth dependent. This behavior brings with it a problem regarding the correct selection of the frequency of the sinusoidal AC force applied in the CSM method, because we are facing a particular case where the natural frequency of the system changes during the test, a fact that implies a risk of resonance.

The issue of having large amplitude of response (Z_0) is a real problem when the selection of the input frequency is not done wisely. There are cases where it could be useful to force the system to enter in resonant, for example in contact detection where if the input frequency is set just above the natural frequency of free hanging system when the indenter gets in contact with the sample is observed a variation of the phase angle; an approach like this, it is connected to ultrasensitive measurement.

In addition to this, it is imperative to mention that depending on the test conditions not just the natural frequency of the system changes (implying the attention that we need to give to the resonance); the global response of the system can exhibit an evolution from an overdamped to an underdamped response as a result of the increasing contact stiffness value with depth. This aspect is clearer when going deeper in the simple harmonic oscillation model applied to two different test benches (see Table 24); one of them available in the Politecnico di Torino's laboratory, for the case of bulk materials where it can be observed that one of them along with the indentation depth (evaluated as contact stiffness) is always representing an underdamped response while the other one exhibit a change in the dynamic response (see Figure 36).

Table 24: Free hanging oscillation constant for Anton Paar Bench (Politecnico di Torino) and Agilent Machine G200.

Free hanging Oscillator Constants			
Anton Paar (Politecnico di Torino) (Anton Paar TriTec SA)		Agilent Machine (Hay paper (Hay, Agee, & Hebert, 2010))	
K (N/m)	1557,57	K (N/m)	92,02
m (g)	11,732	m (g)	11,6
D (N.s/m)	0,2278	D (N.s/m)	2,66
fn (Hertz)	57,99	fn (Hertz)	14,18



It is imperative to clarify the definition of damping factor used for the purpose of evaluating the dynamic response of the system (see Table 25) which is described by Fasana and Marchesiello (Fasana & Marchesiello, 2006) where the dynamic response of a system is divided into

- Overdamped response, $\zeta > 1$
- Critically damped response, $\zeta = 1$
- Underdamped response, $\zeta < 1$

Table 25: Damping coefficient simple harmonic model

Critical Damping (D_{cr})	Damping Factor (ζ)
$D_{cr} = 2\sqrt{K_e m}$	$\zeta = \frac{D}{D_{cr}}$

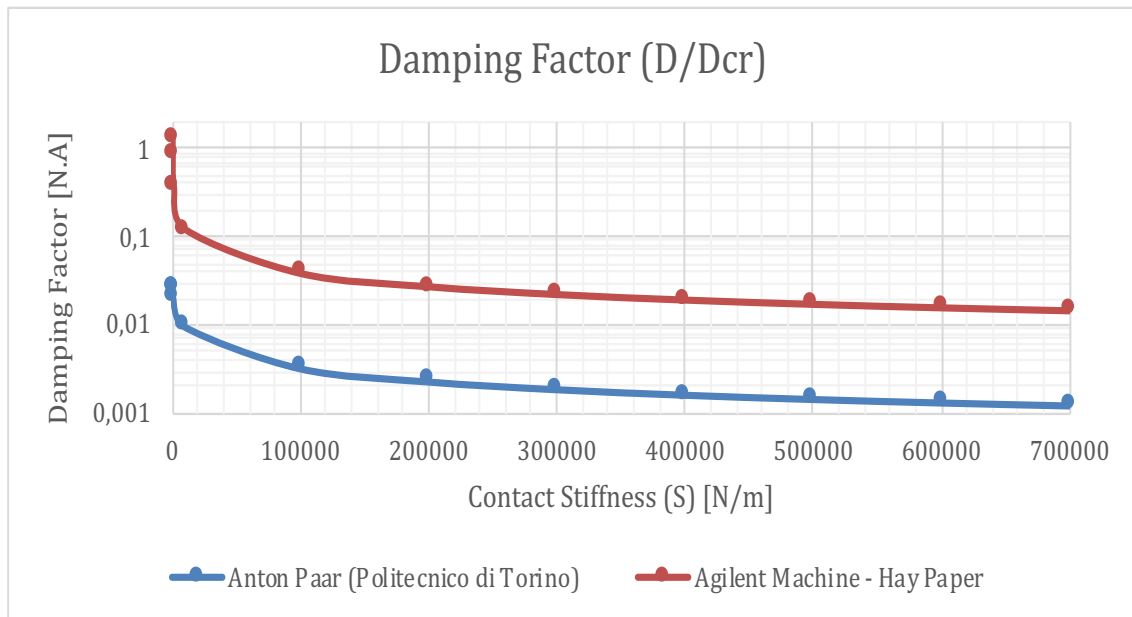


Figure 36: Damping factor for Anton Paar Bench (Politecnico di Torino) and Agilent Machine G200.

Hence, it is relevant to choose the correct input frequency for the AC component of the load, for example Hay (Hay, Agee, & Hebert, 2010) suggested a range between $0.5\omega_n$ and $5\omega_n$ applied to the free hanging oscillator system and complement this with a restriction in the lower limit where is necessary to cut-off the environmental noise (in general described by a frequency of 10 Hz). At this point for the specific test bench at



Politecnico di Torino's laboratory we identified a short band where the input force does not enter in resonance during the test.

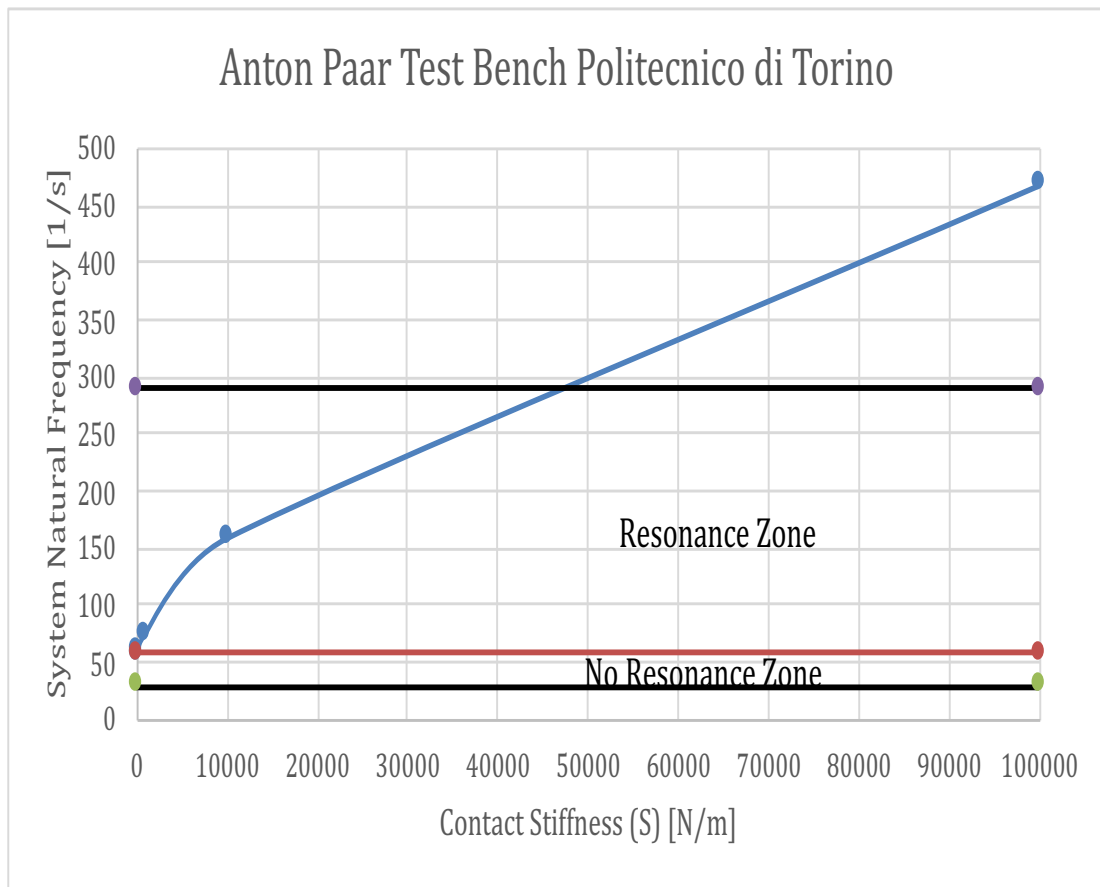


Figure 37: Suggested range of input frequency CSM test applied to test bench of Politecnico di Torino

Indentation Test Machine – Scheme for Continuous Stiffness Measurement

Going into more deeper details of the CSM approach, it is critical to understand the test setup and how this is used to make the measurements. To comprehend the signal acquisition in the technique, the best way to do is referring to the original model, the one proposed by Oliver and Pethica (United States of America Brevetto n. 4,848,141, 1989) which can be split into 4 macro groups (see Figure 38).

- Red rectangle: Indenter + sample
- Blue rectangle: signal sensor
- Green rectangle: unit control group and processing (Lock-in amplifier)
- Purple rectangle: Force source signal



Until now, we have deeply described the indenter + sample group. Still, it is necessary to understand how the rest of the elements works

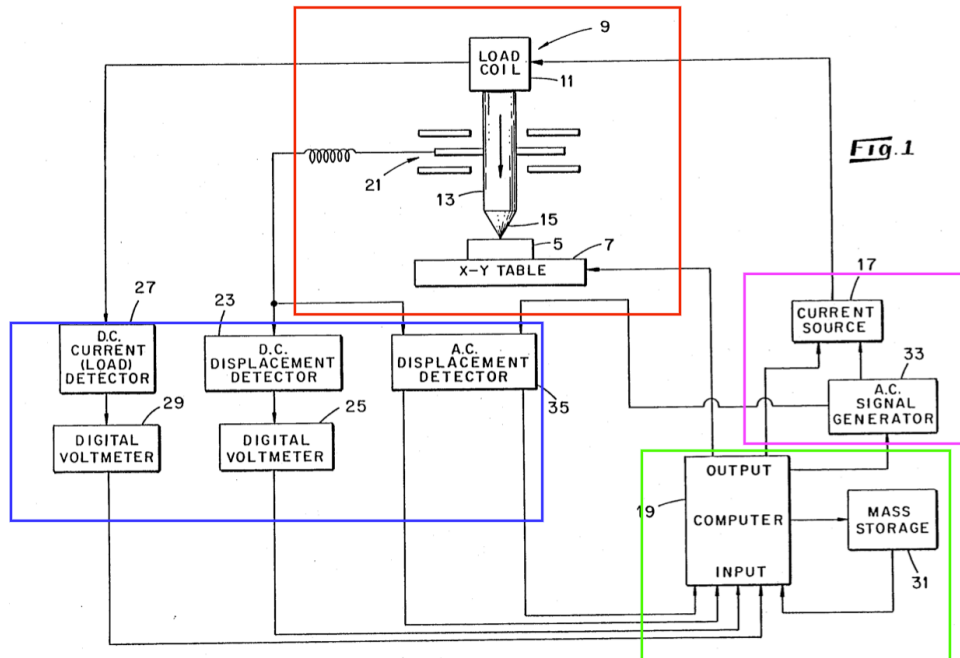


Figure 38: Original schematic arrangement of a CSM test rig (United States of America Brevetto n. 4,848,141, 1989)

Force Source Input Signal and Sensors

The operative process of CSM defines the introduction of an oscillating signal into the DC load that describes the force applied in the sample at any instance of time. Following this scheme, the load used to deform the materials can be divided in 2 signals, a DC which represent the mean value of the applied load and the sinusoidal varying (AC) component (see Table 26 – notice that the change in the notation from $F \rightarrow P$ to identify the load was just for convenience when referring to IIT variables).

Table 26: Excitation force in terms of DC and AC signal (Sudharshan Phani, Oliver, & Pharr, 2020)

DC Load signal	AC Load signal
$P_{DC} = P_{DCo} e^{\left(\frac{1}{P} \frac{dP}{dt}\right)t}$	$P_{AC} = P_{ACo} \cos(2\pi f \cdot t)$
$P_{(t)} = P_{DC} + P_{AC}$	



Observing the form of the signals, we can initiate to define the parameters to impose in the machine for the indentation cycle. Starting from the DC signal,

- P_{DC_0} : Exponential loading pre-factor (typically of the order of few μN).
- $\frac{1}{P} \frac{dP}{dt}$: Indentation strain rate or strain rate.

The last term mentioned has the greatest impact in the form of the load signal applied to the indenter and defines a classification in the CSM methods: Constant Strain Rate (CSR) test; graphically, it can be observed the load force of CSM-CSR in comparison with ISO 15477 in Figure 39 where the loading phase mean value is associated to the DC input.

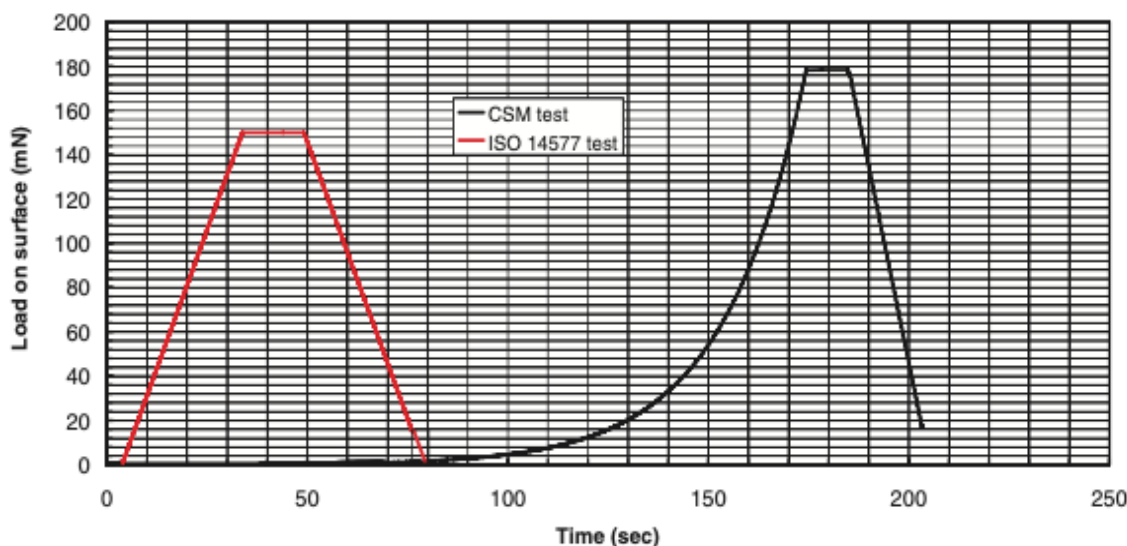


Figure 39: Force-time algorithms used for CSM and ISO 14577 tests (Hay, Agee, & Hebert, 2010)

About the AC signal, this is just a sinusoidal signal impose to the DC signal with the aim of create a response capable of describing a oscillating behavior in the indentation depth that allows to determine contact stiffness (S) using the simple harmonic oscillator model by the use of the AC component of the $h(t)$ function (as it can be observed in Figure 38 the input and output signal are always split into DC and AC component). The particularity of this AC force oscillation is that needs to be defined in a way that the great majority of deformation during a CSM oscillation cycle is elastic (Merle, Higgings, & Pharr, 2019), an assumption that it is verified when estimating the plasticity effect in bulk materials (a topic later discussed in this text)



As final remark, the ratio P_{ACo}/P_{DCo} in general is a low value that can utterly define the loop control method for the oscillation force and displacement response.

Computer – Phase Lock Amplifier [PLA] (Lock in Amplifier)

This group in the test rig represents the control unit of the bench, where one of the most critical items is the lock in amplifier which has the function of filtering the AC signals (input and output) to determine amplitude ratio and phase angle among the force and the displacement response with the objective of determining the contact stiffness.

For a better comprehension of the lock in amplifier working principle, you can refer to the appendix on this text, where it is done a special focus on how this can affect the values of oscillating depth (AC component of the $h(t)$ response) due to PLA time constant and the way to correct it.

Factors Affecting CSM Test

As per Instrumented Indentation Method, CSM has its own sources of error that can compromise the measurement and mechanical properties estimation. In general, continuous stiffness measurement is still an indentation and common issues from a procedure IIT approach are still present in the dynamic technique, among those effect we can find the initial penetration depth, indentation size effect (ISE) and the instrument compliance. To consider these common factors in the CSM methodology, the same procedure is applied as per IIT, but in relationship with the instrument compliance some insights are important to keep it mind during the calibration process of the machine. These recommendations born from the standards (ISO 14577-2) and adapted to the specific case of each test bench/manufacturer, to introduce this concept it will be described the process done by Agilent Technologies regarding their Nano indenter G200 User's guide (Agilent Technologies, 2013). In the same way, it is remarkable to mention that Continuous Stiffness Measurement has its own source of error due the nature itself of the method such as the plasticity effect in bulk materials.

Instrument Compliance

From IIT theory, it has been characterized the effect of the frame stiffness into the indentation depth and the total compliance (C) (referred to the spring elements), where



the model used to simulate its influence was an arrange of series spring that conducts to a correlation describe in Figure 40 where $C_f = 1/K_f$.

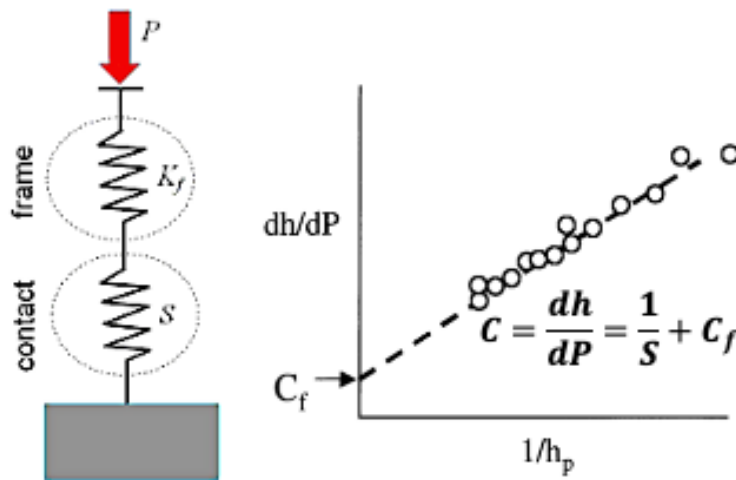


Figure 40: Model description for instrument compliance.

Parting from this definition, the manufacture (Agilent Technologies) states that the procedure is the same as per ISO 14577-2, where they fixed as material to determine the Frame Stiffness the fused silica by doing an IIT test at one location (Agilent Technologies, 2013). Then, they use the C_f measured as input parameter in the CSM test in the sample material to study, but by doing this, they identified 3 cases of interest.

1. Contact stiffness of the fused silica is less than 1 % of frame stiffness measure with fused silica.
2. Contact stiffness of the fused silica is more than 1 % of frame stiffness, but Hardness is the only result of interest.
3. Contact stiffness of the fused silica is more than 10 % of frame stiffness and the Young's modulus is a property to evaluate.

About the first situation, it is the desirable response because it means the frame stiffness does not significantly influence the Young's modulus value, and the assumption of using instrument compliance estimated with fused silica as input parameter is valid for the purpose of the measure. However, when we encounter case 2, with the intention of applying the same approach (C_f as input parameter in CSM test), notice that the manufacturer remarks that hardness estimation does not suffer any effect from stiffness frame error (see Figure 41), but for Young's modulus the case 2 means that the test bench



is measuring different values of frame stiffness depending on the position of load application (see Figure 42) which results in what we can observe in Figure 43.

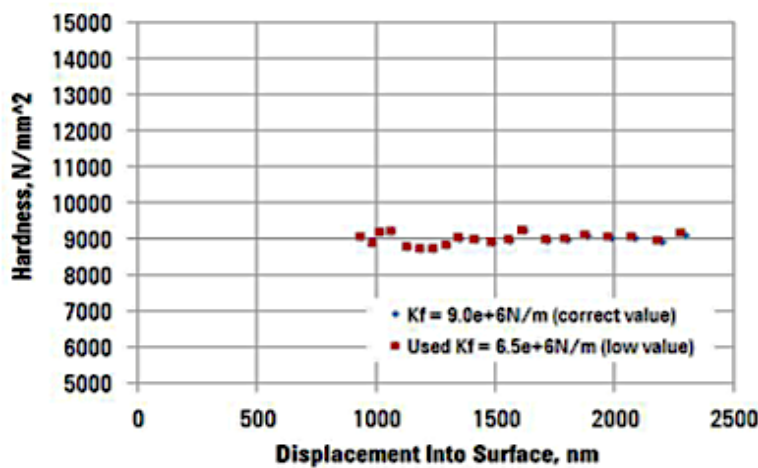


Figure 41: No apparent effect of frame stiffness on modulus (Agilent Technologies, 2013)

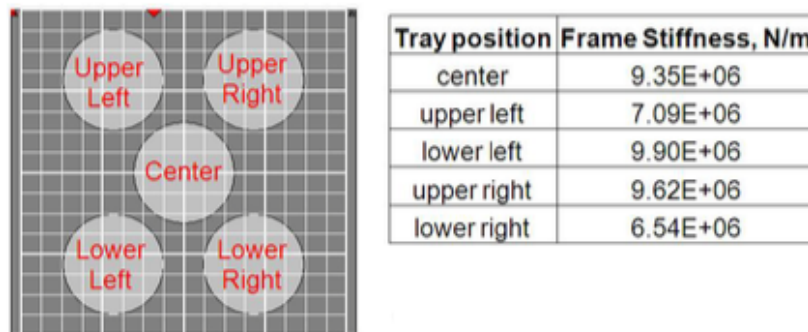


Figure 42: Variation due to sample tray position (Agilent Technologies, 2013)

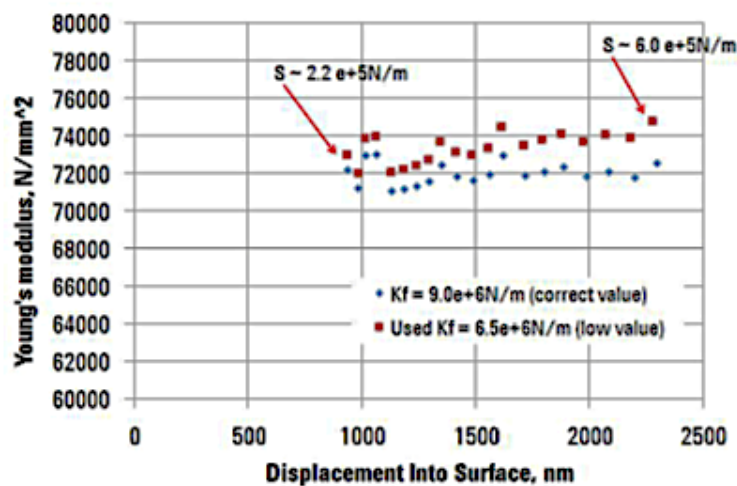


Figure 43: Effect of frame stiffness of modulus (Agilent Technologies, 2013)



Therefore, when we are observing contact stiffness of the fused silica is more than 1 % of frame stiffness, it is important to be conscience that Young's modulus value is not accurate, but if the application allows it, still can be used. Finally in the worst of the scenarios (case 3), Agilent Technologies advises to use the test sample instead of the fused silica to perform the study of the instrument compliance, considering a test set up similar in indentation depth and load range to the one desired to applied in the CSM.

Plasticity Effect – Bulk Materials

The CSM plasticity issue as described by Merle (Merle, Higgings, & Pharr, 2019) is evidence when the assumption that a major part of deformation during a CSM oscillation cycle is elastic is not accomplished. This aspect is verified when analyzing the phase angle function in terms of the indentation depth which for bulk materials; characterized by being unable to exhibit damping properties as the viscoelastic materials, $D_c = 0$ which conducts to a mean value of the phase angle of zero).

When the response of the system shows a phase angle dependency of the indentation penetration (see Figure 44). In this situation, the AC force oscillations do not create elastic deformation and plastic yield effect (additionally to the one produced by the DC input) is observed (see Figure 45), in other words intermittent plastic deformation.

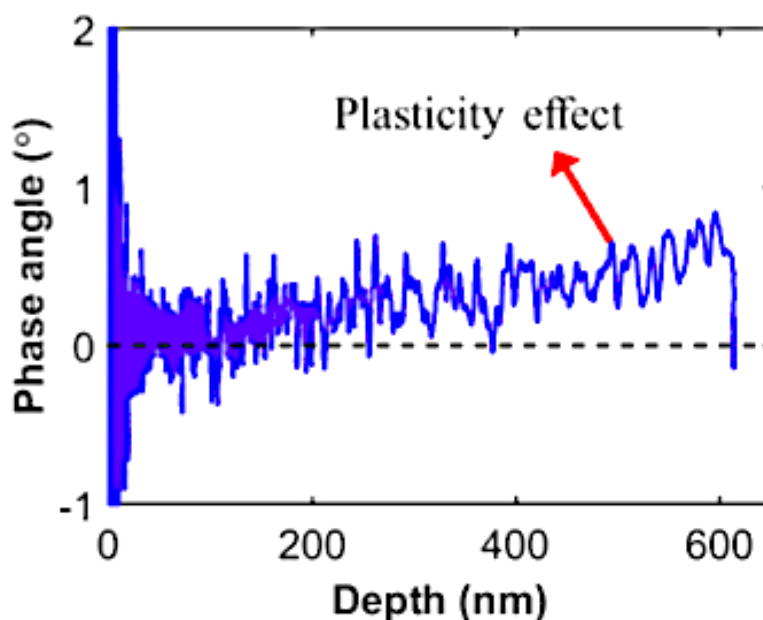


Figure 44: Phase angle-displacement variation, during a constant strain rate CSM test for fused silica (Sudharshan Phani, Oliver, & Pharr, 2020)



The presence of plasticity creates distortions/noise in the displacement signal fed to the lock-in amplifier, resulting in a wrong evaluation of the harmonic amplitude, and this ultimately yields an underestimation of the contact stiffness and an overestimation of the measured phase angle.

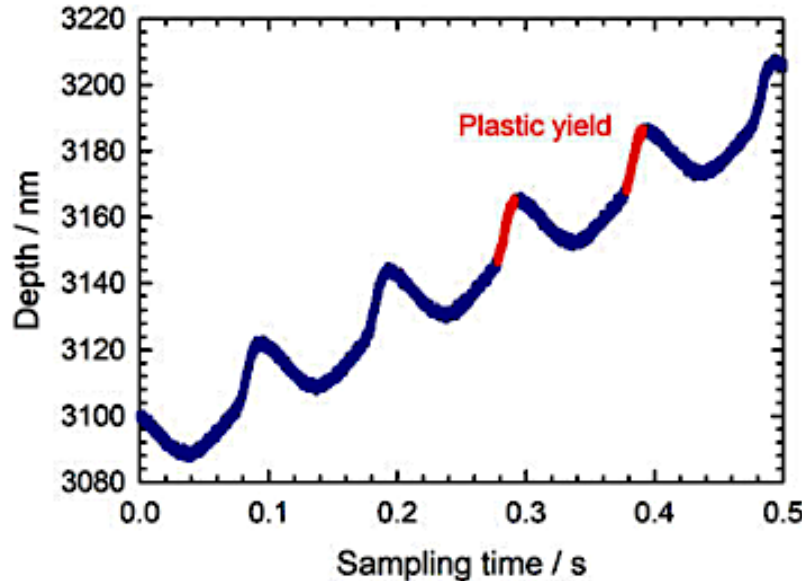


Figure 45: Experimental observation of cyclic plastic yield. (Merle, Higgings, & Pharr, 2019)

With the objective of controlling the plasticity effect, it is defined a parameter called compliance error fraction (C_{err}) which use data obtained from Finite Element Analysis (FEA) to correct the total compliance measure parameter (C_{msd}) as can be seen in Table 27 where ΔC_{plas} is the compliance error due to plasticity, C_{inp} is the input compliance obtained using the FEA derived quasi-static indentation loading and unloading parameters.

Table 27: Plasticity error estimation (Sudharshan Phani, Oliver, & Pharr, 2020)

Empirical equation for plasticity error	Relationship plasticity error and compliance measurement
$C_{err} = \frac{\Delta C_{plas}}{C_{inp}} = [AX^{-0.85}(e^X - 1)\phi]^B$	$C_{err} = \frac{\Delta C_{plas}}{C_{inp}} = \frac{C_{msd} - C_{inp}}{C_{inp}}$
$X = \frac{1}{P} \frac{dP}{dt} \frac{1}{f} \frac{P_{DCo}}{P_{ACo}}$	

A and B equal to 0.025 and 1.5, respectively and ϕ is in degrees.



Indentation strain rate and Material Sensitivity

The continuous stiffness measurement when analyzing in detail the hardness curves in terms of the depth is observed that the trend described is precisely the one that we should obtain if we superimpose multiple IIT. Hence, when it is necessary to do some verification about the correct setting of the parameters in CSM, it is useful time to time do a cross checking with the instrumented indentation test.

One of those parameters to validate is the indentation strain rate, because of the nature of the major part of indentation machines (force control system), the strain rate is normally set as a constant (input parameter) to fix. When doing this, it is possible to face a situation (not easily to appreciate) where there is an overestimation of the hardness with the depth; the cause related to the sensitivity regarding the strain rate which defines a distinction about how susceptible the materials are. A study concerning this aspect was done by Leitner (Leitner, Maier-Kiener, & Kiener, 2017) where he and his colleagues found that depending on the material, there are some of them which shows discrepancies between multiple IIT and CSM test (see Figure 46).

The variable that creates this difference between both approaches is connected to creep evaluation strategies present in instrumented indentation test (see Figure 47), when comparing two different materials (one sensitive to strain rate) and perform CSM with low strain rate. Evidencing how the impact of these parameter for those cases where the sample is affected by load cycle comporting to variation on the subsequent mechanical properties estimated.

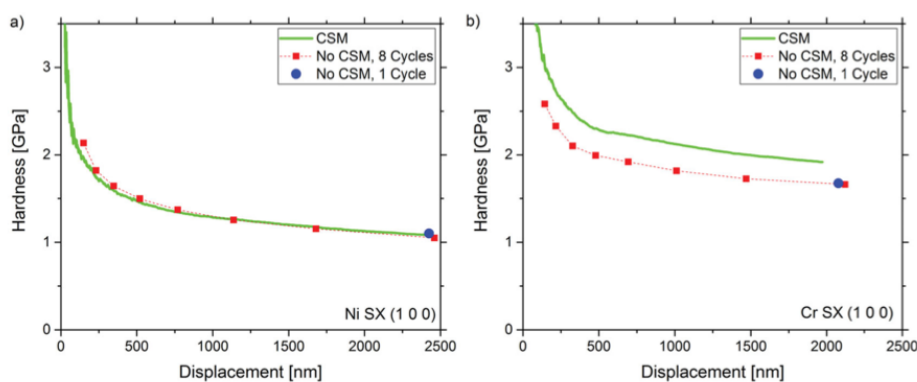


Figure 46: Comparison of hardness—displacement profiles for (a) Ni SX and (b) Cr SX for tests with and without CSM. (Leitner, Maier-Kiener, & Kiener, 2017)

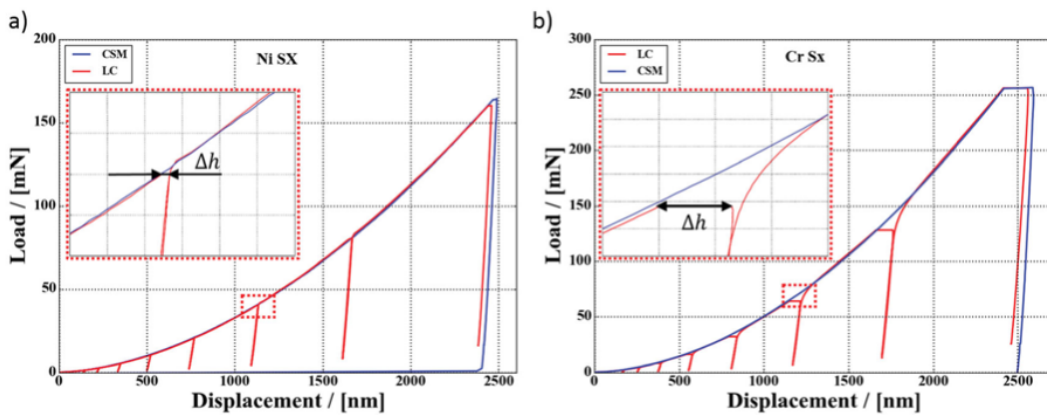


Figure 47: Load—displacement curves of LC (multiple unloading IIT) and CSM measurements on Ni SX and Cr (Leitner, Maier-Kiener, & Kiener, 2017)

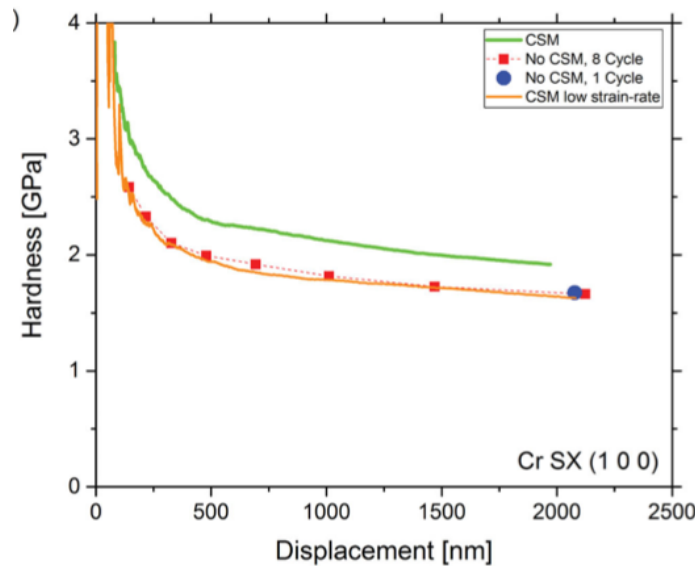


Figure 48: Comparison with Low strain-rate CSM experiments (Leitner, Maier-Kiener, & Kiener, 2017)

METHOD APPLICATIONS

Nowadays, the range of materials present in the market and the increasing demand of a high performance of these in several applications field has become more and more required, and for this purpose, the precision and capability of the techniques applied into the characterization of materials needed to be even more reliable, as we anticipate at the beginning of this work. Hence, this chapter has the premise of presenting and analyzing the application of Continuous Stiffness Measurement in practical cases of use, that goes from studies on superficial properties of components (especially those who suffered heat



treatment), following application in the thin film technologies (specific case of coating properties definition), analysis of viscoelastic materials, and others which are described in the next sections as evidence of application fields.

Surface Mechanical Properties – Heat Treated Materials

Until now, it has been reviewed the theoretical and experimental approach of the continuous stiffness measurement method, all the explanations were given with particular attention of identifying hardness and elastic modulus of the sample of interest. Still, the models presented were presented from the point of view of bulk materials; now the objective is to extend the model to real cases where in general the components and materials show a behavior in terms of mechanical properties that changes with the indentation depth (even for bulk materials), in line with this purpose is opportune to refer to one of the critical factors in a dynamic hardness test, the indentation size effect (ISE).

According to the ISE theory, during an indentation test it is observed in the initial contact phase of the indenter with the material a trend H vs h not constant over the range (see Figure 26) evidencing a relationship which depends on the load applied (it is mentioned a dependency hardness with the load because normally the indentation test are trial force controlled instead of indentation controlled). It is precisely this comportment that allows to identify a minimum and maximum value of displacement/force for a given indenter where the material exhibits mechanical properties different than the core (substrate).

As a result of this, diverse approaches have been formulated with the goal of defining correlations that can describe the indentation size effect range in terms of thickness of the layer, hardness, and Young's modulus. Therefore, if the reason behind of the indentation test has to do with the determination of substrate thickness and their properties; is relevant to consider what Indentation Size Effect theory established that can be shortened into three macro layers in a dynamic hardness test.

1. Work-hardened zone: this represents the initial depths in an indentation test. It is given this name because the initial contact depth phase usually contains a fraction of deformed material which properties are different from the substrate due to



specifically this deformation that activated a work-hardened process in the surface of the sample.

2. Intermediate zone: just after the work-hardened phase, we found a further layer where properties such as hardness and elastic modulus are still different from the core material. But the reason is not related to a deformation instead the causes could be connected to the presence of other layers made of a different material (as per coating – thin film application) or changes in the mechanical properties due to chemical and/or temperature process aimed to improve or modify outer behavior of the sample.
3. Load independent zone: in practice it is defined by a presence of a mono-substrate where there is no dependency of the load in hardness and elastic modulus values.

The classification just done it is reflected into Figure 26. However, there are situations where the discretization of each layer is more visible looking at the elastic properties of the sample (E), which is a situation more common in thin film use (see Figure 49). Even though, for thin films application may be the case where is more evident the change a layer to other, it is a casualty for that specific context. When, the situation is related to heat or chemical treatment samples, the efforts to differentiate the degree of depth of these processes affect the surface of the sample is harder. Hence, FEM simulations and mathematical models have been developed to correctly identify the phase change, these start from an analysis of the contact stiffness.

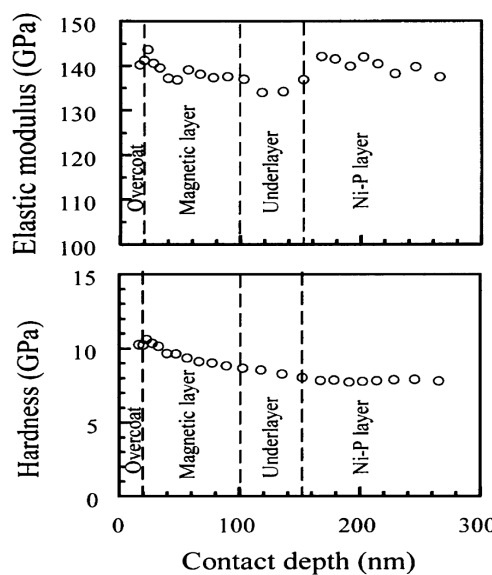


Figure 49: Elastic modulus, and hardness as a function of contact depth for a magnetic rigid disk with a multilayered structure (Xiaodong & Bharat, 2002)



The reason behind of using S is related to the assumption of linearity of this parameter with 1/h; for homogeneous materials is a valid argument. Although, when we speak of a multilayered material in general the linearity is lost (see Figure 50) due to the influence of Young's modulus, except for heat treated materials where the outer surface and the substrate exhibit the same values because heat treatment (Annealing, normalizing, hardening and tempering) affects the microstructure of the sample impacting in mechanical properties such as hardness and yield strength creating a marked difference between the surface and the core, with not global impact (surface + substrate) in the Young's modulus (consistent with the fact that the Young's modulus essentially characterizes the atomic bonds strength that are not sensitive to the heat treatment (Mouginot, Spatig, & Seifert, 2020)) which is the reason why in this work it is considered to split surface heat treated and thin film layers.

There are different methodologies to evaluate the effect in hardness and elastic properties when it is the case of studying multilayered components, for the specific application of the heat-treated materials, we found Nix and Gao model (Nix & Gao, 1998) (see Table 28) developed a model interested in describing the hardness and indentation depth (insights about the Young's modulus were not done for this specific case due to the reason mentioned before).

Table 28: Nix and Gao Model for ISE evaluation

Nix and Gao Model	
$\frac{H}{H_o} = \sqrt{\left(1 - \frac{h^*}{h}\right)}$	
$H_o = 3\sqrt{3}\alpha\mu b\sqrt{\rho_s}$	$h^* = \frac{81}{2}ba^2 \left(\tan \theta \frac{\mu}{H_o}\right)^2$

Where H_o is the hardness in the limit of infinite depth (NO ISE), h^* is a characteristic length (related to indenter shape), α is a constant in general with value $\frac{1}{2}$, μ the shear modulus, b is the Burgers vector and ρ_s is the density of statistically stored dislocation.

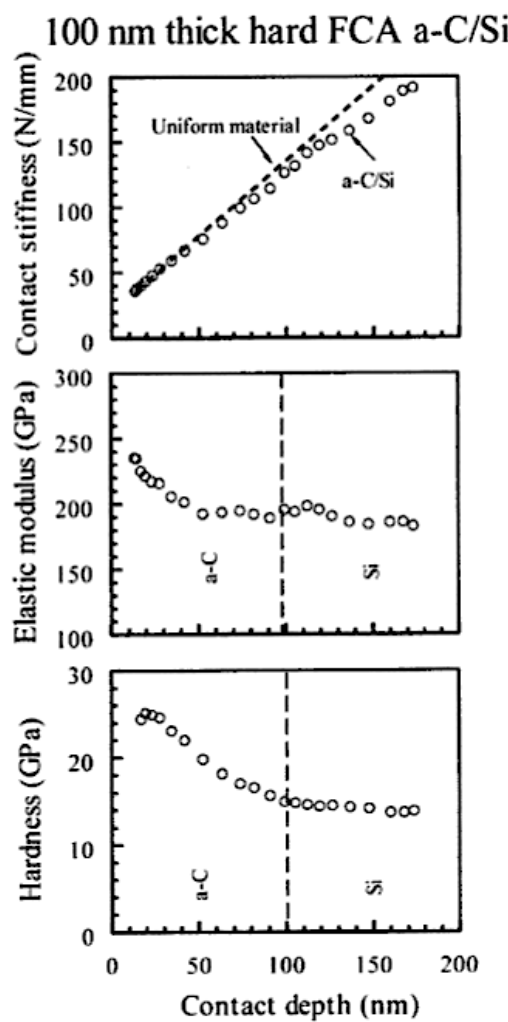


Figure 50: Contact stiffness, elastic modulus, and hardness as a function of contact depth for hard FCA a-C/Si (Bharat Bhushan, 2002)

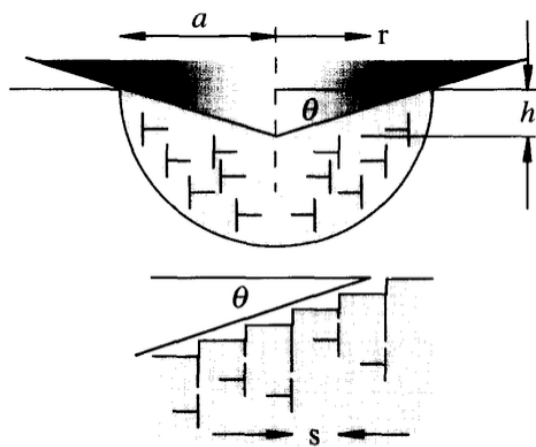


Figure 51: Geometrically necessary dislocations created by a rigid conical indentation (Nix and Gao (Nix & Gao, 1998))



However, Nix and Gao model offers a great fit for bulk materials and hardened ones (see Figure 52), the correlations lack of real applications in a manufacturing context because it does not add any new information of practical use, the potential of this Nix-Gao proposal relies on non-continuous indentation, for example IIT. For this reason, other models are preferred capable of giving details on the interaction of surface and substrate.

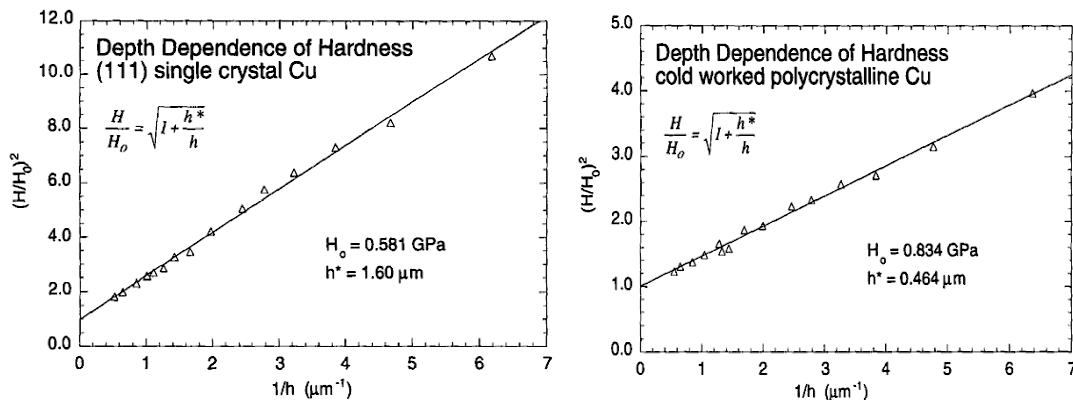


Figure 52: Depth dependence of hardness plotted according to Nix-Gao model (Nix & Gao, 1998)

Welding: CSM Hardness profile characterization

One of the interests of CSM in the surface treated material is the local affected zone (in the literature known as Heat Affected Zone – HAZ (Bailey, 1994)) after the welding process which is a method to join two or more components usually in several industries especially in the joining of metals or thermoplastic materials. The reason behind of considering welding as part of the CSM surface heat treated applications is a consequence of the present of a local temperature delta when joining component by welding techniques, this locally gradients create a similar effect of heat treatment around the joined area as we can appreciate in Figure 53.

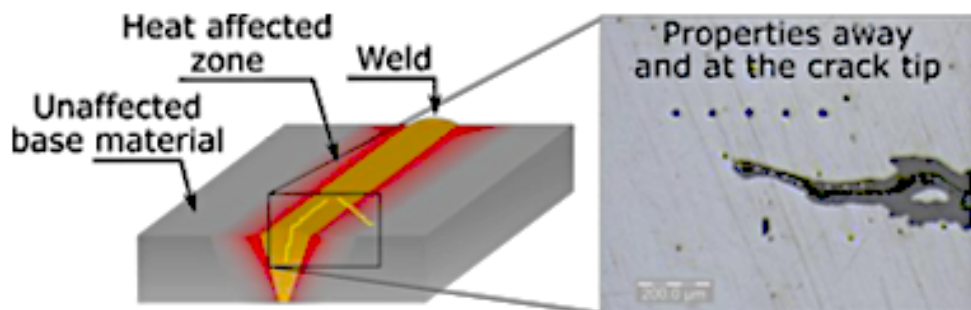


Figure 53: Discretization of welding area (Sedmak & Nohava)



At this point the dynamic indentation technique is able to develop a hardness profile capable of describing how this property change near and away the welding point (see Figure 54)

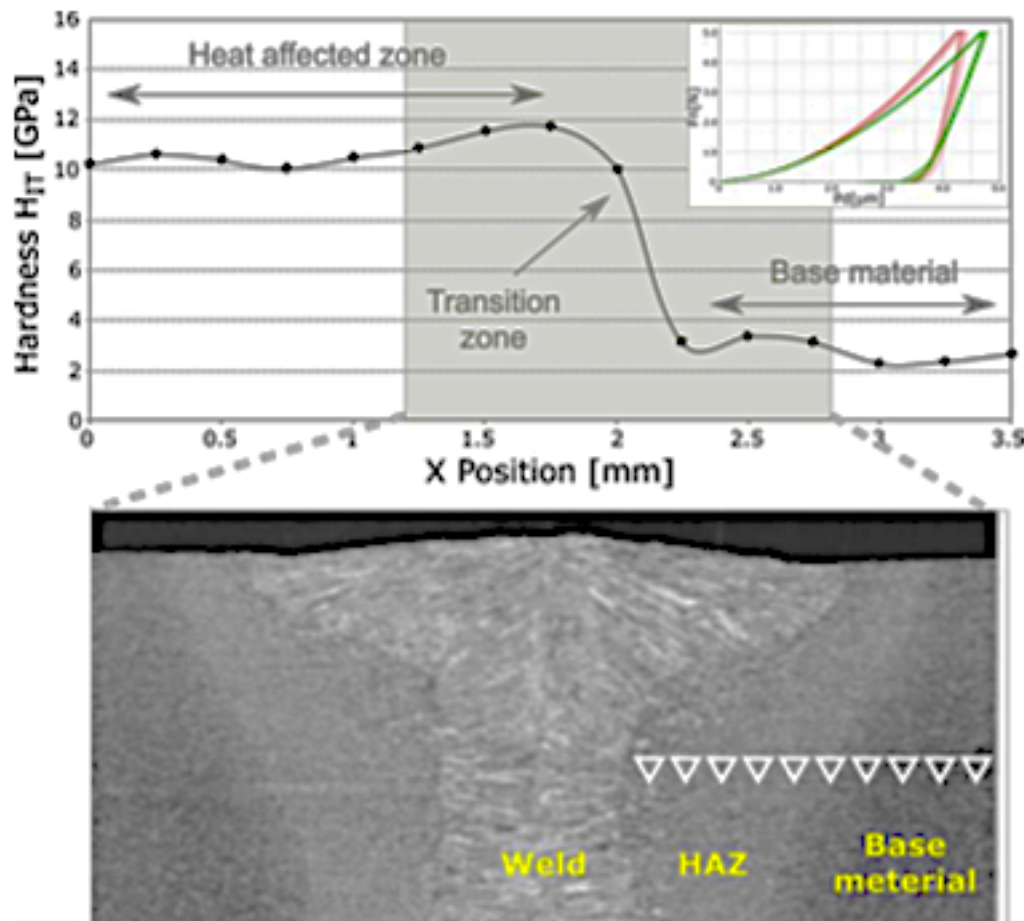


Figure 54: Cross-section of the heat affected zone and the corresponding hardness profile at fixed indentation depth (Sedmak & Nohava)

Thin Film Characterization

The use of thin film has to do with the definition of a layer of materials applied/added to a component with the objective to improve their performance or add complementary characteristic non-intrinsic of the material itself. It is possible to encounter with applications when the term “thin film” is related to an approach of multiple sheets of different materials, in that case we refer to a multilayered film; in the opposite we are facing a monolayer application.



In a context where it is necessary to perform a characterization of a thin film, in general in a range between micrometers and nanometer in thickness (Torr International Services LLC, s.d.). Several properties could be considered, limiting this to the reach of indentation technique, we mean mechanical behavior (hardness, elastic modulus, creep properties, other...) Still, with the goal of estimating these properties we cross with two specific circumstances: the thickness of the layer unknown and the most favorable one, the film thickness is known (several methods to determine thickness can be used, for example throughout of magnetic induction methods).

Film thickness known

When the thickness of every layer in a multilayered component are known, the scope of a dynamic indentation test is to identify the mechanical performance of the surface when is applied a load onto it. Although, this analysis does not finish in giving a data of the evolution of the hardness with the indentation depth, the study goes beyond that barrier by characterizing the interaction of thin film and the substrate with focus on the contribution (at a specific depth) of the film and the core material in the value of hardness determined.

In general, the methods of analysis for continuous indentation dataset to achieve this objective are linked to the relative indentation depth defined as the indentation depth (h) to film thickness (t) ratio, h/t . One of the starting methodologies applied was developed by Jonsson and Hogmark (Jonsson & Hogmark, 1984) where it is required the conventional data from a CSM test on both coated and uncoated substrates (see Figure 55) and the film thickness.

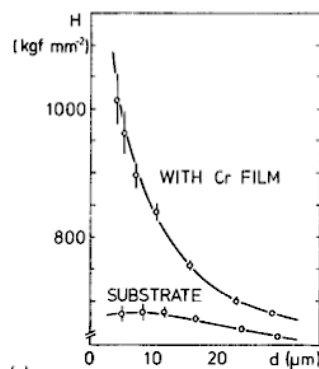


Figure 55: Hardness vs impression diagonal on substrates with and without a film (Jonsson & Hogmark, 1984)



Looking at the graph, it is clear the impact of applying a film in the overall hardness of the component, but to notice when the indentation depth increases there is a convergence in the value of substrate and substrate + film hardness which approximate to the hardness of the core material; evidencing that the effect of the hardness increasing by the film is limited to a specific range. Considering this, Jonsson and Hogmark formulated a model trying to describe the impact of the substrate in the thin film layer hardness, defining what they called composite hardness (H_c), a variable that depends on the intrinsic hardness of the coating (H_f) and the substrate (H_s) together with the volume fraction (a_f) of the coating material (see Figure 56) which counts the contribution of the coating in the composite hardness.

Table 29: Jonsson and Hogmark Model for thin film model

Volume fraction	Composite Hardness
$a_f = 1 - \left(1 - \frac{Ct}{h}\right)^2$	$H_c = a_f H_f + (1 - a_f) H_s$

In the equations above, it is important to mention 2 aspects, the first one is the fact the volume fraction function can have values between 0 and 1. The second aspect has to do with the mechanism of deformation during the indentation, the authors (Jonsson and Hogmark) established that during the pressing of the indenter on the sample is possible to perceive a plastic deformation or fracture of the thin layer (film) making this info important in the definition of the constant (C) in the model, specifically for a Berkovich indenter.

- Coating undergoes fracture ($C=0.0915$)
- Coating undergoes plastic deformation ($C=0.1746$)

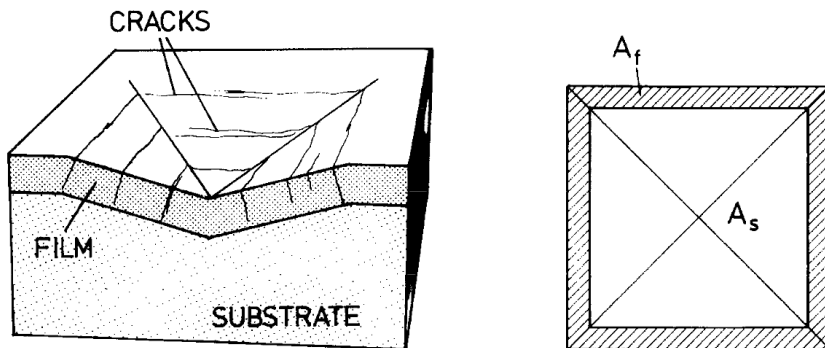


Figure 56: Load-supporting areas A_f and A_s of the film and the substrate respectively (Jonsson & Hogmark, 1984)



Table 30: Remarks on Volume fraction and Composite hardness

$a_f = 1$	$h < C_t$
$H_c = H_f$	$h < C_t$

Then, having the full frame of the Jonsson and Hogmark theory (even specific keys point in the range of a fully contribution in hardness just by the film, see Table 30) allows the afterwards studies that have been conducted to test the model and analyze its capabilities in real applications. Among those studies, it is necessary to mention the work of (Puchi-Cabrera, Staia, & Lost, 2015) done regarding 2024-T6 aluminum alloy coated with a diamond-like carbon film, employing electroless NiP as intermediate layer (see Figure 57)

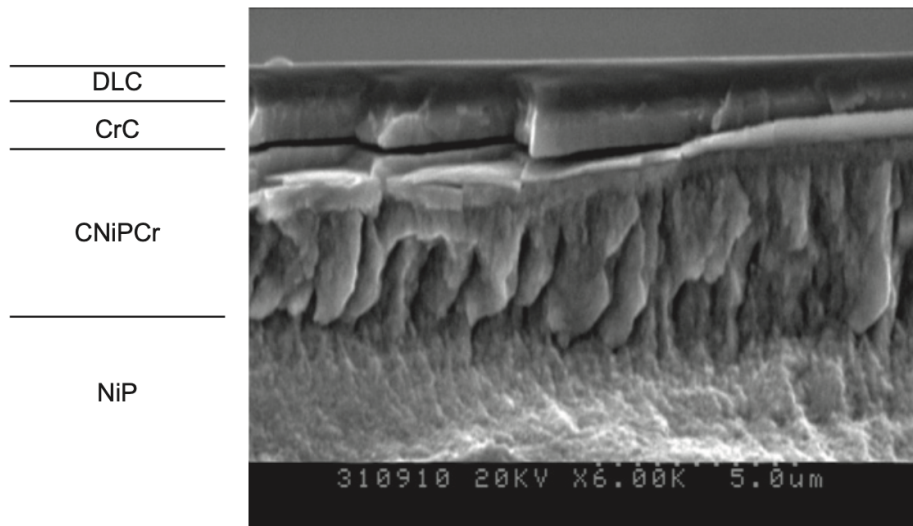


Figure 57: SEM cross section view of the coated system under investigation after fracture, showing the DLC, CrC and CNiPCr layers, as well as the NiP substrate (Puchi-Cabrera, Staia, & Lost, 2015)

The analysis performed by Puchi-Cabrera implied the modification of the Jonsson and Hogmark model to extend its use on multilayer coating (see Table 31). The robustness of this, later in the work was compared to a more complex model, in relation to the number of variables involved, proposed by Puchi-Cabrera having as result that the model published in 1984 in its simplicity still describe quite well the hardness behavior function of the indentation depth (see Figure 58) and more important how each layer contributes in the hardness value measured continuously with depth (see Figure 59).

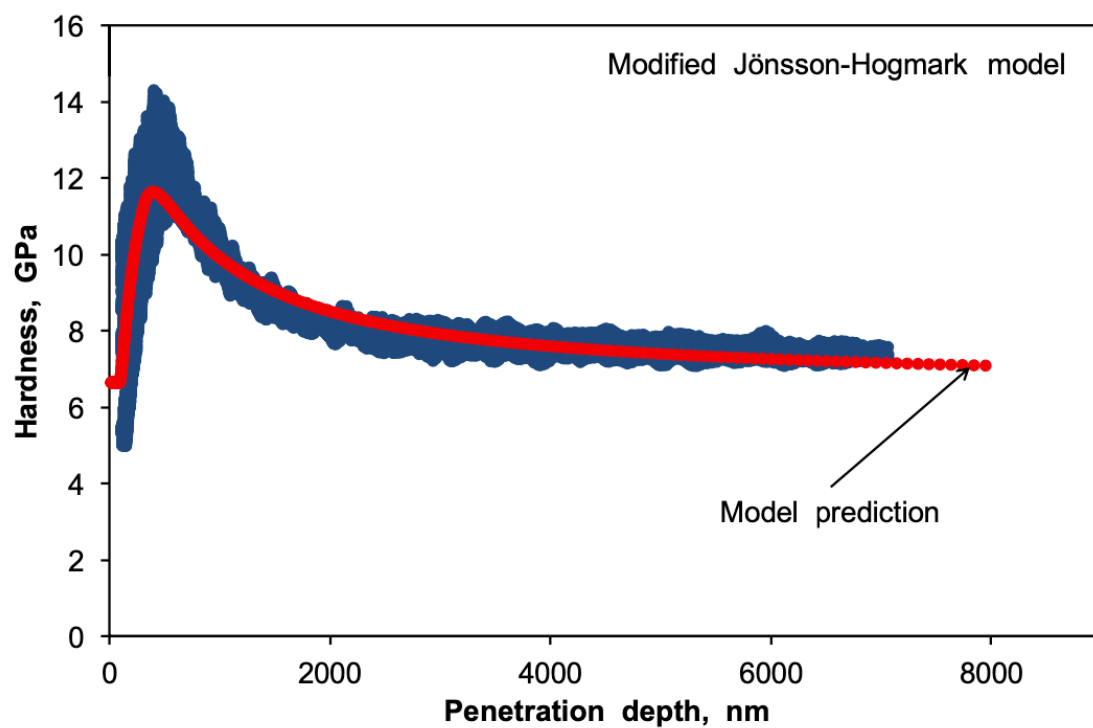


Figure 58: Change in the experimental values of the composite hardness as a function of penetration depth 2024-T6 aluminum alloy coated (Puchi-Cabrera, Staia, & Lost, 2015)

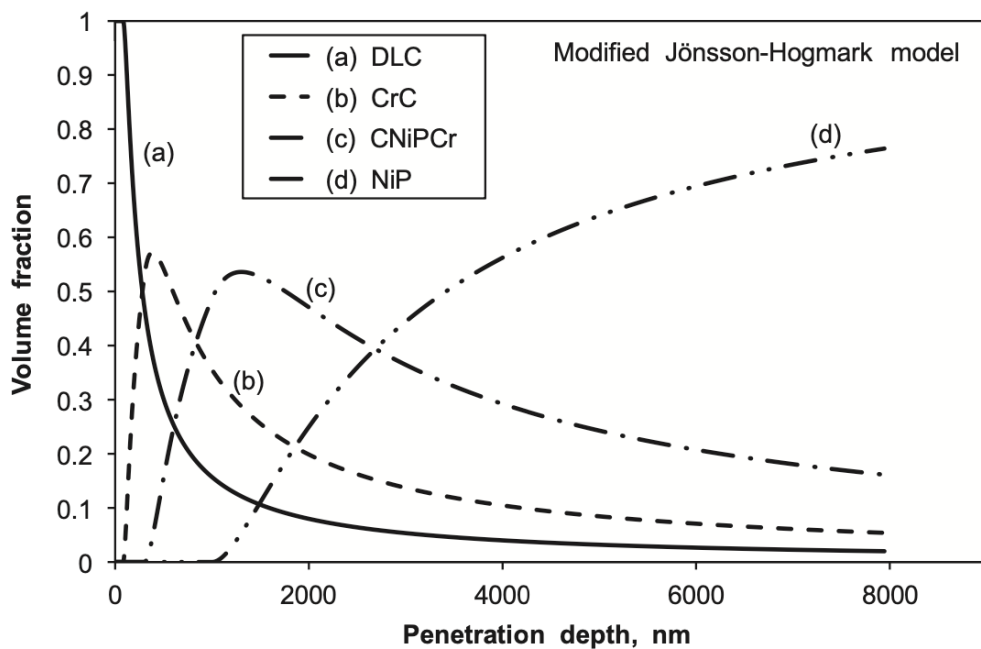


Figure 59: Change in the volume fraction of each coating contributing to the composite hardness, according to the JH model, as a function of penetration depth (Puchi-Cabrera, Staia, & Lost, 2015)



Table 31: Puchi-Cabrera modified Jonsson and Hogmark model for multilayered films
(Puchi-Cabrera, Staia, & Lost, 2015)

Modified Jonsson and Hogmark model
Volume Fraction function in terms of the layers <ul style="list-style-type: none"> For the first layer of material $a_f^{(1)} = \begin{cases} 1 & \text{if } h < C^{(1)} t_f^{(1)} \\ 1 - \left(1 - \frac{C^{(1)} t_f^{(1)}}{h}\right)^2 & \text{otherwise.} \end{cases}$ <ul style="list-style-type: none"> For the j-layer of material $a_f^{(j)} = \begin{cases} 1 - \sum_{i=1}^{j-1} a_f^{(i)} & \text{if } h < \sum_{i=1}^j C^{(i)} t_f^{(i)} \\ \left\{ 1 - \left[1 - \frac{\sum_{i=1}^j C^{(i)} t_f^{(i)}}{h} \right]^2 \right\} - \left\{ 1 - \left[1 - \frac{\sum_{i=1}^{j-1} C^{(i)} t_f^{(i)}}{h} \right]^2 \right\} & \text{otherwise.} \end{cases}$ <ul style="list-style-type: none"> For the substrate $a_f^{(S)} = 1 - \sum_{i=1}^N a_f^{(i)}.$
Composite Hardness function $H_c = \sum_{i=1}^N a_f^{(i)} H_f^{(i)} + a_f^{(S)} H_s.$

It is relevant to mention that this model can be applied to heat treated materials because the outer surface can be considered a layer, but the process will need to determine the impact (thickness) of the treated sample throughout different tools or going through an iterative process based on the information described in unknown thin film thickness chapter.



Unknow film thickness

Not having knowledge of the film thickness is a suitable scenario when prototyping is the context to work on where the results from new setups or manufacturing techniques cannot be entirely predicted. It is here where the dynamic indentation test enters as a control loop to provide information to refine the methods applied to produce a component.

Until now, it has been described how indentation dataset can be useful to determine hardness, Young's modulus, and interaction among the layers (in case of multilayered materials) when knowing the film thickness, but how to proceed in case of the opposite. As it was mentioned before, the definition of the film thickness can be done by other means such as magnetic induction equipment; even though in case of the only data available comes from the indentation test. It is important to clarify that even in that context is possible to estimate the layer thickness going through an iterative process that starts from a first guess of the film thickness by analyzing the contact depth and elastic modulus curves.

During the explanation of the heat-treated surfaces hardness, it was detailed how in some opportunities, the E and H curves in terms of indentation depth are capable of evidencing the layer change during the displacement of the indenter (see Figure 49). However, it is possible to approximate the thickness value by examining the contact stiffness curves (in simple situations like 1 film+1 substrate or multilayered if there is not interested in determining each layer thickness), taking advantage of trend of total compliance characterized by the contact stiffness parameter in relation to 2 asymptotic limits as it is seen in Tricoteaux paper (Tricoteasux, et al., 2010) (see Figure 60). By doing this, it is feasible to get an approximation of the zones of influence of the substrate during the evaluation of the elastic properties of the sample.

Although, it is promising the capability of the continuous stiffness measurement with a further analysis to estimate thin film thickness, we suggest limiting this feature as a good approximation, for more accurate values to perform a deeper study in the indentation data or choose other alternative methods to complement CSM results.

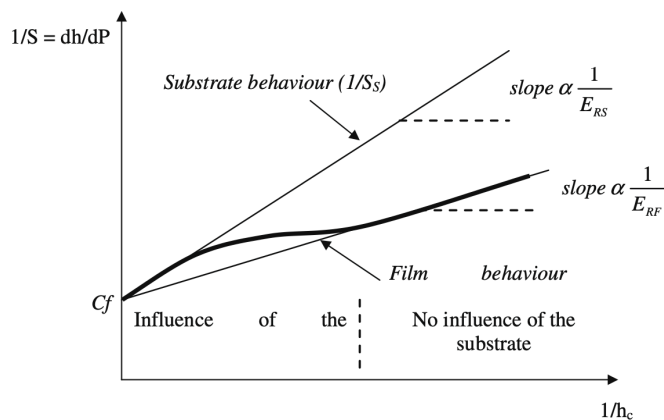


Figure 60: Schematic representation of S variation for the coated system (hard film on soft substrate). (Tricoteasux, et al., 2010)

Material Characterization for Battery Cell Manufacturing

When we discuss about the applications area of the thin film coating, one of the fields where there are important uses is related to the production of battery cells. A topic nowadays becoming more and more relevant in relationship with the trend of electrification of the powertrain in automotive industry where Lithium-ion batteries are one of the most used.

However, why the battery cell manufacture relates to indentation techniques, to answer this we need to investigate in the composition of a battery (see Figure 61). It is observed that a battery is built of a series of layer from different materials where among the factors to evaluate the performance of a cell, we find the homogeneity of the electrode coating (crucial to guarantee capacity and long lifetime of the battery and its ability to absorb many charging/discharging cycles (Nohava, Characterization of electrodes in lithium-ion batteries by nanoindentation)) and their mechanical properties which are estimated during a dynamic indentation test.

It is possible to perform two kinds of test regarding the hardness measurement depending on the dimension of the battery cell, where for small areas is enough a single indentation to get hardness and elastic modulus. Although, when the cell is bigger is needed to perform grid indentation with the objective of build a map which describes mechanical properties (see Figure 62) by doing this, it is possible to evaluate the



homogeneity of the battery by a statistically analysis of the hardness and elastic modulus grid.

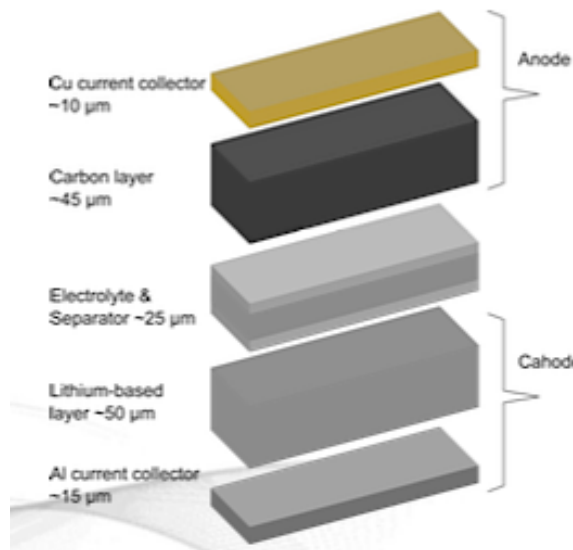


Figure 61: Lithium-ion battery structure showing approximate thickness of the components (Nohava, Characterization of electrodes in lithium-ion batteries by nanoindentation)

In the same order of ideas, a less studied application of nanoindentation in the battery field has to do with the aging of the battery, in general analyzed from the point of view chemical degradation due to the cycle of charging/discharging of the battery cell. However, it is not only characteristic that changes during the lifetime service, but the mechanical properties of the layers also composing the battery are affected by the aging of the battery too (see Figure 63)

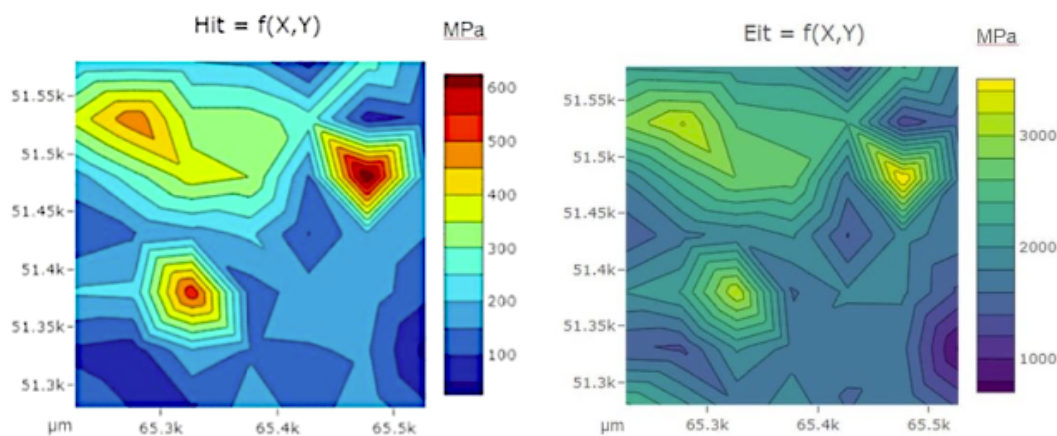


Figure 62: Distribution of hardness and elastic modulus on Li-ion cathode coating (area 300 x 300 μm).

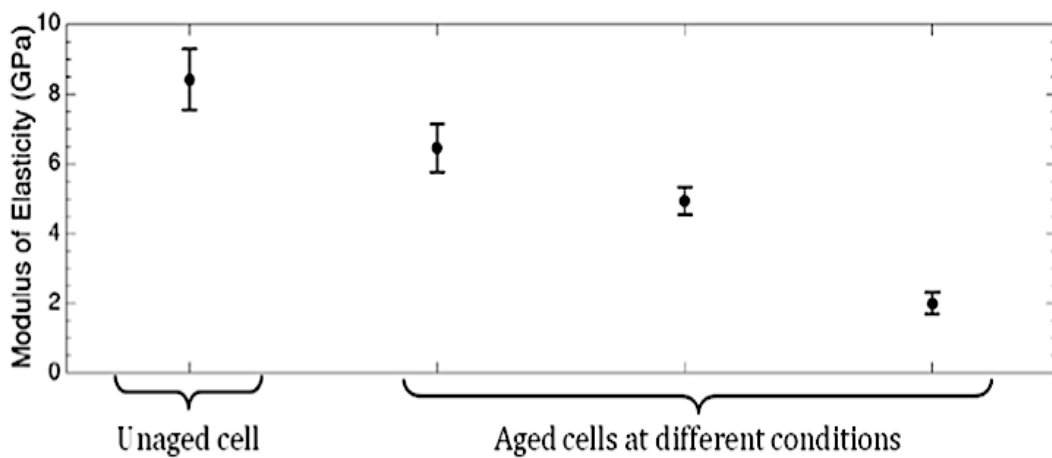


Figure 63: evolution of elastic modulus of LiFePO₄ coating after aging measured by nanoindentation (Demirocak & Bhushan, 2015)

Viscoelastic Material – Glass Transition Temperature

Previously it was mentioned the potential of continuous stiffness measurement to estimate characteristic of polymers such storage and loss modulus. Although, these measurements can be of interest in the characterization of polymeric materials, the real capability of the dynamic indentation technique is when the test is applied in conjunction with a sweep related to the temperature test conditions. Because by doing this the indentation technique is capable of the estimating the glass transition temperature (T_g) of the polymer defined as temperature at which the polymers change from hard to soft mechanical behavior (Pacakova, 2005) due to the sensitivity of ratio storage modulus to increase when the material is about this limit.

Analysis in relation to the glass transition temperature determination by CSM method has been performed for example onto Polydimethylsiloxane (PDMS) by Noble (Noble, 2018) having as result an estimation of T_g around -115°C (see Figure 66) which is a proof of the capability of the Sinus mode to characterize polymers and the relevance of the technique in the several fields, for example shock absorber in the automotive sector made of polymers.

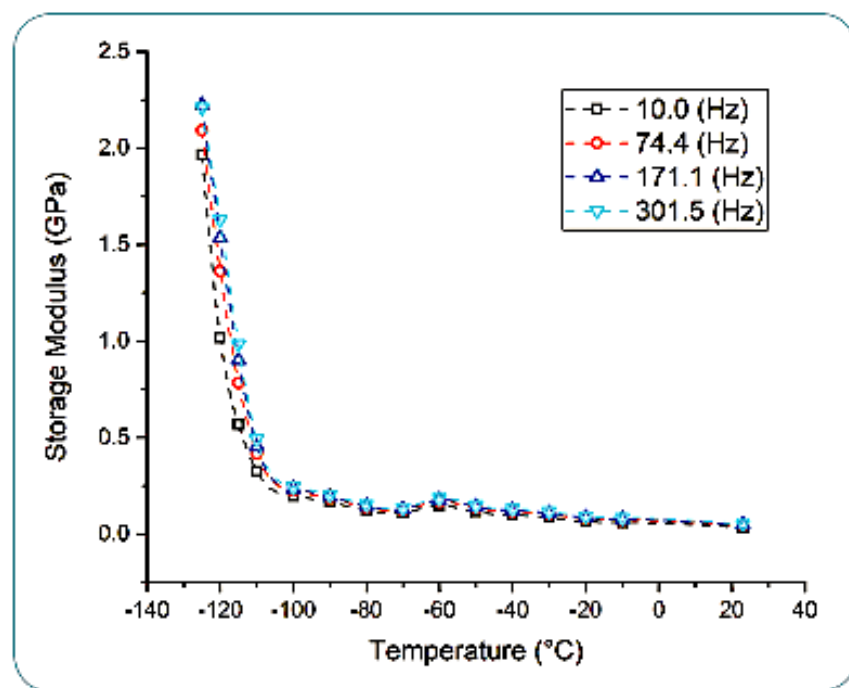


Figure 64: Storage modulus versus temperature for PDMS thin film. (Noble, 2018)

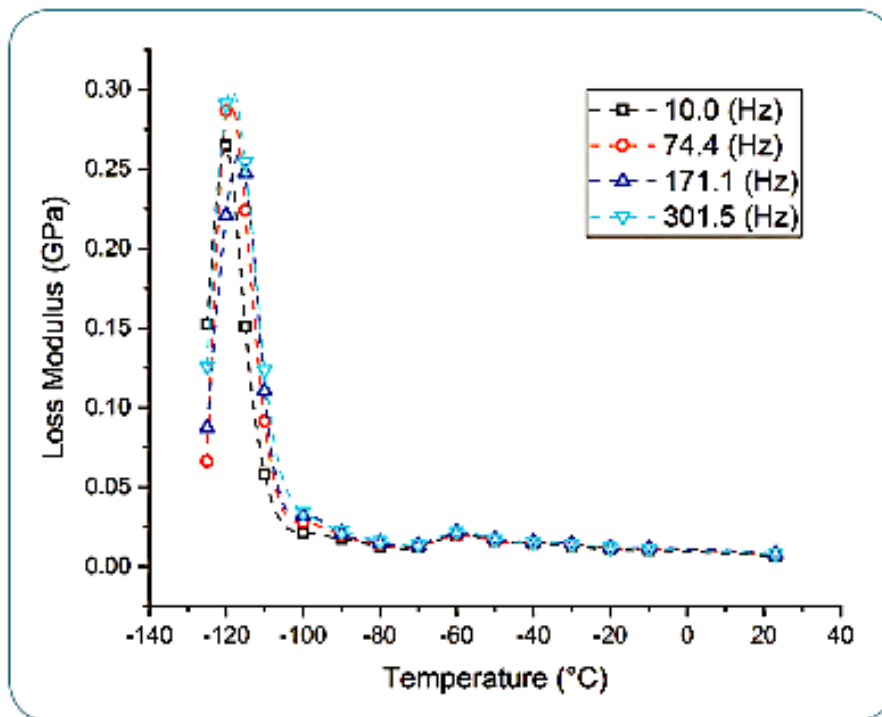


Figure 65: Loss modulus versus temperature for PDMS thin film (Noble, 2018)

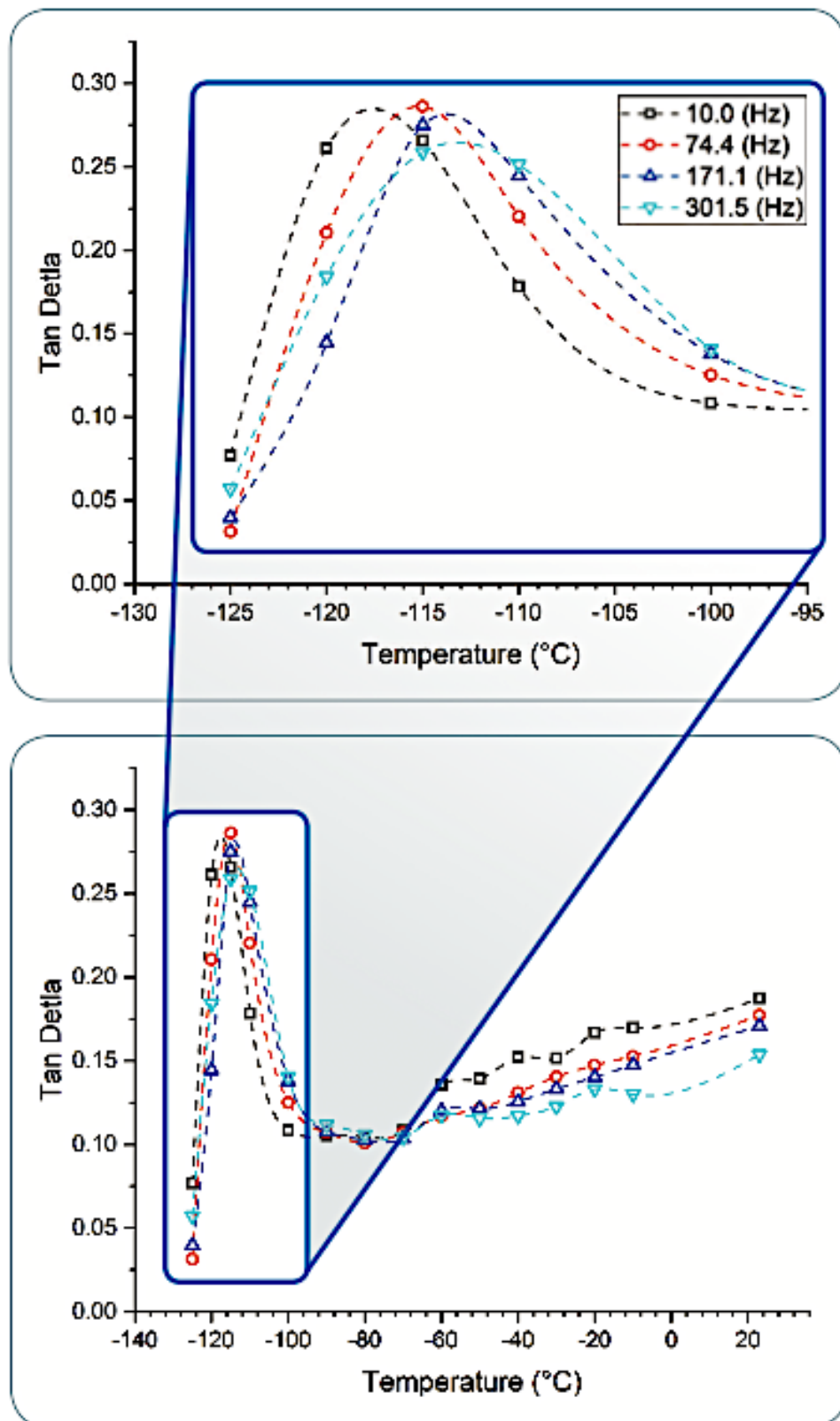


Figure 66: Tangent delta versus temperature for PDMS thin film. The upper graph shows a zoomed view of the data around the Tg temperature (Noble, 2018)



CONCLUSIONS

Nanoindentation techniques have significant use in the characterization of surface properties and thin layer materials, especially dynamic techniques that allows to establish a description of the mechanical properties of the materials without the use of optical measurements by just analyzing force-displacement data. Today, it is available a normative related to how to perform tests of this nature, i.e., ISO 14577 but limited to characterize the material at a specific indentation depth imposing the need of doing multiple tests when it is necessary to investigate the mechanical behavior of the sample along the depth. To overcome this issue, the continuous stiffness measurement is feasible alternative where it is important to mention that in contrast with ISO 14577 is a procedure not fully described by a normative, even though the literature about it presented by several authors, and consequently we encounter with a method where there are no restrictions in terms of the parameters used in the procedure: at first from the input values to perform the trial and secondly from the constructive point of view where the choices done by the manufacturer influence the range of applications and different setup available to realize the CSM test.

Regarding the impact of input values, the most representative aspects are the excitation frequency of the load applied into the indenter during the contact with the sample which determines the possibility of going through resonance during the test and the PLA constant chosen in the lock-in amplifier which impacts in the quality of the filtered indentation depth signal with the purpose of evaluating amplitude and phase shift, the last one particularly critical in the study of viscoelastic materials.

In the same order of ideas, the setup done by the manufacturer is critical too because defines the behavior of the test bench, in this work it was studied two different manufacturers machines where the results show that equipment producers criteria have a critical impact in the vibration response of the machine, as a proof of this, it was described that Agilent G200 test bench changes from an overdamped response to an underdamped one due to the interaction with the sample in relation to the contact stiffness that rises with the increasing of the indentation depth. In addition to this, always Agilent G200 equipment exhibit an output where in almost all the case the conjunction test bench and sample conduct to pass through resonance; a characteristic when it is investigated in the



Anton Paar equipment available at Politecnico di Torino, it is observed that of course there is a frequency range when the machine enters in resonance, but there is a small range (from 30 to 55 hz) where it is still possible performing CSM test without the risk of resonance avoiding peaks in the indentation depth measurement that may bring inaccuracies because the nature underdamped of the machine.

The statement described above addressed to the conclusion of this dissertation that demonstrates the potential and capability of the continuous stiffness measurement to be applied as method to estimate mechanical properties over a range of materials (from bulk to viscoelastic samples) in scales range even at nanometer length. Although, it is a methodology where is necessary to create a normative that allows an accurate and properly selection of the parameters implemented from both sides (user and manufacturer) with the objective of avoiding discrepancies in the results when the method is repeated in an already tested material.



BIBLIOGRAPHY

- Agilent Technologies. (2013). Agilent Technologies Nano Indenter G200. USA: Agilent Technologies.
- Anton Paar TriTec SA. (n.d.). G71IB002EN-B NHT3 User Manual. Switzerland.
- ASMEC GmbH. (n.d.). ASMEC - Advance Surface Mechanics. Retrieved September 9, 2021, from <https://www.asmec.de/en/information.php?seite=0&useite=20>
- ASTM Standard. (2020). A370 - Standard Test Methods and Definitions for Mechanical Testing of Steel Products. ASTM Standard.
- Bailey, N. (1994). Factors influencing weldability. In Weldability of Ferritic Steels (pp. 1-44). Woodhead Publishing Ltd.
- Bharat Bhushan, X. L. (2002). A review of nanoindentation continuous stiffness measurement technique and its applications. Materials Characterization, 48, 11-36.
- Chicot, D., De Baets, P., Staia, M., Puchi-Cabrera, E., Louis, G., Perez Delgado, Y., & Vleugels, j. (2013). Influence of tip defect and indenter shape on the mechanical properties determination by indentation of a TiB₂-60% B₄C ceramic composite. International Journal of Refractory Metals and Hard Materials, 38, 102-110.
- Chicot, D., Puchi-Cabrera, E., Lost, A., Staia, M., Decoopman, X., Roudet, F., & Louis, G. (2013). Analysis of indentation size effect in copper and its alloys. Material Science and Technology, 29(7), 868-876.
- Chicot, D., Yetna N'Jockm, M., Roudet, F., Decoopman, X., Staia, M., & Puchi-Cabrera, E. (2015). Some improvements for determining the hardness of homogeneous materials from the work-of-indentation. International Journal of Mechanical Sciences.
- Demirocak, D. E., & Bhushan, B. (2015). Probing the aging effects on nanomechanical properties of a LiFePO₄ cathode in a large format prismatic cell. Journal of Power Sources - Elsevier, 280, 256-262.



Emco-Test Prüfmaschinen GmbH. (n.d.). EMCO - TEST. Retrieved September 2021, from <https://www.emcotest.com/en/the-world-of-hardness-testing/hardness-know-how/theory-of-hardness-testing/principles-of-hardness-testing/history-of-hardness-testing/>

Fasana, A., & Marchesiello, S. (2006). Meccanica delle Vibrazioni. Torino - Italy: CLUT.

Fischer-Cripps, A. C. (2002). Nanoindentation. New York, NY: Springer.

Fischer-Cripps, A. C. (2006). Critical review of analysis and interpretation of nanoindentation test data. *Surface & Coating Technology* - Elsevier, 200, 4153-4165.

Germak, A. (n.d.). Docsity: Misure Meccaniche - Dispensa - Meccanica Applicata, Sintesi di Meccanica Applicata. Retrieved 04 2021, from <https://www.docsity.com/it/misure-meccaniche-dispensa-meccanica-applicata/60035/>

Giannakopoulos, A., & Suresh, S. (1999). Determination Of Elastoplastic Properties By Instrumented Sharp Indentation. *Scripta Materialia* - Elsevier Science ltd, 40(10), 1191-1198.

Harding, J. W., & Sneddon, I. N. (1945). The elastic stresses produced by the indentation of the plane surface of a semi-infinite elastic solid by a rigid punch. *Mathematical Proceedings of the Cambridge Philosophical Society*, 41(01), 16-26.

Hay, J., Agee, P., & Hebert, E. (2010). Continuous Stiffness Measurement During Instrumented Indentation Testing. *Experimental Techniques* - Society of Experimentals Mechanics, 86-94.

Instron Company. (n.d.). Instron. Retrieved 08 2021, from <https://www.instron.com/en/our-company/library/glossary/u/ultimate-strength>

ISO Standard. (2014). 6506 -Metallic materials - Brinell Test. ISO Standard.

ISO Standard. (2016). 14577 - Metallic materials — Instrumented indentation test for hardness and materials parameters. ISO Standard.



- ISO Standard. (2018). 4545 - Metallic Materials - Knoop Hardness Test. ISO Standard.
- ISO Standard. (2018). 6507 - Metallic Materials - Vickers Hardness Test. ISO Standard.
- JCGM - BIPM. (n.d.). JCGM - [VIM3] 4.12 sensitivity of a measuring system - sensitivity. Retrieved September 2021, from <https://jcgm.bipm.org/vim/en/4.12.html>
- Jonsson, B., & Hogmark, S. (1984). Hardness Measurements of Thin Films. *Thin Solid Films*, 114, 257-269.
- King, R. (1987). Elastic analysis of some punch problems for a layered medium. *International Journal of Solids and Structures*, 1657-1664.
- Kutz, M. (2006). *Mechanical Engineer's Handbook - Material and mechanical design*. John Wiley & Sons, Inc.
- Leitner, A., Maier-Kiener, V., & Kiener, D. (2017). Dynamic nanoindentation testing: is there an influence on a material's hardness? *Materials Research Letters*, 1-8.
- Loubet, J., Bauer, M., Tonck, A., Bec, S., & Gauthier-Manuel, B. (1993). Nanoindentation with a surface force apparatus. Kluwe Academic Publisher, 429-447.
- Maculotti, G., Genta, G., Lorusso, M., M, P., Ugues, D., & Galetto, M. (2019). Instrumented Indentation Test: Contact Stiffness Evaluation in the Nano-range. *Nanomanufacturing and Metrology* - Springer, 2(1), 16-25.
- Malzbender, J., De With, G., & Den Toonder, J. (2000). The P-h₂ relationship in indentation. *Journal of Material Research*, 15(5), 1209-1212.
- Martens, A. (1898). *Handbuch der Materialienkunde für den Maschinenbau*. Berlin, Germany: Springer.
- Merle, B., Higgings, W. H., & Pharr, G. (2019). Critical issues in conducting constant strain rate nanoindentation tests at higher strain rates. *Journal of Material Research*.



- Michel Yetna, N., Idriss, F. R., Olivier, B., & Didier, C. (2016). Work-of-indentation coupled to contact stiffness for calculating elastic modulus by instrumented indentation. Elsevier, 94, 170-179.
- Mouginot, R., Spatig, P., & Seifert, H.-P. (2020). Dynamic study of contact damping in martensitic stainless steels using nanoindentation. Mechanics of Materials - Elsevier, 149, 1-10.
- Nix, W. D., & Gao, H. (1998). Indentation Size Effect in Crystalline Materials: A law for strain gradient plasticity. Journal of Mechanics and Physics of Solids, 46(3), 411-425.
- Noble, J. (2018). Polymer Thin Film Characterization at Cold Temperatures Using nanoDMA III and xSol Cryo. Minneapolis, MN - USA: Bruker Corporation.
- Nohava, J. (n.d.). Characterization of electrodes in lithium-ion batteries by nanoindentation. Switzerland: Anton Paar.
- Nohava, J. (n.d.). Dynamic mechanical analysis by nanoindentation. Switzerland: Anton Paar.
- Oliver, W. C., & Pethica, J. B. (1989, July 18). United States of America Patent No. 4,848,141.
- Oliver, W. C., & Pharr, G. M. (1992). An improved technique for determining hardness and elastic modulus using load and displacement sensing indentation experiments. Journal of Materials Research, 7(6), 1564-1583.
- Oliver, W. C., & Pharr, G. M. (1992). On the generality of the relationship among contact stiffness, contact area, and elastic modulus during indentation. Journal of Materials Research, 7(3), 613-617.
- Oliver, W. C., & Pharr, G. M. (2004, January). Measurement of hardness and elastic modulus by instrumented indentation: Advances in understanding and refinements to methodology. Journal of Materials Research, 19(1), 3-20.



- Pacakova, V. (2005). Plastics. In Encyclopedia of Analytical Science (pp. 180-187). Prague, Czech Republic: Elsevier Ltd.
- Pharr, G. M., & Bolshakov, A. (2002). Understanding nanoindentation unloading curvers. *Journal of Materials Research*, 17(10), 2660-2671.
- Puchi-Cabrera, E., Staia, M., & Lost, A. (2015). Modeling the composite hardness of multilayer coated systems. *Thin Solid Films* - Elsevier, 578, 53-62.
- Sakai, M. (1993). Energy Principle Of The Indentation-Induced Inelastic Surface Deformation And Hardness Of Brittle Materials. *Acta metall. mater.*, 41(6), 1751-1758.
- Sakai, M. (1999). The Meyer hardness: A measure for plasticity? *Journal of Material Research*, 14(9), 3630-3639.
- Sedmak, P., & Nohava, J. (n.d.). Contribution of nanoindentation and tribology to investigation of welds. Switzerland: Anton Paar.
- Sidney R., C., & Estelle, K.-C. (2013). Dynamic nanoindentation by instrumented nanoindentation and force microscopy: a comparative review. *Beilstein Journal of Nanotechnology*, 4, 815-833.
- Sneddon, I. N. (1965). The relation between load and penetration in the axisymmetric boussinessq problem for punch of arbitrary profile. *International Journal of Engineering Science*, 3(47), 47-57.
- Stillwell, N., & Tabor, D. (1961). Elastic Recovery of Conical Indentations. *Proc. Phys. Soc. Lond.*
- Sudharshan Phani, P., Oliver, W., & Pharr, G. (2020). Understanding and modeling plasticity error during nanoindentation with continuous stiffness measurement. *Materials and Design* - Elsevier Ltd, 194, 1-11.
- Tan, M. (2006). A study of indentation work in homogeneous materials. *Journal of Materials Research*, 21(6), 1363-1374.



Torr International Services LLC. (n.d.). Torr International Services LLC. Retrieved 11
12, 2021, from <http://www.torr.com/thin-film-nanotechnology>

Tricoteasux, A., Duarte, G., Chicot, D., Le Bourhis, E., Bemporad, E., & Leasage, J. (2010). Depth-sensing indentation modeling for determination of Elastic modulus of thin films. *Mechanics of Materials*, 42, 166-174.

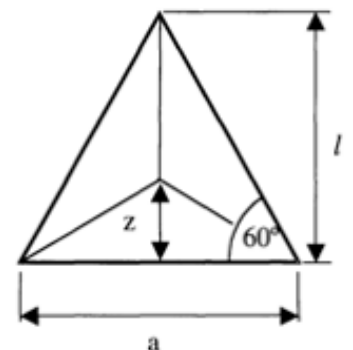
Xiaodong, L., & Bharat, B. (2002). A review of nanoindentation continuous stiffness measurement technique and its applications. *Materials Characterization*, 48, 11-36.

Yenat, M., Chicot, D., Ndjaka, J., Lesage, J., & Decoopman, X. (2015). A criterion to identify sinking-in and piling-up in indentation of materials. *International Journal of Mechanical Sciences*, 90, 145-150.



APPENDIX

Berkovitch indenter



Projected area

$$\tan 60 = \frac{l}{a/2}$$

$$l = \frac{\sqrt{3}}{2} a$$

$$A_{\text{proj}} = \frac{al}{2}$$

$$= \frac{\sqrt{3}}{4} a^2 \quad 0.433a^2$$

Surface area

$$A_{\text{surf}} = 3 \frac{ab}{2}$$

$$\sin 65.3 = \frac{z}{b}$$

$$z = \frac{a}{2} \tan 30$$

$$= \frac{a}{2\sqrt{3}}$$

$$b = \frac{a}{2\sqrt{3} \sin 65.3}$$

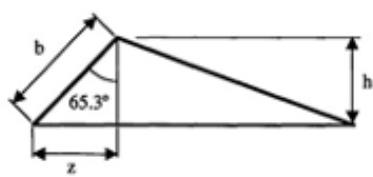
$$A_{\text{surf}} = 3 \frac{a^2}{4\sqrt{3} \sin 65.3}$$

$$0.477a^2$$

$$a = 2\sqrt{3}h \tan 65.3$$

$$A_{\text{surf}} = 27.05h^2$$

Equivalent cone angle:
70.32°



The formulation above were taken from Fischer-Cripps material (Fischer-Cripps, Nanoindentation, 2002)

Instrument Compliance – ISO 14577-2

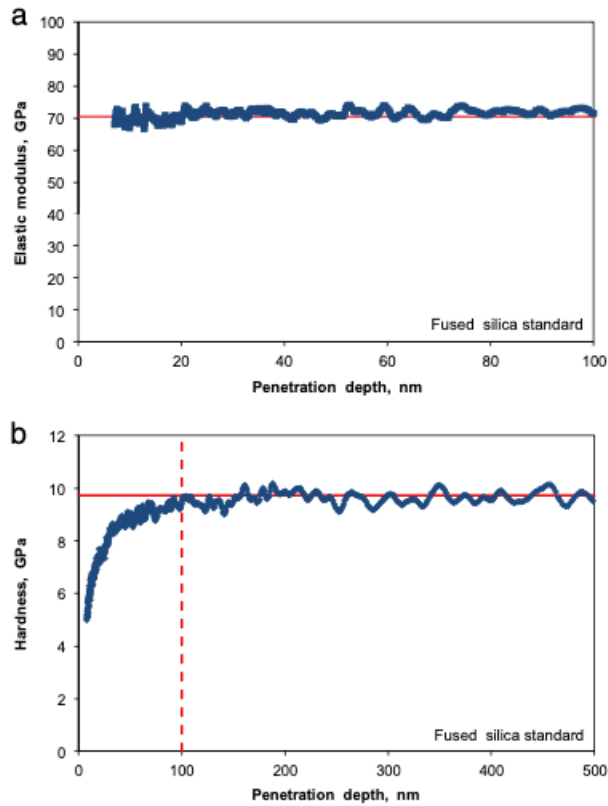
If the area function is not known, a combined iterative procedure is used. Using the area function of the perfect indenter (ISO 14577-1: -, A.4), and initial estimation of C_f and E_r is obtained by plotting C (uncorrected for machine compliance) versus $1/\sqrt{A_p(h_c)}$ for the largest indentations. Then, the new area function using all other indentations is calculated by

$$A_p(h_c) = \frac{\pi}{4} \frac{1}{E_r^2} \frac{1}{(C - C_f)^2}$$

Using the new area function, the estimation of C_f and E_r is repeated. The new values of C_f and E_r influence the area function (iterative process done several times until convergence is achieved).



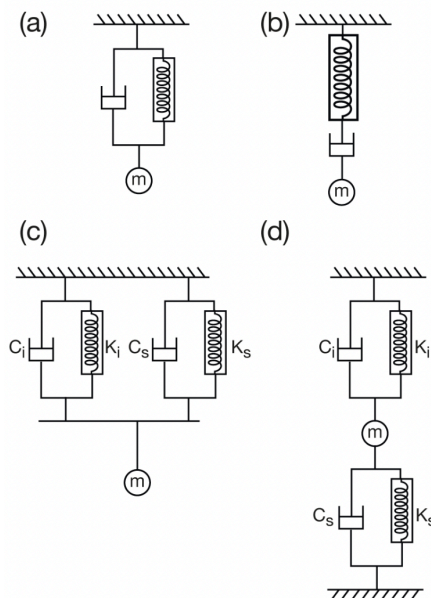
Fused Silica – No presence of ISE



Calibration curves for the Berkovich indenter employed in the present investigation, by means of fused silica standard. No ISE is present in the measurement (Puchi-Cabrera, Staia, & Lost, 2015)



Fundamental models for a viscoelastic mechanical system



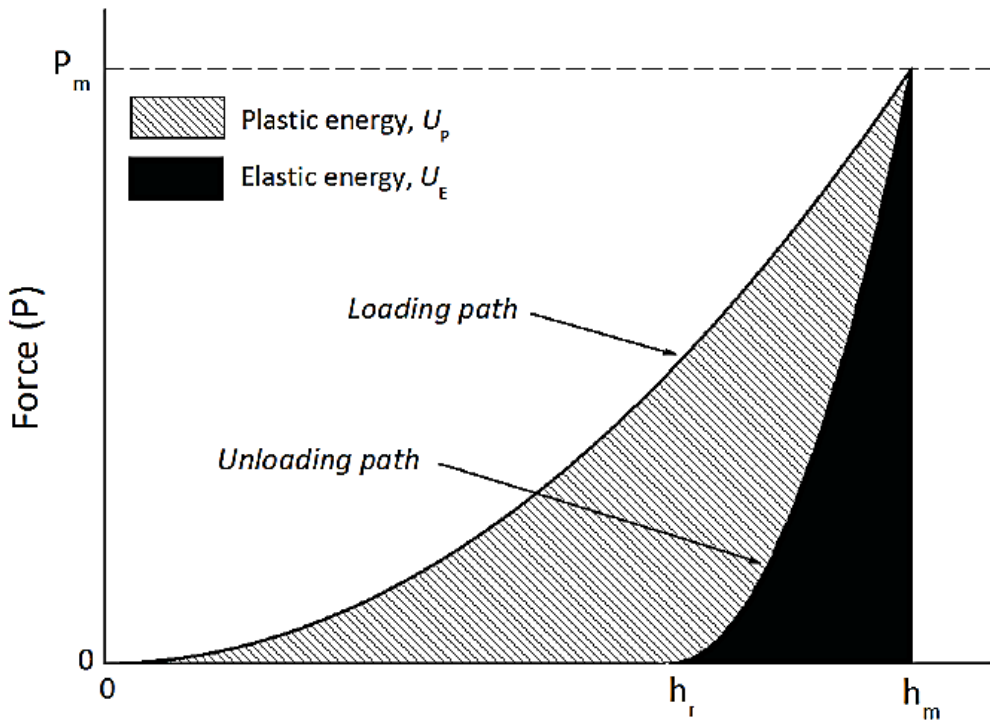
(a) Voigt model (b) Maxwell model (c)
Generalized Voigt model with 2
components (d) Voigt–Kelvin model.
(Sidney R. & Estelle, 2013)

Work of Indentation

When evaluating mechanical properties of materials through indentation mechanism, there is a peculiar approach concerning energetic models to identify and estimate physical quantities on the materials of interest. One of those method is what is known as Work of indentation, which is an analysis of the indentation process by a discretization of the deformation mechanism: elastic and plastic.

At this point, as it was anticipated in the main body of this document, the load – indentation depth curves can graphically delimitate the quantity of energy to produce elastic and plastic deformation into the material to test. For this purpose, the methodology applied concerns the determination of the area under the curves giving as result and new definition of hardness that considers this approach involving energy of deformation.

This definition of hardness states that the resistance of a material can be estimate by the energy/work necessary to create a unit of volume deformed. To get results in terms of values that can be compared to other scales of hardness, the volume deformed was limited to the corresponding to a plastic deformation.



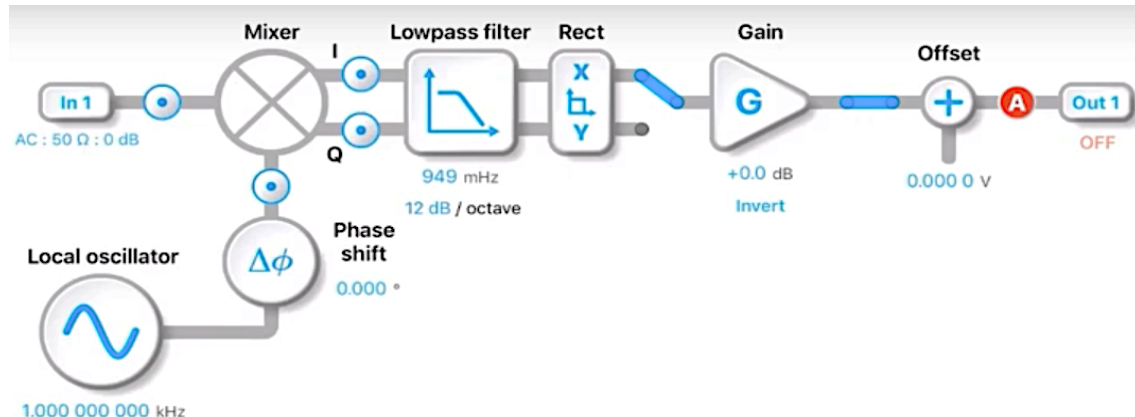
The most relevant aspects of the theory of Work-of-Indentation (methodology formulated by Stilwell and Tabor, then utterly enhanced for several author like Sakai, (Sakai, Energy Principle Of The Indentation-Induced Inelastic Surface Deformation And Hardness Of Brittle Materials, 1993), Yenat (Yenat, Chicot, Ndjaka, Lesage, & Decoopman, 2015), Chicot (Chicot, et al., 2013)) have to do with relationship H/E and the capacity of this method of model to described sinking-in and piling-up just by a simple variable (κ), the value of this change in terms of the phenomenon described, κ is approximately 5 when sinking in is the predominant deformation mode, instead when we face onto piling up κ is around 7.

$$1 - \frac{U_p}{U_p + U_e} = \kappa \frac{H}{E_r}$$

The factor which acts as discriminant about the possible values of κ resides on for example the criteria developed by Yenat (Yenat, Chicot, Ndjaka, Lesage, & Decoopman, 2015) regarding the relationship h_f/h_{\max} .



Lock-in Amplifier Working Principle – PLA time constant effect



Before, starting the explanation of the mechanism of a Lock-in Amplifier, it is important to mention that the next information is described in Sudharshan's work (Sudharshan Phani, Oliver, & Pharr, 2020).

A phase lock amplifier (PLA) is used to determine the amplitude of displacement oscillation in response to an imposed load oscillation during a CSM based indentation test. The PLA measures the amplitude of the signal at the reference frequency, which, in this case, is the frequency of the imposed force oscillation. Even if the displacement oscillation has components from other frequencies due to noise and/or any other nonlinearities in the system, the PLA will specifically determine the amplitude only at the reference frequency. For example, without a loss of generality, an arbitrary displacement signal (D) can be shown to be a sum of multiple sinusoidal waves (sine or cosine function) with different amplitudes (A_1, A_2, A_3), oscillating at different frequencies (f_1, f_2, f_3) and phase angles (ϕ_1, ϕ_2, ϕ_3), respectively as shown in the following equation,

$$D(t) = A_1 \sin(2\pi f_1 t + \phi_1) + A_2 \sin(2\pi f_2 t + \phi_2) + A_3 \sin(2\pi f_3 t + \phi_3) + \dots$$

In order to determine the amplitude, A_1 of the oscillation at a frequency f_1 , a simple mathematical procedure is used. The input signal is multiplied (elementwise) by the reference signal, which is a unit sine wave oscillating at a frequency f_1 , and the resultant product is averaged over a specific time period that is usually an integral



multiple (k) of the time period of the oscillation of the reference signal. The result is the in-phase component (D1)

$$D_1 = \sum_{t=0}^{k/f_1} D(t) \cdot \sin(2\pi f_1 t).$$

Similarly, the out of phase component (D2) is obtained by multiplying the signal with the reference signal phase shifted by 90° , that is

$$D_2 = \sum_{t=0}^{k/f_1} D(t) \cdot \sin(2\pi f_1 t + \pi/2)$$

The amplitude (A1) and the phase (ϕ_1) of the signal at the desired frequency (f1) are then calculated from

$$A_1 = 2\sqrt{D_1^2 + D_2^2}$$

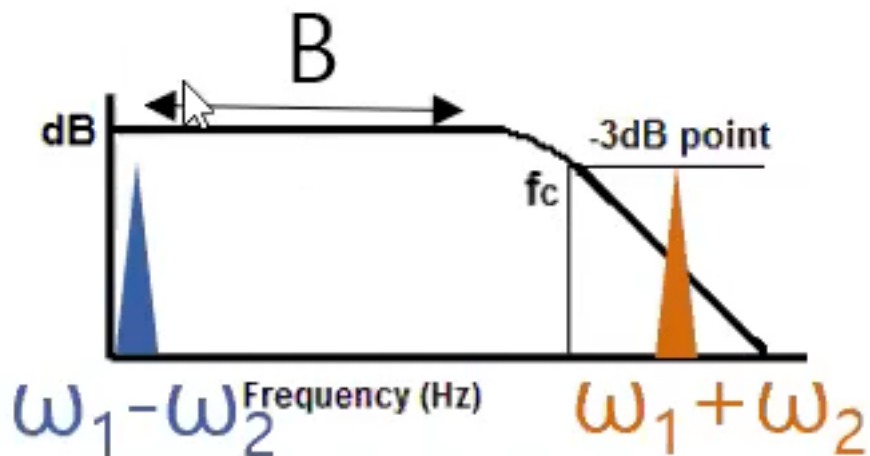
And

$$\phi_1 = \tan^{-1}\left(\frac{D_2}{D_1}\right).$$

The products D1 and D2 are usually averaged for an integral number of time periods of oscillation, which is the natural time constant of the PLA. In certain cases, the averaging is performed twice (double filtering) to suppress the high frequency noise further. The double filtering that is reported in this work involves passing the signals D1 and D2 shown, through a low pass filter twice, i.e., the output of the first filter is fed to the second one. This results in the signals being effectively averaged for twice the time window in each filter. Hence, to a first order approximation, it can be simply treated as a



low pass filter with twice the time constant and the effective time constant is then twice the PLA's natural time constant.



It is the PLA time constant that determines the band witch (B) of the averaging done to the product of D1 and D2.